MORGAN & CLAYPOOL PUBLISHERS

Quantum Radar

Marco Lanzagorta

Synthesis Lectures on Quantum Computing

Marco Lanzagorta & Jeffrey Uhlmann, *Series Editors*

Quantum Radar

Synthesis Lectures on Quantum Computing

Quantum Radar

Marco Lanzagorta

www.morganclaypool.com

ISBN: 9781608458264 paperback
ISBN: 9781608458271 ebook

DOI 10.2200/S00384ED1V01Y201110QMC005

A Publication in the Morgan & Claypool Publishers series
SYNTHESIS LECTURES ON QUANTUM COMPUTING

Lecture #5
Series Editors: Marco Lanzagorta, *ITT Exelis*
Jeffrey Uhlmann, *University of Missouri–Columbia*
Series ISSN
Synthesis Lectures on Quantum Computing
Print 1945-9726 Electronic 1945-9734

Quantum Radar

Marco Lanzagorta
ITT Exelis

SYNTHESIS LECTURES ON QUANTUM COMPUTING #5

MORGAN & CLAYPOOL PUBLISHERS

ABSTRACT

This book offers a concise review of quantum radar theory. Our approach is pedagogical, making emphasis on the physics behind the operation of a hypothetical quantum radar. We concentrate our discussion on the two major models proposed to date: interferometric quantum radar and quantum illumination. In addition, this book offers some new results, including an analytical study of quantum interferometry in the X-band radar region with a variety of atmospheric conditions, a derivation of a quantum radar equation, and a discussion of quantum radar jamming.

This book assumes the reader is familiar with the basic principles of non-relativistic quantum mechanics, special relativity, and classical electrodynamics. Our discussion of quantum electrodynamics and its application to quantum radar is brief, but all the relevant equations are presented in the text. In addition, the reader is not required to have any specialized knowledge on classical radar theory.

KEYWORDS

radar, quantum radar, quantum information, quantum sensors, quantum electrodynamics, quantum optics, classical electrodynamics, radar cross sections

To family:

Michelle, my sweetheart, the rarest of all beauties.

Angelina, my loving mother.

Mary, my favorite Mamie.

Oscar, Toby, Benny, and Hugo, my furry sons who bring inspiration, joy, and excitement to my life.

Be kind, adopt a shelter pet.

Contents

Preface

One of the major scientific thrusts from recent years has been to try to harness quantum phenomena to dramatically increase the performance of a wide variety of classical information processing devices. In particular, it is generally accepted that quantum computers and communication systems promise to revolutionize our information infrastructure.

These advances in quantum information science have had a considerable impact on the development of *quantum sensors*. That is, sensing devices that exploit quantum phenomena in order to increase their sensitivity. The interaction between quantum information science and quantum sensing is substantial. For example, quantum sensors can be described mathematically as noisy quantum channels. In addition, quantum control techniques developed in the context of quantum computation are useful to harness quantum sensing hardware.

It is important to remark that, while quantum sensing is not as mature as quantum computation, it offers simpler engineering challenges. Indeed, a quantum computer requires a large number of qubits on arbitrary superpositions and the application of a large variety of gates. On the other hand, quantum sensors require a small number of qubits on specific entangled states and only require a small set of quantum operations. As a consequence, it appears that the development of quantum sensors offers an enticing near term option for the practical application of the quantum information technologies required for the construction of a hypothetical quantum computer.

Such is the case of quantum radar, which offers the prospect of detecting, identifying, and resolving RF stealth platforms and weapons systems. Preliminary results show that quantum radar using entangled photons can provide a quadratic increase of resolution over non-entangled photons. Furthermore, the "effective visibility" of certain targets is increased if observed with a quantum radar instead of a classical radar. Also, quantum radar is more resilient against the use of jamming countermeasures. And perhaps more important, a quantum sidelobe structure offers a new channel for the detection of RF stealth targets.

This book offers a concise review of quantum radar theory. Our approach is pedagogical. The motivation for quantum radar is presented in Chapter 1. The equations that describe photons and their interactions with matter are discussed in Chapter 2. The reflection of photons by a mirror is considered in Chapter 3, which offers a novel quantum description of specular reflections using quantum electrodynamics and interferometry. In Chapter 4 we review classical radar and associated cross sections. Quantum radar theory is discussed in detail in Chapter 5, with special emphasis on interferometric quantum radar and quantum illumination devices. Finally, Chapter 6 presents a detailed discussion of quantum radar cross sections as well as examples for spherical and rectangular targets. This book offers some new results, including an analytical study of quantum interferometry

in the X-band radar region with a variety of atmospheric conditions, a derivation of a quantum radar equation, and a discussion of quantum radar jamming.

This book assumes the reader is familiar with the basic principles of non-relativistic quantum mechanics, special relativity, and classical electrodynamics. Our discussion of quantum electrodynamics and its application to quantum radar is brief, but all the relevant equations are presented in the text. In addition, the reader is not required to have any specialized knowledge on classical radar theory.

Marco Lanzagorta
July 2011

Acknowledgments

I am grateful to Keye Martin for his advice and encouragement. I am also thankful to James McCracken, James Troupe, and Jeffrey Uhlmann for reviewing this manuscript and for providing valuable corrections, suggestions, and insights. Special thanks to Bryan O'Gorman, who produced the first version of the radar cross section simulation codes. And of course, I deeply appreciate the encouragement and perseverance provided by my editor Mike Morgan. And last but not least, I am thankful to Pam Lamb because her administrative support makes my life so much simpler.

I kindly acknowledge the support received by the Office of Naval Research Quantum Information Science Basic Research Challenge program and ITT Exelis.

Marco Lanzagorta
October 2011

CHAPTER 1

Introduction

Radar is a standoff sensing technology that was originally developed during the first half of the 20th century [105]. While the reflection of radio waves by solid objects was first observed by Heinrich Hertz in 1886, it was not until the years that followed World War One that scientists realized that radar could become a new battlefield technology. During the inter-war period, all major military powers such as the US, the United Kingdom, France, Germany, Japan, Italy and the Soviet Union, performed radar research.

The first pulse-based radar system, able to detect and estimate the range of a target, was developed at the US Naval Research Laboratory in 1934. Subsequently, radar proved to be an important tool during World War Two [85]. For example, the British were the first to exploit radar to detect airborne targets, giving them advance notice of incoming aircraft attacks. Arguably, radar gave a crucial advantage to the Allies during the Battle of Britain [11]. Since then, radar has become a widespread technology not only in the modern battlefield, but also in the civilian world.

1.1 THE NEED FOR IMPROVED RADAR SYSTEMS

There is a critical need to improve the performance of current radar systems and increase the probability of detection, identification, and discrimination of stealth platforms and other objects. In particular, improved standoff sensors are required for the following applications:

Military: Stealth technology was exclusive to the US for the last decades of the 20th century [1, 86]. However, stealth technology is becoming widespread. For example, China recently unveiled their plans to build their J-20 stealth fighter [100]. As a consequence, the ability to provide an early warning system against an enemy attack is severely diminished.

Space Exploration: There is an incredibly large amount of natural and man-made debris surrounding our planet [54]. From small rocks to old satellites, these objects pose a great risk to the manned and unmanned exploration of space. For instance, the STS-118 was damaged by a small object, producing a hole several centimeters in diameter in its hull [64].

Planetary Defense: The past few years have witnessed a renewed interest on mitigation strategies for planetary defense (tracking asteroids, comets, and other astronomical bodies which could be on a collision path with Earth) [78]. In this regard, the Shoemaker-Levy 9 event, where a comet impacted the surface of Jupiter, made clear the possibility of further extinction level events on our planet [107].

As we will see, quantum information technology may be the key to improved long range sensor systems.

1.2 FROM QUANTUM INFORMATION TO QUANTUM SENSORS

One of the major scientific thrusts in recent years has been to try to determine the many ways in which quantum phenomena could be harnessed to dramatically increase the performance of a wide variety of classical information processing devices. In particular, it is generally accepted that quantum computers and communication systems promise to revolutionize our information infrastructure [81].

Arguably, the main motivation of most quantum information science efforts has been the creation of a quantum computer able to run Shor's algorithm for crypto-analysis applications. Even though a full-blown quantum computer able to factorize a large number is still far into the future, many theoretical and experimental results have shown that it is possible to harness quantum phenomena for computation and communication purposes.

As a side effect, advances in quantum information science have had a considerable impact on the development of *quantum sensors*: sensing devices that exploit quantum phenomena in order to increase their sensitivity. Examples of quantum sensors recently proposed by the scientific community include magnetometers, photodetectors, and gravitometers.

Furthermore, the interaction between quantum information science and quantum sensing has been substantial; for example, quantum sensors can be described mathematically as noisy quantum channels. In addition, quantum control techniques developed in the context of quantum computation are useful to harness quantum sensing hardware.

It is important to remark that while quantum sensing is not as mature as quantum computation, it offers simpler engineering challenges. For instance, a quantum computer requires a large number of qubits on arbitrary superpositions with coherence times long enough to perform complex computations using a large variety of gates. On the other hand, quantum sensors require a small number of qubits on a specific entangled state and only require a handful of quantum operations.

As a consequence, it appears that the development of quantum sensors offers an enticing near term option for the practical application of the quantum information technologies required for the construction of a hypothetical quantum computer.

1.3 QUANTUM RADAR TECHNOLOGY

Quantum radar offers the prospect of detecting, identifying, and resolving RF stealth platforms and weapons systems. In the electronic battlefield, quantum radar may become a revolutionary technology just as RF stealth technology was during the last three decades of the 20th century. The use of quantum radar for planetary defense and space exploration is also worth considering.

By exploiting entanglement, quantum radar offers the prospect of enhanced target detection capabilities. These systems rely on quantum states of light (photons) sustained on an entangled

superposition. One half of these states is sent towards the target and the other remains in the receiver. Signal detection is enhanced by exploiting the existing correlation between the emitted photons bounced back by the target and the ones kept inside the radar. As such, quantum radar offer the possibility of detecting, identifying, and resolving stealth targets.

Preliminary results show that quantum radar using entangled photons can provide a quadratic increase of resolution over non-entangled photons [67, 97]. Furthermore, the "effective visibility" of a target is increased if observed with a quantum radar instead of a classical radar, and a quantum sidelobe structure offers a new channel for the detection of RF stealth targets [61].

Although there are practical engineering challenges, it is fair to say that some members of the scientific community have shown skepticism about the prospect of building a quantum radar. However, to date there are no theoretical or experimental results that suggest that photons in the 9 GHz frequency cannot be entangled, transmitted, and detected.

Furthermore, a group at the University of Leiden in the Netherlands has already proposed a mechanism to generate entangled microwave photons using quantum dots [27]. This paper is cited in the celebrated review on quantum entanglement by the Horodecki group [47]. On the other hand, the Universidad del Pais Vasco in Spain has developed theoretical models for single photon detectors operating in the microwave regime [88, 89]. In addition, research performed at NRL has shown that a theoretical quantum radar operating in the 9 GHz regime is able to enhance target detection even if atmospheric attenuation is taken into consideration [97]. Also, a new analysis presented in Chapter 5 shows that supersensitive quantum interferometry is feasible up to about 300 km even in the presence of an attenuating atmosphere. Both of these results were performed using the entanglement attenuation formulas derived by the Mitre group [32, 33] based on a quantization scheme of the electromagnetic field in an attenuating environment [52, 68].

It is important to note that photons in the 9 GHz frequency correspond to the radar-microwave regime. Indeed, the X band in radar corresponds to the 8-12 GHz region and is extensively used for missile guidance, marine radar, weather, ground surveillance, and airport traffic control [31, 59, 95, 96]. Therefore, a quantum radar operating in this band would be extremely useful in a variety of operational environments of civilian and military interest.

1.4 THE QUANTUM RADAR RESEARCH COMMUNITY

There are several groups that are currently performing research on topics related to quantum radar and standoff quantum sensing. Among these, Jeff Shapiro and Seth Lloyd at MIT [34, 48, 67, 93, 94], James Smith at the US Naval Research Laboratory (NRL) [97], Jonathan Dowling at Louisiana State University [26, 50, 65], John Myers at Harvard University [71, 79], Yanhua Shih at the University of Maryland [77], Robert Boyd at the University of Rochester [72], Usha Devi at the University of Bristol [102], Enrique Solano at the Universidad del Pais Vasco [88, 89], Ned Allen at Lockheed Martin [2], James Troupe at the Naval Surface Warfare Center (NSWC) at Dahlgren, and Marco Lanzagorta at ITT Exelis [61, 62]. Furthermore, the Defense Advanced Research Projects Agency (DARPA) promoted the interest on quantum radar during their program on Quantum Sensors [17]

and the Office of Naval Research (ONR) recently held a technical workshop to discuss the feasibility of quantum radar [82].

1.5 SUMMARY

Quantum radar is a promising technology that could have a strong impact on the civilian and military realms. Although quantum sensing technology is not as mature as quantum computation, the engineering of a full-blown multi-qubit quantum computer is a much harder challenge than the design of deployable quantum sensors. As a consequence, quantum radar is a high risk, high payoff proposal. By any means, the concept of a quantum radar is worth investigating in further detail.

CHAPTER 2

The Photon

The photon is the elementary excitation of the quantum electromagnetic field. That is, electromagnetic fields are made of photons. Quantum Electrodynamics (QED) is the relativistic theory that describes the dynamics of photons and its interactions with matter [6, 40, 90, 106]. High precision experiments at the European Organization for Nuclear Research (CERN) have shown that, to date, QED is the most accurate physical theory known to man [24].

In this chapter and the next we will briefly review the basic structure of quantum electromagnetic fields as they relate to non-relativistic matter fields. This specific class of applications of QED is usually referred as *quantum optics* [13, 68, 73, 92]. A detailed discussion of QED or quantum optics is outside the scope of the present book, and the reader is encouraged to pursue the rich literature available on the topic. Our emphasis is to present those equations that are required to understand quantum radar mechanisms such as pulse generation and propagation, as well as the interaction between a quantum radar pulse and a non-relativistic material target.

2.1 MAXWELL EQUATIONS

The electromagnetic fields in vacuum obey Maxwell equations:

$$\begin{aligned} \nabla \cdot \mathbf{E} &= 0 \\ \nabla \cdot \mathbf{B} &= 0 \\ \nabla \times \mathbf{B} &= \frac{1}{c}\frac{\partial \mathbf{E}}{\partial t} \\ \nabla \times \mathbf{E} &= -\frac{1}{c}\frac{\partial \mathbf{B}}{\partial t} \end{aligned} \tag{2.1}$$

which can be rewritten as:

$$\begin{aligned} \nabla^2 \mathbf{E} - \frac{1}{c^2}\frac{\partial^2 \mathbf{E}}{\partial t^2} &= 0 \\ \nabla^2 \mathbf{B} - \frac{1}{c^2}\frac{\partial^2 \mathbf{B}}{\partial t^2} &= 0 \end{aligned} \tag{2.2}$$

to explicitly describe electromagnetic waves [8, 51].

The electromagnetic fields can be expressed in terms of vector and scalar potentials, $\mathbf{A}$ and Φ, as follows:

$$\begin{aligned} \mathbf{B} &= \nabla \times \mathbf{A} \\ \mathbf{E} &= -\nabla \Phi - \frac{1}{c}\frac{\partial \mathbf{A}}{\partial t} \end{aligned} \tag{2.3}$$

Furthermore, the potentials are arbitrary to the extent of a scalar function Λ:

$$\begin{aligned} \mathbf{A} &\longrightarrow \mathbf{A}' = \mathbf{A} + \nabla\Lambda \\ \Phi &\longrightarrow \Phi' = \Phi - \frac{1}{c}\frac{\partial\Lambda}{\partial t} \end{aligned} \tag{2.4}$$

This is known as the *gauge freedom* or *gauge invariance* of the electromagnetic fields [51, 90].

2.2 ELECTROMAGNETIC QUANTUM FIELDS

The canonical quantization of the electromagnetic field replaces the classical fields by quantum operators:

$$\begin{aligned} \mathbf{E} &\longrightarrow \hat{\mathbf{E}} \\ \mathbf{B} &\longrightarrow \hat{\mathbf{B}} \end{aligned} \tag{2.5}$$

that satisfy Maxwell equations [68, 73, 92]. As a consequence, those relations between the electromagnetic fields that are true in classical electrodynamics, continue to hold in quantum electrodynamics.

For example, the reflection and refraction of a beam of light traveling across the boundary of two media with different electromagnetic properties can be computed using Maxwell equations and setting the appropriate boundary conditions for the fields [51]. Consequently, excitations of the quantum electromagnetic fields (i.e., photons) obey the exact same properties when they cross a boundary.

In a cavity of volume V, the electromagnetic fields are made of elementary quantum excitations of momentum $\mathbf{k}$, frequency $\omega_{\mathbf{k}}$, and polarization λ. The quantum fields can be expressed as Fourier expansions in terms of these elementary excitations as follows:

$$\begin{aligned} \hat{\mathbf{E}} &= \sum_{\mathbf{k},\lambda} \mathbf{e}_{\mathbf{k}}^{(\lambda)}\, \mathcal{E}_{\mathbf{k}}\, \hat{a}_{\mathbf{k},\lambda}\, e^{-i\omega_{\mathbf{k}}t + i\mathbf{k}\cdot\mathbf{r}} + h.c. \\ \hat{\mathbf{B}} &= \sum_{\mathbf{k},\lambda} \frac{\mathbf{k}\times\mathbf{e}_{\mathbf{k}}^{(\lambda)}}{\omega_{\mathbf{k}}}\, \mathcal{E}_{\mathbf{k}}\, \hat{a}_{\mathbf{k},\lambda}\, e^{-i\omega_{\mathbf{k}}t + i\mathbf{k}\cdot\mathbf{r}} + h.c. \end{aligned} \tag{2.6}$$

where $h.c.$ stands for the hermitian conjugate, $\epsilon_{\mathbf{k}}^{(\lambda)}$ is the polarization vector (with $\lambda = 0, 1$), and:

$$\mathcal{E}_{\mathbf{k}} = \sqrt{\frac{\hbar\omega_{\mathbf{k}}}{2\epsilon_0 V}} \tag{2.7}$$

The annihilation and creation operators, $\hat{a}$ and $\hat{a}^\dagger$, satisfy the commutation relations:

$$\begin{aligned} [\hat{a}_{\mathbf{k},\lambda}\ ,\ \hat{a}_{\mathbf{k}',\lambda'}] &= 0 \\ [\hat{a}^\dagger_{\mathbf{k},\lambda}\ ,\ \hat{a}^\dagger_{\mathbf{k}',\lambda'}] &= 0 \\ [\hat{a}_{\mathbf{k},\lambda}\ ,\ \hat{a}^\dagger_{\mathbf{k}',\lambda'}] &= \delta_{\mathbf{k}\mathbf{k}'}\,\delta_{\lambda\lambda'} \end{aligned} \tag{2.8}$$

In terms of the annihilation and creation operators, the operator that corresponds to the electromagnetic radiation energy is given by the Hamiltonian:

$$\begin{aligned}\hat{\mathcal{H}}_R &= \frac{1}{2}\int dV\left(\epsilon_0\hat{\mathbf{E}}\cdot\hat{\mathbf{E}}+\frac{1}{\mu_0}\hat{\mathbf{B}}\cdot\hat{\mathbf{B}}\right) \\ &= \sum_{\mathbf{k},\lambda}\hbar\omega_k\left(\hat{a}^\dagger_{\mathbf{k}\lambda}\hat{a}_{\mathbf{k}\lambda}+\frac{1}{2}\right)\end{aligned} \tag{2.9}$$

The electromagnetic quantum fields are best defined on an energy eigenvalue occupation number Fock space. That is, the eigenvectors are of the form:

$$|n_{\mathbf{k},\lambda}\rangle \tag{2.10}$$

which represents a state of n elementary quantum field excitations with momentum $\mathbf{k}$ and polarization λ.

The creation and annihilation operators are used to increase or decrease the number of excitations on a quantum state:

$$\begin{aligned}\hat{a}^\dagger_{\mathbf{k},\lambda}\,|n_{\mathbf{k},\lambda}\rangle &= \sqrt{n_{\mathbf{k},\lambda}+1}\;\;|n_{\mathbf{k},\lambda}+1\rangle \\ \hat{a}_{\mathbf{k},\lambda}\,|n_{\mathbf{k},\lambda}\rangle &= \sqrt{n_{\mathbf{k},\lambda}}\;\;|n_{\mathbf{k},\lambda}-1\rangle\end{aligned} \tag{2.11}$$

Therefore, the creation operators can be used to define any quantum state of light from the quantum vacuum state $|0\rangle$. For example, the state of n elementary excitations with momentum $\mathbf{k}$ and polarization λ is given by:

$$|n_{\mathbf{k},\lambda}\rangle = \frac{\left(\hat{a}^\dagger_{\mathbf{k},\lambda}\right)^n}{\sqrt{n!}}|0\rangle \tag{2.12}$$

For most applications of interest to quantum radar, the electromagnetic radiation moves as a beam in a straight line. For these problems, it is useful to use the continuous-mode quantization of the fields instead of discrete cavity modes [68, 92]. Here, the quantization volume is made infinite, the sum is converted into an integral:

$$\sum_{\mathbf{k}} \longrightarrow \frac{2V}{(2\pi)^3}\int d^3k \tag{2.13}$$

and the operators change to:

$$\begin{aligned}\hat{a} &\longrightarrow \sqrt{\frac{(2\pi)^3}{V}}\,\hat{a} \\ \hat{a}^\dagger &\longrightarrow \sqrt{\frac{(2\pi)^3}{V}}\,\hat{a}^\dagger\end{aligned} \tag{2.14}$$

The one-dimensional continuous mode variable is usually taken to be ω along the direction of propagation of the light $\mathbf{k}$, and the creation and annihilation operators can be simply denoted by $\hat{a}^\dagger(\omega)$ and $\hat{a}(\omega)$. Thus, the non-zero commutation relation can be written as:

$$[\hat{a}(\omega), \hat{a}^\dagger(\omega)] = \delta(\omega - \omega') \tag{2.15}$$

Furthermore, in continuous mode quantization, the equal time commutation relations for the actual electromagnetic fields are:

$$\begin{aligned}
[\hat{E}_i(\mathbf{r}, t),\ \hat{B}_j(\mathbf{r}', t)] &= -i\hbar c^2 \frac{\partial}{\partial l}\delta^3(\mathbf{r} - \mathbf{r}') \\
[\hat{E}_i(\mathbf{r}, t),\ \hat{B}_i(\mathbf{r}', t)] &= 0 \\
[\hat{E}_i(\mathbf{r}, t),\ \hat{E}_j(\mathbf{r}', t)] &= 0 \\
[\hat{B}_i(\mathbf{r}, t),\ \hat{B}_j(\mathbf{r}', t)] &= 0
\end{aligned} \tag{2.16}$$

where (i, j, l) form a cyclic permutation over the three vector components of the electromagnetic fields. As a consequence, orthogonal components of $\mathbf{E}$ and $\mathbf{B}$ can not be measured simultaneously [92].

2.3 THE PHOTON

In the *radiation gauge*, the vector and scalar potentials satisfy:

$$\begin{aligned}
\nabla \cdot \mathbf{A} &= 0 \\
\Phi &= 0
\end{aligned} \tag{2.17}$$

and the electromagnetic fields are given by:

$$\begin{aligned}
\mathbf{E} &= -\frac{\partial \mathbf{A}}{\partial t} \\
\mathbf{B} &= \nabla \times \mathbf{A}
\end{aligned} \tag{2.18}$$

In this gauge, Maxwell's equations are reduced to a single wave equation for the vector potential $\mathbf{A}$:

$$\nabla^2 \mathbf{A} - \frac{\partial^2 \mathbf{A}}{\partial t^2} = 0 \tag{2.19}$$

The canonical quantization of the vector potential leads to:

$$\hat{\mathbf{A}} = \sum_{\mathbf{k},\alpha} \left(\mathbf{A}_{\mathbf{k}\alpha} \hat{a}_{\mathbf{k}\alpha} + \mathbf{A}^*_{\mathbf{k}\alpha} \hat{a}^\dagger_{\mathbf{k}\alpha} \right) \tag{2.20}$$

where:

$$\mathbf{A}_{\mathbf{k}\alpha} = \sqrt{4\pi} \frac{\mathbf{e}^\alpha}{\sqrt{2\omega}} e^{-i(\omega t - \mathbf{k}\cdot\mathbf{r})} \tag{2.21}$$

with:

$$\omega = |\mathbf{k}| \tag{2.22}$$

and the field components satisfy the orthogonality condition:

$$\int \mathbf{A}_{\mathbf{p}\alpha} \cdot \mathbf{A}^*_{\mathbf{q}\beta}\, d^3x = \frac{2\pi}{\omega}\delta_{\mathbf{pq}}\delta_{\alpha\beta} \tag{2.23}$$

In the above equations, $\mathbf{e}^\alpha$ are the two field polarization vectors (with $\alpha = 0, 1$). Because of the radiation gauge condition we have that:

$$\nabla \cdot \hat{\mathbf{A}} = \nabla \cdot \sum_{\mathbf{k},\alpha} \left(\mathbf{A}_{\mathbf{k}\alpha}\hat{a}_{\mathbf{k}\alpha} + \mathbf{A}^*_{\mathbf{k}\alpha}\hat{a}^\dagger_{\mathbf{k}\alpha} \right) = 0 \tag{2.24}$$

and as a consequence:

$$\mathbf{k} \cdot \mathbf{e}^\alpha = 0 \qquad \forall \alpha, \mathbf{k} \tag{2.25}$$

This is *the transversality condition* which establishes that the electromagnetic fields are orthogonal to the direction of propagation of the electromagnetic wave.

Also, $\hat{a}_{\mathbf{k}\alpha}$ and $\hat{a}^\dagger_{\mathbf{k}\alpha}$ are the electromagnetic field potential annihilation and creation operators, respectively, and satisfy:

$$\begin{aligned} \langle N_{\mathbf{k}\alpha} - 1 | \hat{a}_{\mathbf{k}\alpha} | N_{\mathbf{k}\alpha} \rangle &= \sqrt{N_{\mathbf{k}\alpha}} \\ \langle N_{\mathbf{k}\alpha} | \hat{a}^\dagger_{\mathbf{k}\alpha} | N_{\mathbf{k}\alpha} - 1 \rangle &= \sqrt{N_{\mathbf{k}\alpha}} \end{aligned} \tag{2.26}$$

The quantum states of the electromagnetic potential are labeled by $N_{\mathbf{k}\alpha}$, that is, N elementary quantum excitations of the electromagnetic vector potential with momentum $\mathbf{k}$ and polarization α.

In the context of quantum electrodynamics, it is customary to define the *photon* as the elementary quantum excitations of the electromagnetic vector potential [90, 106]. However, it can also be defined as the elementary excitations of the actual electromagnetic fields. Indeed, the functional representations of these quantum fields are related by the definition of electromagnetic potentials and by Maxwell equations in a straightforward manner [73].

2.4 PHOTON INTERACTIONS

It is a well known fact that electromagnetic fields interact with charged particles. In minimal coupling quantum electrodynamics, photons are neutral *gauge fields* coupled to charged particles [90, 106]. The equation that describes the interaction between charged particles and photons is given by replacing the standard derivative terms in the non-interacting dynamical equation of the free particle with the *covariant derivative* [90, 106].

For instance, the Dirac Lagrangian for a non-interacting fermion of mass m described by the Dirac spinor ψ is:

$$\mathcal{L} = i\bar{\psi}\gamma^\mu\partial_\mu\psi - m\bar{\psi}\psi \tag{2.27}$$

where γ^μ are the Dirac matrices and ∂_μ is the standard 4-derivative:

$$\partial_\mu = \left(\frac{\partial}{\partial t}, \nabla\right) \tag{2.28}$$

Then, the electromagnetic interaction is introduced by replacing ∂_μ with the covariant derivative D_μ:

$$D_\mu = \partial_\mu - ieA_\mu \tag{2.29}$$

where e the electric charge of the fermion and A_μ is the Lorentz covariant electromagnetic potential:

$$A_\mu = (\phi, -\mathbf{A}) \tag{2.30}$$

Therefore, the interacting fermion is described by the Lagrangian:

$$\begin{aligned} \mathcal{L} &= i\bar{\psi}\gamma_\mu D^\mu \psi - m\bar{\psi}\psi \\ &= i\bar{\psi}\gamma^\mu \partial_\mu \psi - m\bar{\psi}\psi + e\bar{\psi}\gamma^\mu A_\mu \psi \end{aligned} \tag{2.31}$$

That is, the interaction between the charged fermion and a photon is given by the term:

$$I_{f,\gamma} = e\bar{\psi}\gamma^\mu A_\mu \psi \tag{2.32}$$

which involves two fermionic and one photonic fields.

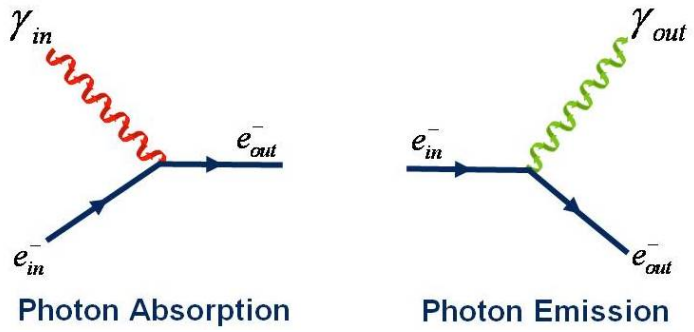

Figure 2.1: Minimal coupling quantum electrodynamics: the interaction between light and matter is described solely in terms of photon absorption or emission processes.

The physical interpretation of this interaction term is shown in Figure 2.1: the interaction between a photon and a fermion is simply described as a process of photonic absorption or as a process of photonic emission [16, 40]. Notice that each of these *Feynman Diagrams* involves two fermionic lines and one photonic line, in accordance with the interaction term $I_{f,\gamma}$. Therefore, all electromagnetic interactions boil down to processes of photonic absorption and/or emission[1].

[1]Even though we derived relativistic expressions, these results are also valid in the non-relativistic regime.

The photon is well described by the equations that emerge from the quantum field treatment of the electromagnetic fields. However, sometimes it is difficult to conceptually understand the dynamics of physical phenomena involving photons. One of the reasons for this shortcoming is that, in strong contrast to other relativistic particles such as the electron, the photon cannot be localized. That is, it is mathematically impossible to build a continuity equation using localization probability distributions that satisfy Einstein's special relativity (see Section 2.6).

Furthermore, the theoretical scope of QED does not include the explicit space-time dependence of the physical processes that it describes [6]. For instance, QED does not describe the continuous evolution in time of a photon being absorbed or emitted by a charged particle. Instead, the theory provides predictions of dynamic observables (energy, momentum, polarization) based on the initial state of the particles before the interaction takes place. Therefore, QED merely provides the transition amplitudes between specified initial and final states of a system of particles [6, 90, 106].

These observations enhance the challenge of properly understanding how an incident photon is reflected by a mirror (clearly, this is a problem closely related to the interaction between a quantum radar pulse and a target). Indeed, the reflection process can be reduced to a scattering problem: the incident photon is being scattered by one or more of the atoms that make the mirror. That is, the incident photon is absorbed by one or more atoms, and subsequently emitted. However, how many atoms scatter the photon? If we cannot localize the photon, then, what atoms are involved in the scattering process? Also, if specific paths make no sense in the context of QED, then, how can we expect to obtain the law of reflections (incident angle equal to outgoing angle of the light beam)? Furthermore, if the scattering process in QED does not involve any geometric angles, how does the scattering atom "know" that it has to send the outgoing photon on a precise direction?

Clearly, picturing the photon as a ball scattered by the atoms in a game of billiards will not lead to the correct answers to these questions. As such, understanding the QED description of specular reflections shows how the commonly held interpretation of the photon as an electron-like particle is completely erroneous and misleading. In the next chapter we will discuss a formal QED description of specular reflections.

2.5 THE CLASSICAL LIMIT

Quantum electrodynamics offers the only theoretical description of electromagnetic fields that is fully consistent with quantum theory. It is also known that the physical properties of a quantum system are equivalent to those of its corresponding classical system when the relevant quantum numbers are large[2] [6, 60]. In the case at hand, classical electrodynamics is recovered in the limit of a large number of photons.

[2]This statement is not exactly true: one could envision a maximally entangled state made of a large number of photons N. Clearly, the limit when N is large does not lead to a description of decoherence. Indeed, the state remains entangled regardless of the value of N. As a consequence, the formal transition to the classical limit needs to involve both a large number of photons and a decoherence process.

However, an infinitely large number of photons also implies an infinitely large energy. Clearly, a more rigorous condition is required to determine when a system has to be described with quantum or classical electrodynamics.

To this end, let us consider a time-dependent quasi-classical electric field $\mathbf{E}$ averaged over a short time interval Δt. We assume that the field has a Fourier representation of the form:

$$\mathbf{E}(\mathbf{x}, t) = \int \tilde{\mathbf{E}}(\mathbf{k}, \omega) e^{-i(\omega t - \mathbf{k}\cdot\mathbf{r})} dk^3 d\omega \tag{2.33}$$

If $\bar{\mathbf{E}}$ is the average field over Δt, then the only Fourier components that will contribute to $\bar{\mathbf{E}}$ are those with frequencies:

$$\omega \leq \frac{1}{\Delta t} \tag{2.34}$$

as for the other components the oscillatory factor $e^{-i\omega t}$ is very small when averaged over Δt. In addition, in a unitary volume, the number of oscillators with frequency between zero and ω is:

$$\left(\frac{\omega}{c}\right)^3 \approx \frac{1}{(c\Delta t)^3} \tag{2.35}$$

We also know that the field energy density is proportional to $\bar{\mathbf{E}}^2$. Therefore, if $\bar{N}_\omega$ is the average number of photons we have that:

$$\bar{N}_\omega \times \hbar\omega \times \left(\frac{\omega}{c}\right)^3 \approx \bar{\mathbf{E}}^2 \tag{2.36}$$

and as a consequence:

$$\bar{N}_\omega \approx \frac{\bar{\mathbf{E}}^2 c^3}{\hbar\omega^4} \tag{2.37}$$

Then, if the number of photons is large:

$$\bar{N}_\omega \gg 1 \Rightarrow \bar{\mathbf{E}}^2 \gg \frac{\hbar\omega^4}{c^3} \tag{2.38}$$

so is the value of $\bar{\mathbf{E}}^2$, but the electric field is large only *in reference to the averaging time interval* Δt. That is:

$$|\bar{\mathbf{E}}| \gg \frac{\sqrt{\hbar c}}{(c\Delta t)^2} \tag{2.39}$$

This is the meaningful condition that establishes when an electric field can be treated classically (and a similar condition can be deduced for the magnetic field) [6].

For example, for experiments where Δt is very small, the fields are required to be very strong if they are to be considered classically. In practice, however, Δt is related to the time during which the field changes in an appreciable manner. Thus, for a static field $\Delta t \to \infty$ and the classicality condition can be satisfied by arbitrary fields. In other words, all static fields are classical fields.

On the other hand, let us assume now a time-dependent field that changes in an appreciable manner over a time interval Δt. Then, if the field is sufficiently weak, it can never be considered as a classical field and has to be described using quantum electrodynamics.

2.6 PHOTON LOCALIZATION

Non-relativistic quantum mechanics prescribes that the localization of a subatomic particle (i.e., an electron) described by the wave function $\Psi(\mathbf{x})$ is probabilistically distributed in space [40, 60]. That is, we can define a probability density for localizing the particle in the volume element d^3x as follows:

$$\rho(\mathbf{x}) \equiv |\Psi(\mathbf{x})|^2 \tag{2.40}$$

Together with the probability flux density:

$$\mathbf{j}(\mathbf{x}) \equiv -\frac{i}{2m}\left(\Psi^*(\mathbf{x})\nabla\Psi(\mathbf{x}) - \Psi(\mathbf{x})\nabla\Psi^*(\mathbf{x})\right) \tag{2.41}$$

they satisfy the continuity equation for particle localization:

$$\frac{\partial\rho(\mathbf{x})}{\partial t} + \nabla\cdot\mathbf{j}(\mathbf{x}) = 0 \tag{2.42}$$

A similar relation emerges for relativistic spin-1/2 particles described by the Dirac equation [40]:

$$j^\mu(x) \equiv -e\bar{\Psi}(x)\gamma^\mu\Psi(x) = \left(\rho, \mathbf{j}\right) \implies \partial_\mu j^\mu(x) = 0 \tag{2.43}$$

In the case of photons, however, it is *mathematically impossible* to build a current J^μ that satisfies a gauge invariant and Lorentz covariant continuity equation of the form [6]:

$$\partial_\mu J^\mu(x) = 0 \tag{2.44}$$

with a positive definite time-component (i.e., a positive definite localization probability density). Indeed, gauge invariance requires that the 4-vector electromagnetic field A^μ can only appear as the antisymmetric tensor:

$$\begin{aligned} F_{\mu\nu} &= \partial_\mu A_\nu - \partial_\nu A_\mu \\ &= -i(k_\mu A_\nu - k_\nu A_\mu) \end{aligned} \tag{2.45}$$

Therefore, the photon localization current has to be a positive definite function of the form:

$$J^\mu \propto \mathcal{F}(F^{\mu\nu}, F^*_{\mu\nu}, k_\mu) \tag{2.46}$$

However, because of the transversality condition[3]:

$$k^\alpha F_{\alpha\beta} = 0 \tag{2.47}$$

it is easy to verify that all possible combinations of $F^{\mu\nu}$, $F^*_{\mu\nu}$, and k_μ will either cancel to zero or depend explicitly on k_μ (which violates the positive definite condition).

Furthermore, the fact that the photon cannot be localized also implies that we cannot define a consistent wave function for the photon. Indeed, the wave function is defined to characterize the spatial localization of quantum particles such as electrons.

[3]This condition establishes that in an electromagnetic wave, the electromagnetic fields $\mathbf{E}$ and $\mathbf{B}$ are perpendicular to the propagation vector $\mathbf{k}$.

2.7 PHOTON DETECTION

The quantum electric field can be separated into its positive and negative frequency terms as:

$$\hat{\mathbf{E}}(\mathbf{r},t) = \hat{\mathbf{E}}^{(+)}(\mathbf{r},t) + \hat{\mathbf{E}}^{(-)}(\mathbf{r},t) \tag{2.48}$$

where:

$$\begin{aligned}
\hat{\mathbf{E}}^{(+)}(\mathbf{r},t) &= \sum_{\mathbf{k},\alpha} \mathbf{E}_{\mathbf{k}\alpha}(\mathbf{r},t)\hat{a}_{\mathbf{k}\alpha} \\
&= i \sum_{\mathbf{k},\alpha} \sqrt{2\pi\omega}\, \mathbf{e}^{\alpha}\, e^{-i(\omega t - \mathbf{k}\cdot\mathbf{r})}\, \hat{a}_{\mathbf{k}\alpha} \\
\hat{\mathbf{E}}^{(-)}(\mathbf{r},t) &= \sum_{\mathbf{k},\alpha} \mathbf{E}^{*}_{\mathbf{k}\alpha}(\mathbf{r},t)\hat{a}^{\dagger}_{\mathbf{k}\alpha} \\
&= -i \sum_{\mathbf{k},\alpha} \sqrt{2\pi\omega}\, \mathbf{e}^{\alpha *}\, e^{i(\omega t - \mathbf{k}\cdot\mathbf{r})}\, \hat{a}^{\dagger}_{\mathbf{k}\alpha}
\end{aligned} \tag{2.49}$$

Thus, $\hat{\mathbf{E}}^{(+)}(\mathbf{r},t)$ and $\hat{\mathbf{E}}^{(-)}(\mathbf{r},t)$ involve the annihilation and creation of photons, respectively.

A detector at the position $(\mathbf{r},t)$ measures a photon by destroying it (using, for instance, the photoelectric effect). Therefore, $\hat{\mathbf{E}}^{(+)}(\mathbf{r},t)$ is the only term of the quantum electric field operator that contributes to this measurement process. Furthermore, the transition amplitude of the detector signaling a photon is given by:

$$a_f(\mathbf{r},t) = \langle f|\hat{\mathbf{E}}^{(+)}(\mathbf{r},t)|i\rangle \tag{2.50}$$

where the electric field went from the initial state $|i\rangle$ to the final state $|f\rangle$ through the annihilation of a photon. The transition probability is then given by:

$$w_f(\mathbf{r},t) = |a_f(\mathbf{r},t)|^2 = \left|\langle f|\hat{\mathbf{E}}^{(+)}(\mathbf{r},t)|i\rangle\right|^2 \tag{2.51}$$

The final state of the electromagnetic field is of no interest to the measurement process, and therefore we need to sum over all the possible final states:

$$\begin{aligned}
W(\mathbf{r},t) &= \sum_{f} w_f(\mathbf{r},t) \\
&= \sum_{f} \left|\langle f|\hat{\mathbf{E}}^{(+)}(\mathbf{r},t)|i\rangle\right|^2 \\
&= \sum_{f} \langle i|\hat{\mathbf{E}}^{(-)}(\mathbf{r},t)|f\rangle \cdot \langle f|\hat{\mathbf{E}}^{(+)}(\mathbf{r},t)|i\rangle \\
&= \langle i|\hat{\mathbf{E}}^{(-)}(\mathbf{r},t) \cdot \hat{\mathbf{E}}^{(+)}(\mathbf{r},t)|i\rangle \\
&= \langle \hat{\mathbf{E}}^{(-)}(\mathbf{r},t) \cdot \hat{\mathbf{E}}^{(+)}(\mathbf{r},t)\rangle
\end{aligned} \tag{2.52}$$

where we have used the fact that the final states form a complete basis of the Hilbert space:

$$\sum_f |f\rangle\langle f| = 1 \tag{2.53}$$

Therefore, we can define the expectation value of the measured intensity as:

$$\begin{aligned} \langle \hat{I}(\mathbf{r},t)\rangle &\equiv W(\mathbf{r},t) \\ &= \langle \gamma_i |\, \hat{\mathbf{E}}^{(-)}(\mathbf{r},t)\cdot\hat{\mathbf{E}}^{(+)}(\mathbf{r},t)\,|\gamma_i\rangle \\ &= Tr\left(\rho_i\, \hat{\mathbf{E}}^{(-)}(\mathbf{r},t)\cdot\hat{\mathbf{E}}^{(+)}(\mathbf{r},t)\right) \end{aligned} \tag{2.54}$$

where the expectation value of the electric quantum field operator is taken on the initial state of the photon field $|\gamma_i\rangle$ [92], and Tr is the matrix trace operator.

Finally, it is necessary to mention that the *First Order Correlation Function* is defined as:

$$G^{(1)}(\mathbf{r}_1,\mathbf{r}_2;t_2-t_1) \equiv \langle \hat{\mathbf{E}}^{(-)}(\mathbf{r}_1,t_1)\cdot\hat{\mathbf{E}}^{(+)}(\mathbf{r}_2,t_2)\rangle \tag{2.55}$$

Then, it terms of this function the expectation value of the measured intensity is given by:

$$\langle \hat{I}(\mathbf{r},t)\rangle = G^{(1)}(\mathbf{r},\mathbf{r};0) \tag{2.56}$$

2.8 THE PHOTON WAVE FUNCTION

We can presume that the photon in question was produced by some form of atomic decay. In such a case we can use the Weisskopf-Wigner theory of spontaneous emission of photons between two atomic energy levels [13, 92]. Working in the rotating wave approximation, one can approximate the state of the emitted photon as:

$$|\gamma_0\rangle = \sum_{\mathbf{k}} g_{\mathbf{k}} \frac{e^{-i\mathbf{k}\cdot\mathbf{r}_0}}{(\nu_{\mathbf{k}}-\omega)+i\Gamma/2}|1_{\mathbf{k}}\rangle \tag{2.57}$$

where ω is the frequency difference between the atomic energy levels E_a and E_b, $\mathbf{r}_0$ is the position of the atom, Γ is the inverse of the lifetime of the excited state of the atom:

$$\Gamma \equiv \frac{1}{\tau} = \frac{1}{4\pi\epsilon_0}\frac{4\omega^3|\hat{\vec{\mu}}|^2_{ab}}{3\hbar c^3} \tag{2.58}$$

and:

$$|g_{\mathbf{k}}|^2 = \frac{\nu_{\mathbf{k}}}{2\hbar\epsilon_0 V}\,|\hat{\vec{\mu}}_{ab}\cdot\mathbf{e}_{\mathbf{k}}|^2 \tag{2.59}$$

with:

$$\hat{\vec{\mu}}_{ab} = \langle a|\hat{\vec{\mu}}|b\rangle \tag{2.60}$$

the transition amplitude of the electric dipole moment of the atom between the states a and b.

Within the theoretical framework of the Weisskopf-Wigner model is possible to give an "operational" definition of a *photon wave function* [73, 92]. Indeed, suppose we have a single photon produced by atomic spontaneous emission. For added simplicity, also assume that the electric field is polarized in the direction $\vec{\epsilon}$. Then, the first order correlation function is given by:

$$\begin{aligned} G^{(1)}(\mathbf{r},\mathbf{r};0) &= \langle\gamma_0|\,\hat{\mathbf{E}}^{(-)}(\mathbf{r},t)\cdot\hat{\mathbf{E}}^{(+)}(\mathbf{r},t)\,|\gamma_0\rangle \\ &= \langle\gamma_0|\hat{E}^{(-)}(\mathbf{r},t)\vec{\epsilon}^{\,*}\cdot\hat{E}^{(+)}(\mathbf{r},t)\vec{\epsilon}\,|\gamma_0\rangle \\ &= \langle\gamma_0|\hat{E}^{(-)}(\mathbf{r},t)\hat{E}^{(+)}(\mathbf{r},t)|\gamma_0\rangle \\ &= \langle\gamma_0|\hat{E}^{(-)}(\mathbf{r},t)\left(\sum_i|\gamma_i\rangle\langle\gamma_i|\right)\hat{E}^{(+)}(\mathbf{r},t)|\gamma_0\rangle \end{aligned} \tag{2.61}$$

where we have assumed that the photon states form a complete basis of the Hilbert space. However, because γ_0 represents a single photon state, only the vacuum contributes to this term:

$$\begin{aligned} \Longrightarrow G^{(1)}(\mathbf{r},\mathbf{r};0) &= \langle\gamma_0|\hat{E}^{(-)}(\mathbf{r},t)|0\rangle\langle 0|\hat{E}^{(+)}(\mathbf{r},t)|\gamma_0\rangle \\ &= \left|\langle 0|\hat{E}^{(+)}(\mathbf{r},t)\,|\gamma_0\rangle\right|^2 \end{aligned} \tag{2.62}$$

Furthermore, as discussed in the previous section, $G^{(1)}(\mathbf{r},\mathbf{r};0)$ is the probability of measuring a photon at the detector site. Therefore, the function:

$$\Psi_\gamma(\mathbf{r},t) \equiv \langle 0|\hat{E}^{(+)}(\mathbf{r},t)\,|\gamma_0\rangle \tag{2.63}$$

can be understood as a photon wave function[4].

If we write the quantum electric field as:

$$\hat{\mathbf{E}}^{(+)}(\mathbf{r},t) = i\sum_{\mathbf{k},\alpha}\sqrt{2\pi\omega}\,\mathbf{e}^\alpha\,e^{-i(\omega t-\mathbf{k}\cdot\mathbf{r})}\,\hat{a}_{\mathbf{k}\alpha} \tag{2.64}$$

and transform the summation into an integral, we get the spherical wave function:

$$\Psi_\gamma(\mathbf{r},t) = \frac{\mathcal{E}_0}{\Delta r}\Theta\left(t-\frac{\Delta r}{c}\right)\,e^{-(i\omega+\Gamma/2)(t-\Delta r/c)} \tag{2.65}$$

where:

$$\begin{aligned} \mathcal{E}_0 &= -\frac{\omega^2\,|\hat{\vec{\mu}}|_{ab}\,\sin\eta}{4\pi\epsilon_0\,c^2\,\Delta r} \\ \Delta r &= |\mathbf{r}-\mathbf{r}_0| \end{aligned} \tag{2.66}$$

and η is the angle between the electric dipole $\vec{\mu}$ and $\Delta\mathbf{r} = \mathbf{r}-\mathbf{r}_0$ [92]. Notice that $\mathcal{E}_0$ is independent of $\mathbf{r}$ in the far field. Indeed, $|\hat{\vec{\mu}}|_{ab}$ depends linearly on $\mathbf{r}$, canceling the dependence on $\mathbf{r}$ introduced in the denominator of the expression for $\mathcal{E}_0$.

[4]Of course, this statement is approximately true only within the context of the specific experiments discussed in this text involving quasi-monochromatic fields. Any attempt to generalize the concept of a photon wave function will ultimately lead to contradictions [73].

2.9 PROPAGATION IN ATTENUATING MEDIA

Any realistic description of a classical or quantum radar needs to account for the attenuation losses due to the atmosphere. We consider two major contributions to atmospheric attenuation: absorption and scattering [43]. Absorption is the process when the light is absorbed by the medium and its energy is dissipated as heat. On the other hand, scattering is the process when light is absorbed by the medium and re-emitted in some direction with minimal thermodynamic energy dissipation. In this section we will briefly discuss the description of attenuation in the classical and quantum realms.

2.9.1 ATTENUATION OF CLASSICAL LIGHT

In the context of classical electrodynamics, the energy flux of a parallel beam of light $\Phi(r)$ is attenuated due to absorption as:

$$\Phi(r) = \Phi(0)\, e^{-\chi_a r} \tag{2.67}$$

where χ_a is the absorption attenuation coefficient. If scattering losses are present, then the total attenuation coefficient becomes:

$$\chi_c = \chi_a + \chi_b \tag{2.68}$$

where χ_b is the scattering attenuation coefficient [91].

In the classical context, the process of absorption is well described through Maxwell equations in material media:

$$\begin{aligned}
\nabla \cdot \mathbf{D} &= 4\pi\rho && (2.69)\\
\nabla \cdot \mathbf{B} &= 0 && (2.70)\\
\nabla \times \mathbf{H} &= \frac{4\pi}{c}\mathbf{J} + \frac{1}{c}\frac{\partial \mathbf{D}}{\partial t} && (2.71)\\
\nabla \times \mathbf{E} &= -\frac{1}{c}\frac{\partial \mathbf{B}}{\partial t} && (2.72)
\end{aligned}$$

along with the constitutive equations:

$$\begin{aligned}
\mathbf{D} &= \mathbf{E} + 4\pi\mathbf{P} && (2.73)\\
\mathbf{H} &= \mathbf{B} - 4\pi\mathbf{M} && (2.74)
\end{aligned}$$

If we assume a linear response medium, then we can write:

$$\mathbf{P} = \chi_e \mathbf{E} \tag{2.75}$$

and therefore:

$$\mathbf{D} = \epsilon \mathbf{E} \tag{2.76}$$

with:

$$\epsilon = 1 + 4\pi\chi_e \tag{2.77}$$

And similarly:

$$\mathbf{B} = \mu \mathbf{H} \tag{2.78}$$

where χ_e is the electric susceptibility, ϵ is the dielectric constant, and μ the magnetic permeability of the medium [51].

Using a simple molecular model based on damped harmonic oscillators, the dynamics of a molecular electron in the presence of an electric field E are described by:

$$m\left(\ddot{x} + \gamma x + \omega_0^2 x\right) = -eE \tag{2.79}$$

where m, e, and ω_0 are the electron's mass, charge, and binding energy, respectively, and γ is the damping coefficient [51].

Using this model for an arbitrarily large number of multi-electron molecules is possible to derive the dielectric constant as:

$$\epsilon(\omega) = 1 + \frac{4\pi N e^2}{m} \sum_j \frac{f_j}{\omega_j^2 - \omega^2 - i\omega\gamma} \tag{2.80}$$

where N is the number of molecules per volume, the summation is done over the number of electrons per molecule, ω_j is the frequency of the harmonic oscillator tied to the j^{th}-electron, γ_j is the damping constant of the j^{th}-electron, ω is the frequency of the light traversing the medium, and f_i is the degeneracy of the electronic states and satisfies:

$$\sum_j f_j = Z \tag{2.81}$$

where Z is the number of electrons per molecule.

Even though this expression for the dielectric constant is accurate, we need a quantum-mechanical model to describe the dynamics of the absorbing molecules. This is necessary to accurately determine γ_j, ω_j, and f_j. Then, using Maxwell's equations we find that the absorption coefficient is given by:

$$\chi_a \propto \frac{2\omega}{c} \Im\left(\sqrt{1 + \frac{4\pi N e^2}{m} \sum_j \frac{f_j}{\omega_j^2 - \omega^2 - i\omega\gamma}}\right) \tag{2.82}$$

where $\Im$ represents the imaginary part of the argument.

The estimation of the scattering coefficient χ_b is much more difficult to do following elementary principles [91]. One is required to use the Rayleigh scattering or Mie scattering formalism, which leads to accurate but rather complex formulae [8, 51]. Furthermore, the total scattering coefficient will depend on the size, density, and distribution of the scattering centers. In most cases, one is required to search the literature for empirical values of χ_b [91].

2.9.2 ATTENUATION OF QUANTUM LIGHT

The quantization of the electromagnetic field in attenuating media is much more complicated than in vacuum [21, 49, 55, 69]. The consistent theoretical treatment of attenuating media requires the quantization of interacting electromagnetic, matter, and reservoir fields [49].

A full treatment of this problem is outside the scope of the present book, but we can say that the expressions for the quantized fields are very long and complicated. While this quantization procedure is so robust that it allows the prediction of the dielectric constant of the medium, the resulting expressions are too difficult for any analytical study, and it is very difficult to integrate phenomenological values of the attenuation constant into the theory.

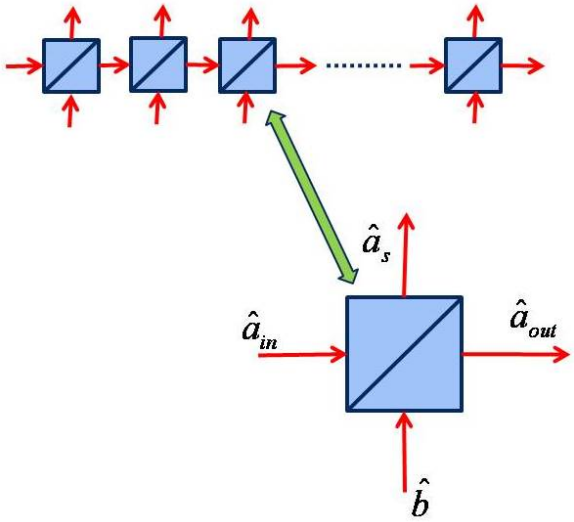

Figure 2.2: The attenuation of light (scattering + absorption) can be modeled using a chain of beam-splitters [52, 68].

However, it is possible to obtain simplified equations if one assumes that the medium is adequately described by a chain of beam splitters as shown in Figure 2.2 [52, 68]. The incident light in each beam splitter is represented by the operator $\hat{a}_{in}$. The light that is scattered or absorbed by the medium is represented by $\hat{a}_s$. Also, the possible contributions from the medium to the light field are represented by $\hat{b}$. Finally, the net output of light is described by $\hat{a}_{out}$. Then, the traversal of the chain of beam splitters modifies the annihilation quantum operator into:

$$\hat{a}(\omega) \longrightarrow e^{ikz-\chi_c(\omega)z/2}\,\hat{a}(\omega) + i\sqrt{\chi_c(\omega)}\int_0^z dx\, e^{(ik-\chi_c(\omega)/2)(z-x)}\,\hat{b}(\omega) \tag{2.83}$$

where:

$$k = \frac{\omega\,\eta(\omega)}{c} \tag{2.84}$$

and $\eta(\omega)$ is the refraction index of the medium [52, 68]. As usual, the expression for the creation operator is the Hermitian-conjugate of $\hat{a}(\omega)$.

This quantization scheme offers a simpler phenomenological theory where it is relatively easy to plug the experimental values for the attenuation coefficient χ_c. However, because of the presence of attenuation due to an external field $\hat{b}(\omega)$, the quantum light field has to be treated as an *open quantum system* [74].

As an example, let us consider a *NOON state*:

$$\begin{aligned} |NOON\rangle &= \frac{1}{\sqrt{2}}\left(|N\rangle_1|0\rangle_2 + |0\rangle_1|N\rangle_2\right) \\ &= \frac{1}{\sqrt{2}}\left(\frac{(a_1^\dagger)^N}{\sqrt{N!}}|0\rangle_1|0\rangle_2 + \frac{(a_2^\dagger)^N}{\sqrt{N!}}|0\rangle_1|0\rangle_2\right) \\ &= \frac{1}{\sqrt{2N!}}(a_1^\dagger)^N|0\rangle_1|0\rangle_2 + \frac{1}{\sqrt{2N!}}(a_2^\dagger)^N|0\rangle_1|0\rangle_2 \\ &= \frac{1}{\sqrt{2}}\left(\frac{(a_1^\dagger)^N}{\sqrt{N!}} + \frac{(a_2^\dagger)^N}{\sqrt{N!}}\right)|0\rangle_1|0\rangle_2 \end{aligned} \tag{2.85}$$

After propagating each component across distances L_1 and L_2 over two different media characterized by refraction indices η_1 and η_2, and attenuation coefficients χ_{c1} and χ_{c2}, we get:

$$\begin{aligned} |NOON\rangle' &= \frac{1}{\sqrt{2N!}}e^{-i\omega\eta_1/c-\chi_{c1}(\omega)/2)(NL_1)}\left(\hat{a}_1^\dagger\right)^N|0\rangle_1|0\rangle_2 \\ &+ \frac{1}{\sqrt{2N!}}e^{-i\omega\eta_2/c-\chi_{c2}(\omega)/2)(NL_2)}\left(\hat{a}_2^\dagger\right)^N|0\rangle_1|0\rangle_2 \\ &+ |\Phi\rangle \end{aligned} \tag{2.86}$$

where $|\Phi\rangle$ is a state that represents those states that have been scattered outside the NOON basis due to the $\hat{b}(\omega)$ contribution to $\hat{a}(\omega)$.

2.10 SUMMARY

The photon is the elementary excitation of the quantum electromagnetic field. Furthermore, the photon is a non-localizable particle; that is, it is mathematically impossible to build a continuity equation for the photon current. As a consequence, it is impossible to write down a wave equation for the photon.

In spite of these complexities, it is possible to write down expressions for the probability of photon detection as well as an approximate photon wave function for monochromatic light.

Finally, it is possible to build a quantum theory for the attenuation of light considering a chain of beam splitters. This quantization scheme produces equations where one can insert phenomenological values of the attenuation coefficient to analyze the state of attenuated photons.

CHAPTER 3

Photon Scattering

As we discussed in the previous chapter, in the large photon number limit, Quantum Electrodynamics (QED) leads to Classical Electrodynamics (CED). Indeed, the electromagnetic quantum fields $\hat{\mathbf{E}}$ and $\hat{\mathbf{B}}$ satisfy the same Maxwell equations as the classical fields $\mathbf{E}$ and $\mathbf{B}$ [90, 106]. As a consequence, those physical phenomena that are described by CED can also be described with QED.

Such is the case of specular reflections, that is, the reflection of light by a mirror. By imposing the right boundary conditions on the classical electromagnetic fields one can use Maxwell equations to derive the well known "Law of Reflections" (the incident and outgoing rays of light form equal angles with respect to the normal at the mirror surface) [8, 51]. Therefore, it is to be expected that photons, the elementary excitations of the quantum electromagnetic field, will be reflected by a mirror following a similar law.

Nevertheless, it is highly valuable to develop a description of specular reflections exclusively using QED fundamental processes of absorption and emission of photons [62]. First of all, it is an enlightening educational exercise to use the tools of Quantum Field Theory (QFT) and QED in a different context to their traditional use in high energy physics. Second, this problem makes evident the conceptual problems of interpreting the photon as an electron-like quantum particle. And equally important, the derived formulas found in this effort can be directly applied to quantum sensing. In particular, as we will see in the following chapters, a QED description of specular reflections is of fundamental importance for the understanding of Quantum Radar and Quantum Radar Cross Sections (QRCS) [61].

Unfortunately, a quantum description of specular reflections that explicitly uses fundamental QED processes is not readily available in the scientific literature. Indeed, it is not found in traditional textbooks on QFT, QED, or quantum optics, and neither in the scientific literature from recent years. A few classical optics books talk about the subject, but completely avoid all technical details [43]. And even though Richard Feynman provides an outstanding layman-level discussion to the subject matter in one of his books, he avoids fundamental QED processes in favor of a quantum path integral approach [30].

In order to overcome this deficiency, this chapter will provide a quantum description of specular reflections that exclusively uses fundamental QED processes of absorption and emission of photons[1]. Our approach is pedagogical in nature and attempts to bridge the gap between our understanding of classical and quantum physics. Clearly, this is a topic that deserves further discussion and analysis.

[1]This chapter is based on a paper written by the author [62].

3.1 PHYSICAL PROPERTIES OF THE SPECULAR REFLECTION OF LIGHT

The reflection of light by a mirror is a well understood physical phenomena [8, 43]. The *Law of Reflections* relates the incident and reflected angles of a beam of light and was first derived by Hero of Alexandria in 10-70 AD. The formal mathematical description of this phenomena was first given by Fresnel in the early 1800s using wave optics. Subsequently it was found that Fresnel's equations could be easily derived using Maxwell equations by imposing the adequate boundary conditions on the mirror's surface.

However, the Law of Reflections is not the only physical property that characterizes specular reflections. The reflection of light by a mirror is characterized by the following five fundamental physical properties [8, 43]:

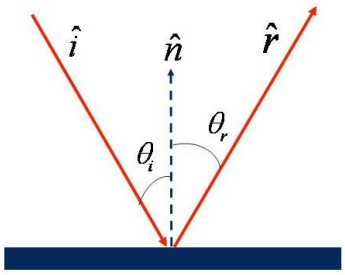

Figure 3.1: The geometry of light reflected by a mirror.

P1: The Law of Reflection. The angle of incidence θ_i is equal to the angle of reflection θ_r (see Figure 3.1).

P2: Coplanarity. The incident ray $\hat{\mathbf{i}}$, the reflected ray $\hat{\mathbf{r}}$, and the normal to the mirror $\hat{\mathbf{n}}$ are found in the same plane Π (see Figure 3.1).

P3: Fermat's Principle. The light travels on the path of least traversal time. That is, light travels over the shortest path.

P4: In/Out Frequency Invariance. The frequency of the incident light ω_i is equal to the frequency of the reflected light ω_r.

P5: Quartic Frequency Cross Section. The scattering of light by a mirror is due to Rayleigh scattering processes with a cross section $d\sigma \propto \omega^4$.

Therefore, the ultimate goal of this chapter is to adequately describe all of the above five physical properties in terms of QED fundamental processes of absorption and emission of photons.

3.2 ATOM-PHOTON SCATTERING

The physical process of interest for the present discussion is the atomic scattering of radiation of the form:

$$A_i + \gamma_i \longrightarrow A_f + \gamma_f \tag{3.1}$$

That is, an atom A_i and a photon γ_i interact with each other in a process that ultimately leads to the atom A_f and a photon γ_f in presumably different quantum states. However, conservation of energy dictates that:

$$E_i + \hbar\omega_i = E_f + \hbar\omega_f \tag{3.2}$$

where E_a refers to atomic energies and $\hbar\omega_b$ to photon energies.

Depending on the energy of the final states, there are four types of atom-photon scattering processes [16]:

- **Rayleigh Scattering:** Low-energy elastic scattering ($\omega_i = \omega_f$).
- **Raman Scattering:** Low-energy inelastic scattering ($\omega_i \neq \omega_f$).
- **Thomson Scattering:** High-energy elastic scattering ($\omega_i = \omega_f$).
- **Compton Scattering:** High-energy inelastic scattering ($\omega_i \neq \omega_f$).

In the present chapter we will assume the low energy regime. That is, we will only consider the case of low energy photons[2]. We still need to show, however, that Rayleigh Scattering is the process that characterizes specular reflections.

3.2.1 THE TRANSITION AMPLITUDE

At the lowest order in non-relativistic perturbation theory we have two possible time-ordered diagrams that contribute to the process of photon scattering by an atom (Figure 3.2)[3]:

I The atom A_i absorbs the photon γ_i transforming into the intermediate A_n state. Subsequently, the atom emits a photon γ_f and goes to the A_f state.

$$A_i + \gamma_i \longrightarrow A_n \longrightarrow A_f + \gamma_f \tag{3.3}$$

II The atom A_i emits the photon γ_f and transforms into the intermediate state A_n. Subsequently, the atom absorbs the photon γ_i and enters into the A_f state.

$$A_i + \gamma_i \longrightarrow A_n + \gamma_f + \gamma_i \longrightarrow A_f + \gamma_f \tag{3.4}$$

[2] In this context, the energy of a photon is considered low or high relative to the ionization energy of the interacting atom. For quantum radar applications, we are indeed below the ionization limit.

[3] Note, however, that in relativistic quantum field theory both time-ordered diagrams would be represented by a single Feynman diagram. It is also worth noticing that while the photon is always a relativistic particle, we have chosen the atom to be in non-relativistic kinematic states. As all the particle propagators in the relevant diagrams refer to atoms, we can use non-relativistic perturbation theory to describe the dynamics of the atom [40].

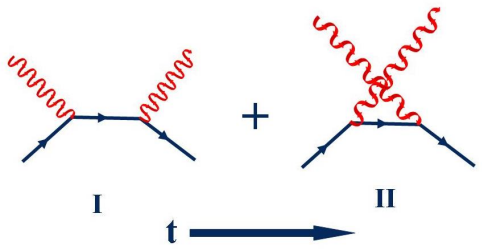

Figure 3.2: The two lowest order time-ordered diagrams in non-relativistic perturbation theory that contribute to the process of photon scattering by an atom.

The vertices of the diagrams shown in Figure 3.2 represent fundamental QED processes of absorption or emission of photons as described in Chapter 2. These vertices are described by those energy terms in the Hamiltonian that couple radiation and matter. From left to right, as seen in Figure 3.2, the four vertices in these diagrams represent:

V^a_{ni}: A_i absorbs a photon ω_i and transforms into A_n.

V^e_{fn}: A_n emits a photon ω_f and transforms into A_f.

V^e_{ni}: A_i emits a photon ω_f and transforms into A_n.

V^a_{fn}: A_n absorbs a photon ω_i and transforms into A_f.

Explicitly, in terms of atomic and photonic quantum states, these vertices are given by:

$$\begin{aligned} V^a_{ni} &= \langle A_n| \otimes \langle 0| \ \hat{V}^a \ |A_i\rangle \otimes |\omega_i\rangle \\ V^e_{fn} &= \langle A_f| \otimes \langle \omega_f| \ \hat{V}^e \ |A_n\rangle \otimes |0\rangle \\ V^e_{ni} &= \langle A_n| \otimes \langle \omega_f| \ \hat{V}^e \ |A_i\rangle \otimes |0\rangle \\ V^a_{fn} &= \langle A_f| \otimes \langle 0| \ \hat{V}^a \ |A_n\rangle \otimes |\omega_i\rangle \end{aligned} \tag{3.5}$$

where $\hat{V}^a$ and $\hat{V}^e$ are quantum operators that represent the atomic absorption and emission of a photon, respectively. And also, to simplify notation we have rewritten the initial state of the photon as:

$$|\omega_i\rangle = |1_{\mathbf{k}_i,\alpha_i}\rangle \tag{3.6}$$

with $\omega_i = |\mathbf{k}_i|$.

Therefore, non-relativistic perturbation theory prescribes the transition amplitude $\tilde{V}_{fi}$ for the atom-photon scattering process as follows [6, 60]:

$$\tilde{V}_{fi} = \sum_n \left(\frac{V^e_{fn} V^a_{ni}}{\mathcal{E}_i - \mathcal{E}^I_n} + \frac{V^a_{fn} V^e_{ni}}{\mathcal{E}_i - \mathcal{E}^{II}_n} \right) \tag{3.7}$$

where $\mathcal{E}_i$ is the initial energy, $\mathcal{E}_n^I$ is the intermediate energy for diagram I, and $\mathcal{E}_n^{II}$ is the intermediate energy for diagram II[4]. These energies are clearly given by:

$$\begin{aligned} \mathcal{E}_i &= E_i + \hbar\omega_i \\ \mathcal{E}_n^I &= E_n \\ \mathcal{E}_n^{II} &= E_n + \hbar\omega_i + \hbar\omega_f \end{aligned} \tag{3.8}$$

In minimal coupling QED, the interaction between light and matter is given by a term in the energy that couples a charged particle field with the quantum electromagnetic field [90, 106]. However, in the present case, mirrors are made of neutral atoms. The energy terms that describe how neutral atomic quantum fields interact with the electromagnetic quantum field involve the atom's electric and magnetic multipole moments [13, 73, 92]. For the case of small frequencies, all transitions can be considered in the electric dipole approximation [6, 13, 73, 92]. Then, higher atomic electric and magnetic multipole moments can be safely ignored in the present discussion.

The electric dipole $\vec{\mu}$ is defined as:

$$\vec{\mu} \equiv \sum q_i \mathbf{r}_i \tag{3.9}$$

where q_i represents the electric charge in the system with position $\mathbf{r}_i$ [51]. Clearly, $\vec{\mu}$ depends on the physical structure of the atom and may result in a very complex term. However, in our discussion it is not necessary to assume any specific form for $\vec{\mu}$.

As discussed above, the only energy term that couples the atom quantum field with the electromagnetic quantum field is given by the electric dipole coupling:

$$\hat{V} = -\hat{\vec{\mu}} \cdot \hat{\mathbf{E}} \tag{3.10}$$

where $\hat{\vec{\mu}}$ is the atom's electric dipole operator and $\hat{\mathbf{E}}$ is the electromagnetic quantum field.

The electric dipole interaction does not distinguish between absorption and emission processes. Thus, the emission and absorption couplings are exactly the same:

$$\hat{V}^a = \hat{V}^e = \hat{V} \tag{3.11}$$

In the radiation gauge we can write $\hat{\mathbf{E}}$ as:

$$\begin{aligned} \hat{\mathbf{E}} &= -\frac{\partial \hat{\mathbf{A}}}{\partial t} \\ &= \sum_{\mathbf{k},\alpha} \left(\mathbf{E}_{\mathbf{k}\alpha} \hat{a}_{\mathbf{k}\alpha} + \mathbf{E}^*_{\mathbf{k}\alpha} \hat{a}^\dagger_{\mathbf{k}\alpha} \right) \end{aligned} \tag{3.12}$$

where:

$$\begin{aligned} \mathbf{E}_{\mathbf{k}\alpha} &= i\omega \mathbf{A}_{\mathbf{k}\alpha} \\ &= i\sqrt{2\pi\omega}\ \mathbf{e}^\alpha\ e^{-i(\omega t - \mathbf{k}\cdot\mathbf{r})} \end{aligned} \tag{3.13}$$

[4]It can be shown that the energy terms in the denominator of the transition amplitude form the time-ordered description of the atom propagator in relativistic QED [40].

and therefore:

$$\begin{aligned}\hat{V} &= -\hat{\vec{\mu}}\cdot\hat{\mathbf{E}} \\ &= -\hat{\vec{\mu}}\cdot\sum_{\mathbf{k},\alpha}\left(\mathbf{E}_{\mathbf{k}\alpha}\hat{a}_{\mathbf{k}\alpha}+\mathbf{E}^{*}_{\mathbf{k}\alpha}\hat{a}^{\dagger}_{\mathbf{k}\alpha}\right) \\ &= -\hat{\vec{\mu}}\cdot i\sum_{\mathbf{k},\alpha}\sqrt{2\pi\omega}\left(\mathbf{e}^{\alpha}\,e^{-i(\omega t-\mathbf{k}\cdot\mathbf{r})}\,\hat{a}_{\mathbf{k}\alpha}-\,\mathbf{e}^{\alpha *}\,e^{i(\omega t-\mathbf{k}\cdot\mathbf{r})}\,\hat{a}^{\dagger}_{\mathbf{k}\alpha}\right) \\ &= -i\sum_{\mathbf{k},\alpha}\sqrt{2\pi\omega}\left(\hat{\vec{\mu}}\cdot\mathbf{e}^{\alpha}\,e^{-i(\omega t-\mathbf{k}\cdot\mathbf{r})}\,\hat{a}_{\mathbf{k}\alpha}-\hat{\vec{\mu}}\cdot\,\mathbf{e}^{\alpha *}\,e^{i(\omega t-\mathbf{k}\cdot\mathbf{r})}\,\hat{a}^{\dagger}_{\mathbf{k}\alpha}\right)\end{aligned} \tag{3.14}$$

Notice that in the above expression, the operator $\hat{\vec{\mu}}$ only acts on atomic states, while the operator $\hat{a}_{\mathbf{k}\alpha}$ only acts on photon states. As a consequence, they commute with each other.

For added simplicity, we can consider the case where the photon states are described by plane waves and the wavelength is larger than the size of the scattering atoms. This is the *electric dipole approximation* and implies that:

$$e^{i\mathbf{k}\cdot\mathbf{r}}\approx 1+i\frac{2\pi}{\lambda}r+\ldots\approx 1 \tag{3.15}$$

where $|\mathbf{r}|$ is consider to be of the order of the size of an atom [6, 73].

Therefore, the first transition amplitude of relevance is given by:

$$\begin{aligned}V^{a}_{ni} &= \langle A_n|\otimes\langle 0|\;\hat{V}\;|A_i\rangle\otimes|\omega_i\rangle \\ &= -i\sum_{\mathbf{k},\alpha}\sqrt{2\pi\omega}\,\langle A_n|\hat{\vec{\mu}}|A_i\rangle\cdot\mathbf{e}^{\alpha}\,e^{-i\omega t}\,\langle 0|\hat{a}_{\mathbf{k}\alpha}|\omega_i\rangle \\ &\quad +i\sum_{\mathbf{k},\alpha}\sqrt{2\pi\omega}\,\langle A_n|\hat{\vec{\mu}}|A_i\rangle\cdot\,\mathbf{e}^{\alpha *}\,e^{i\omega t}\,\langle 0|\hat{a}^{\dagger}_{\mathbf{k}\alpha}|\omega_i\rangle \\ &= -i\sqrt{2\pi\omega_i}\,\langle A_n|\hat{\vec{\mu}}|A_i\rangle\cdot\mathbf{e}^{i}\,e^{-i\omega_i t} \\ &= -i\sqrt{2\pi\omega_i}\left(\mathbf{e}^{i}\cdot\hat{\vec{\mu}}_{ni}\right)e^{-i\omega_i t}\end{aligned} \tag{3.16}$$

where we have defined:

$$\hat{\vec{\mu}}_{ab}\equiv\langle A_a|\,\hat{\vec{\mu}}\,|A_b\rangle \tag{3.17}$$

and A_a, A_b represent atomic states. Similarly, for V^{e}_{fn} we get:

$$V^{e}_{fn}=i\sqrt{2\pi\omega_f}\left(\mathbf{e}^{f *}\cdot\hat{\vec{\mu}}_{nf}\right)e^{i\omega_f t} \tag{3.18}$$

And similar expressions can be derived for V^{e}_{ni} and V^{a}_{fn}.

3.2.2 THE SCATTERING CROSS SECTION

In terms of transition amplitudes, the scattering cross section is given by [60]:

$$d\sigma=2\pi|\tilde{V}_{fi}|^{2}\frac{\omega_f^{2}\,d\Omega}{(2\pi)^{3}} \tag{3.19}$$

and therefore, for the atom-photon scattering case in consideration we have:

$$d\sigma = \left| \sum_n \left\{ \frac{(\hat{\vec{\mu}}_{fn} \cdot \mathbf{e}^{f*})(\hat{\vec{\mu}}_{ni} \cdot \mathbf{e}^{i})}{\omega_{ni} - \omega_i} + \frac{(\hat{\vec{\mu}}_{fn} \cdot \mathbf{e}^{i})(\hat{\vec{\mu}}_{ni} \cdot \mathbf{e}^{f*})}{\omega_{nf} + \omega_i} \right\} \right|^2 \frac{\omega_i \omega_f^3}{\hbar^2 c^4} d\Omega \tag{3.20}$$

where we have defined:

$$\omega_{ab} \equiv \frac{E_a - E_b}{\hbar} \tag{3.21}$$

The above equation reveals a few interesting facts. First of all, the cross section is zero if the electric dipole is orthogonal to the polarization vector of the photon. In other words, the atom cannot absorb or emit a photon in the direction of its electric dipole. This is a well known physical property of the dipole radiation approximation in classical electrodynamics [51].

Second, the scattering cross section is very small except when the frequency of the incident photon ω_i is close to one of the atomic frequencies ω_{ni}. The atomic frequencies may correspond to energy levels in atoms, for instance, but they may also encompass rotational and vibrational energy levels for the case of molecules.

3.2.3 THE SCATTERING TENSOR

It is convenient to define the *Scattering Tensor* as [6]:

$$(\mathcal{C}_{ab})_{fi} \equiv \frac{1}{\hbar} \sum_n \left\{ \frac{(\hat{\mu}_a)_{fn}(\hat{\mu}_b)_{ni}}{\omega_{ni} - \omega_i} + \frac{(\hat{\mu}_b)_{fn}(\hat{\mu}_a)_{ni}}{\omega_{nf} + \omega_i} \right\} \tag{3.22}$$

and use it to rewrite the scattering amplitude in a much simpler form:

$$d\sigma = \omega_i (\omega_i + \omega_{if})^3 \left| (\mathcal{C}_{ab})_{fi} \, (\mathbf{e}_a)^{f*} (\mathbf{e}_b)^{i} \right|^2 \frac{d\Omega}{c^4} \tag{3.23}$$

Furthermore, we can decompose the scattering tensor into scalar (0), symmetric (S), and antisymmetric (A) components:

$$\mathcal{C}_{ab} = \mathcal{C}^0 \delta_{ab} + \mathcal{C}^S_{ab} + \mathcal{C}^A_{ab} \tag{3.24}$$

which are given by:

$$\begin{aligned} \mathcal{C}^0 &= \frac{1}{3} \mathcal{C}_{aa} \\ \mathcal{C}^S_{ab} &= \frac{1}{2} (\mathcal{C}_{ab} + \mathcal{C}_{ba}) - \mathcal{C}^0 \delta_{ab} \\ \mathcal{C}^A_{ab} &= \frac{1}{2} (\mathcal{C}_{ab} - \mathcal{C}_{ba}) \end{aligned} \tag{3.25}$$

and summation over repeated indices is implied. Then, the transition amplitudes for the three components of the scattering tensor operator are given by:

$$
\begin{aligned}
(\mathcal{C}^0)_{fi} &= \frac{1}{3}\sum_n \frac{\omega_{ni}+\omega_{nf}}{(\omega_{ni}-\omega_i)(\omega_{nf}+\omega_i)}(\hat{\mu}_a)_{fn}(\hat{\mu}_a)_{ni} \\
(\mathcal{C}^S_{ab})_{fi} &= \frac{1}{2}\sum_n \frac{\left(\omega_{ni}+\omega_{nf}\right)\left((\hat{\mu}_a)_{fn}(\hat{\mu}_b)_{ni}+(\hat{\mu}_b)_{fn}(\hat{\mu}_a)_{ni}\right)}{(\omega_{ni}-\omega_i)(\omega_{nf}+\omega_i)} - (\mathcal{C}^0)_{fi}\delta_{ab} \\
(\mathcal{C}^A_{ab})_{fi} &= \frac{2\omega_i+\omega_{if}}{2}\sum_n \frac{(\hat{\mu}_a)_{fn}(\hat{\mu}_b)_{ni}-(\hat{\mu}_b)_{fn}(\hat{\mu}_a)_{ni}}{(\omega_{ni}-\omega_i)(\omega_{nf}+\omega_i)}
\end{aligned}
\tag{3.26}
$$

3.2.4 FREQUENCY INVARIANCE

Let us consider now the scattering of a photon by N identical atoms. The scattering tensor for the total system is given by the sum of the individual scattering tensors for each atom. If the atoms are close to each other, and all of them have the exact same physical properties, we can expect that the scattering tensor for each of the atoms will be the same. The only possible difference in all the terms will be due to the initial and final states taken in the transition amplitude. That is:

$$
\begin{aligned}
(\mathcal{C}_{ab})^{(Total)}_{fi} &= \sum_{j=1}^{N}(\mathcal{C}_{ab})^{(j)}_{fi} \\
&= \sum_{j=1}^{N}\langle\, \Psi^{(j)}_f \mid \mathcal{C}_{ab} \mid \Psi^{(j)}_i \,\rangle
\end{aligned}
\tag{3.27}
$$

Indeed, the wave functions for the atomic states are not the same, but they are defined within arbitrary phase factors. Thus, the initial and final states for the j^{th} atom can be written as:

$$
\begin{aligned}
\mid \Psi^{(j)}_i \,\rangle &= e^{I\phi^j_i} \mid \Psi_i \,\rangle \\
\mid \Psi^{(j)}_f \,\rangle &= e^{I\phi^j_f} \mid \Psi_f \,\rangle
\end{aligned}
\tag{3.28}
$$

Notice that, in order to avoid confusion with the indices, we use I to denote the imaginary number. The total scattering tensor now takes the following form:

$$
\begin{aligned}
(\mathcal{C}_{ab})^{(Total)}_{fi} &= \sum_{j=1}^{N} e^{I(\phi^j_i-\phi^j_f)}\langle\, \Psi_f \mid \mathcal{C}_{ab} \mid \Psi_i \,\rangle \\
&= \sum_{j=1}^{N} e^{I(\phi^j_i-\phi^j_f)}\,(\mathcal{C}_{ab})_{fi}
\end{aligned}
\tag{3.29}
$$

As a consequence, to compute the differential cross section we need to take the average over the phase factors for each atom separately [6]. However, for the case of Rayleigh scattering, not only

the energy is unchanged, but also the phases of the initial and final states are the same:

$$\phi_i^j = \phi_f^j \tag{3.30}$$

and therefore:

$$\begin{aligned} d\sigma_{Rayleigh} &\propto \left|(\mathbf{e}_a)^{f*}(\mathbf{e}_b)^i\ (\mathcal{C}_{ab})_{fi}^{(Total)}\right|^2 \\ &\propto \left|(\mathbf{e}_a)^{f*}(\mathbf{e}_b)^i \sum_{j=i}^{N} (\mathcal{C}_{ab})_{fi}^{(j)}\right|^2 \\ &\propto \left|(\mathbf{e}_a)^{f*}(\mathbf{e}_b)^i\ N\ (\mathcal{C}_{ab})_{fi}\right|^2 \\ &\propto N^2\left|(\mathbf{e}_a)^{f*}(\mathbf{e}_b)^i\ (\mathcal{C}_{ab})_{fi}\right|^2 \end{aligned} \tag{3.31}$$

On the other hand, for Raman scattering the phase factors for the initial and final states are different:

$$\phi_i^j \neq \phi_f^j \tag{3.32}$$

and:

$$\begin{aligned} d\sigma_{Raman} &\propto \left|(\mathbf{e}_a)^{f*}(\mathbf{e}_b)^i\ (\mathcal{C}_{ab})_{fi}^{(Total)}\right|^2 \\ &\propto \left|(\mathbf{e}_a)^{f*}(\mathbf{e}_b)^i \sum_{j=i}^{N} (\mathcal{C}_{ab})_{fi}^{(j)}\right|^2 \\ &\propto \left|(\mathbf{e}_a)^{f*}(\mathbf{e}_b)^i \sum_{j=1}^{N} e^{I(\phi_i^j - \phi_f^j)}\ (\mathcal{C}_{ab})_{fi}\right|^2 \\ &\propto \left|(\mathbf{e}_a)^{f*}(\mathbf{e}_b)^i\ (\mathcal{C}_{ab})_{fi}\right|^2 + \left|(\mathbf{e}_a)^{f*}(\mathbf{e}_b)^i\ (\mathcal{C}_{ab})_{fi}\right|^2 + \ldots \\ &\quad \ldots + \left|(\mathbf{e}_a)^{f*}(\mathbf{e}_b)^i\ (\mathcal{C}_{ab})_{fi}\right|^2 + \text{ crossed terms} \end{aligned} \tag{3.33}$$

However, all the crossed terms vanish at the time of taking the average over the different phases of the atoms [6]. Therefore:

$$d\sigma_{Raman} \propto N\left|(\mathbf{e}_a)^{f*}(\mathbf{e}_b)^i\ (\mathcal{C}_{ab})_{fi}\right|^2 \tag{3.34}$$

which implies that:

$$\frac{d\sigma_{Rayleigh}}{d\sigma_{Raman}} \approx N \tag{3.35}$$

As a consequence, for a large number of atoms, the contributions from Raman scattering are much smaller than those that arise from Rayleigh scattering:

$$d\sigma_{Rayleigh} \gg d\sigma_{Raman} \text{ for } N \gg 1 \tag{3.36}$$

In the case of radiation scattering, this means that the frequency of the scattered radiation is extremely likely to be the same as the one from the incident radiation. Thus, we have obtained the specular reflection property **P4** solely based on QED arguments.

3.2.5 QUARTIC FREQUENCY DEPENDENCE

In the case of Rayleigh scattering, we have that:

$$\omega_i = \omega_f = \omega \tag{3.37}$$

It is easy to verify that the components of the scattering tensor have the following ω-independent limit values in the low energy regime:

$$\begin{aligned} \lim_{\omega\to 0} (\mathcal{C}^A_{ab})_{fi} &= 0 \\ \lim_{\omega\to 0} (\mathcal{C}^S_{ab})_{fi} &\neq 0 \\ \lim_{\omega\to 0} (\mathcal{C}^0)_{fi} &\neq 0 \end{aligned} \tag{3.38}$$

That is, the scattering cross section only depends on the frequency ω through the term outside the square absolute value of Equation (3.23):

$$\lim_{\omega\to 0} d\sigma \propto \omega_i \left(\omega_i + \omega_{if}\right)^3 \tag{3.39}$$

and as a consequence:

$$\lim_{\omega\to 0} d\sigma \propto \omega^4 \tag{3.40}$$

This means that, in the low energy limit, the Rayleigh scattering has a quartic frequency dependence [6]. In other words, we have shown that the specular reflection property **P5** arises solely from QED considerations.

3.3 MIRROR-PHOTON SCATTERING

In the preceding section we discussed the scattering of light by a set of atoms. We made no assumptions as to the specific geometry of the set of atoms. However, geometric considerations are important to derive the remaining properties of specular reflections. Indeed, the geometry of the mirror relative to the incoming photon embodies the angular information required by the law of reflections.

As we will see, the geometry of the scattering system is ultimately responsible for an interference pattern at the detection point. To arrive to this conclusion we will model a specular surface as a set of scatterers and analyze the interference patterns that they produce. As such, the approach to follow is to perform an interferometric analysis similar to the one used in the description of Young's double slit experiment.

3.3.1 YOUNG'S DOUBLE SLIT EXPERIMENT

As a first step, let us consider the standard setup for Young's double slit experiment (Figure 3.3). The slits in the first screen are located at the points $\mathbf{r}_1$ and $\mathbf{r}_2$. We are interested in estimating the intensity at the measurement point $\mathbf{r}$ on the right-hand side screen at time t.

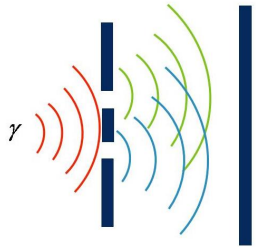

Figure 3.3: Diagramatic description of the standard setup for Young's double slit experiment.

As seen in Figure 3.3, the electromagnetic field at some point $\mathbf{r}$ in the photodetection screen has two contributions, one for each slit. The contribution from slit i is the value of the field in $\mathbf{r}_i$ propagated at the speed of light c across the distance S_i over the time t_i:

$$\hat{\mathbf{E}}_i^{(+)}(\mathbf{r}, t) = \hat{\mathbf{E}}^{(+)}(\mathbf{r}_i, t - t_i) \tag{3.41}$$

where:

$$t_i = \frac{S_i}{c} = \frac{|\mathbf{r} - \mathbf{r}_i|}{c} \tag{3.42}$$

From the classical theory of diffraction, it is know that the electromagnetic field at $(\mathbf{r}, t)$ is given by the linear superposition of both contributions. As a consequence, we have a similar expression for the quantum electromagnetic field:

$$\hat{\mathbf{E}}^{(+)}(\mathbf{r}, t) \approx K_1\, \hat{\mathbf{E}}^{(+)}(\mathbf{r}_1, t - t_1) \;+\; K_2\, \hat{\mathbf{E}}^{(+)}(\mathbf{r}_2, t - t_2) \tag{3.43}$$

where the constants K_1 and K_2 are pure imaginary numbers that depend on the specific geometry of the slits [8, 43].

As discussed in the previous chapter, the expectation value of the intensity at the measurement point is given by:

$$\begin{aligned} \langle \hat{I}(\mathbf{r}, t) \rangle &= Tr\left(\rho\, \hat{\mathbf{E}}^{(-)}(\mathbf{r}, t) \cdot \hat{\mathbf{E}}^{(+)}(\mathbf{r}, t)\right) \\ &= \langle\, \hat{\mathbf{E}}^{(-)}(\mathbf{r}, t) \cdot \hat{\mathbf{E}}^{(+)}(\mathbf{r}, t)\, \rangle \end{aligned} \tag{3.44}$$

which implies, for the case in consideration, that:

$$\begin{aligned} \langle \hat{I}(\mathbf{r}, t) \rangle &= |K_1|^2\, \langle\, \hat{\mathbf{E}}^{(-)}(\mathbf{r_1}, t - t_1) \cdot \hat{\mathbf{E}}^{(+)}(\mathbf{r_1}, t - t_1)\, \rangle \\ &+ |K_2|^2\, \langle\, \hat{\mathbf{E}}^{(-)}(\mathbf{r_2}, t - t_2) \cdot \hat{\mathbf{E}}^{(+)}(\mathbf{r_2}, t - t_2)\, \rangle \\ &+ 2\, Re\left(K_1^* K_2\, \langle\, \hat{\mathbf{E}}^{(-)}(\mathbf{r_1}, t - t_1) \cdot \hat{\mathbf{E}}^{(+)}(\mathbf{r_2}, t - t_2)\, \rangle\right) \end{aligned} \tag{3.45}$$

In terms of the first order correlation functions defined in the previous chapter, the expectation value of the intensity is given by:

$$\begin{aligned}\langle \hat{I}(\mathbf{r},t)\rangle &= |K_1|^2\, G^{(1)}(\mathbf{r}_1,\mathbf{r}_1;0) \\ &+ |K_2|^2\, G^{(1)}(\mathbf{r}_2,\mathbf{r}_2;0) \\ &+ 2\, Re\left(K_1^* K_2 G^{(1)}(\mathbf{r}_1,\mathbf{r}_2;t_1-t_2)\right)\end{aligned} \tag{3.46}$$

If we define:

$$\langle \hat{I}^{(i)}(\mathbf{r},t)\rangle \equiv |K_i|^2\, G^{(1)}(\mathbf{r}_i,\mathbf{r}_i;0) \tag{3.47}$$

and:

$$g^{(1)}(\mathbf{r}_1,\mathbf{r}_2;\tau) \equiv \frac{G^{(1)}(\mathbf{r}_1,\mathbf{r}_2;\tau)}{\sqrt{G^{(1)}(\mathbf{r}_1,\mathbf{r}_1;0)G^{(1)}(\mathbf{r}_2,\mathbf{r}_2;0)}} \tag{3.48}$$

where:

$$\tau = t_2 - t_1 \tag{3.49}$$

then we can write:

$$\begin{aligned}\langle \hat{I}(\mathbf{r},t)\rangle &= \langle \hat{I}^{(1)}(\mathbf{r},t)\rangle + \langle \hat{I}^{(2)}(\mathbf{r},t)\rangle \\ &+ 2\sqrt{\langle \hat{I}^{(1)}(\mathbf{r},t)\rangle\langle \hat{I}^{(2)}(\mathbf{r},t)\rangle}\; Re\left(g^{(1)}(\mathbf{r}_1,\mathbf{r}_2;\tau)\right)\end{aligned} \tag{3.50}$$

If we perform the polar decomposition of $g^{(1)}(\mathbf{r}_1,\mathbf{r}_2;\tau)$:

$$g^{(1)}(\mathbf{r}_1,\mathbf{r}_2;\tau) = \left|g^{(1)}(\mathbf{r}_1,\mathbf{r}_2;\tau)\right|\; e^{i(\alpha-\omega\tau)} \tag{3.51}$$

where:

$$\alpha = \alpha(\mathbf{r}_1,\mathbf{r}_2;\tau) = \arg\left(g^{(1)}(\mathbf{r}_1,\mathbf{r}_2;\tau)\right) + \omega\tau \tag{3.52}$$

and ω is the frequency of the field[5]. Then, we finally obtain:

$$\begin{aligned}\langle \hat{I}(\mathbf{r},t)\rangle &= \langle \hat{I}^{(1)}(\mathbf{r},t)\rangle + \langle \hat{I}^{(2)}(\mathbf{r},t)\rangle \\ &+ 2\sqrt{\langle \hat{I}^{(1)}(\mathbf{r},t)\rangle\langle \hat{I}^{(2)}(\mathbf{r},t)\rangle}\; \left|g^{(1)}(\mathbf{r}_1,\mathbf{r}_2;\tau)\right|\; \cos(\alpha-\omega\tau)\end{aligned} \tag{3.53}$$

The cosine of $\omega\tau$ is the term that varies rapidly along the surface of the detecting screen, producing the interference pattern [92]. Clearly, this term depends on the difference of the distance traveled by the light from each of the slits to the detection point:

$$\omega\tau = \frac{\omega}{c}(S_2 - S_1) \tag{3.54}$$

[5]This specific decomposition is taken so that α becomes a slowly varying function of its variables [92].

Therefore, we can understand S_i as a form of *interferometric distance*.

So far we have derived the observed interference pattern as a consequence of the variations in the source fields $\hat{\mathbf{E}}_1(\mathbf{r}_1, t_1)$ and $\hat{\mathbf{E}}_2(\mathbf{r}_2, t_2)$ at the detection point $(\mathbf{r}, t)$. However, Feynman's path integral formalism provides an alternative interpretation of the results. Within this theoretical framework, it is reasoned that the photon could have taken two paths to arrive to the detector point $(\mathbf{r}, t)$: it either went through $(\mathbf{r}_1, t_1)$ or through $(\mathbf{r}_2, t_2)$. The path uncertainty that the experiment cannot resolve is what ultimately causes the quantum interference in the screen [29].

3.3.2 YOUNG'S DOUBLE SCATTERER EXPERIMENT

Let us now consider Young's experiment, but we replace the slits by two scatterers as shown in Figure 3.4. To simplify the discussion, let us assume that each scatterer is a two level atom. We denote by b_i and e_i the ground and excited states of atom i, respectively. We further presume that a photon is scattered by these atoms at a time t such that:

$$-\delta \ll t \ll \delta \quad \text{and} \quad 0 < \delta \ll 1 \tag{3.55}$$

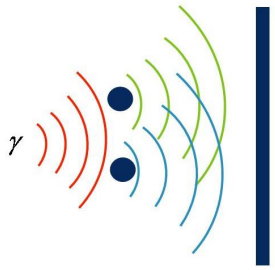

Figure 3.4: Young's interference experiment with two scattering atoms.

For this example, the process of photon scattering is extremely simple [92]. The initial system is made of a photon and two atoms in the ground state. The photon is absorbed by one of the atoms, which is sent from the ground to the excited state. Subsequently, the atom emits the photon and goes back to its ground state. The quantum states of the system before, after, and while the photon has been absorbed are given by:

$$\begin{aligned} |\Psi\rangle_{t<-\delta} &= |\gamma\rangle|b_1 b_2\rangle \\ |\Psi\rangle_{-\delta\le t\le\delta} &= \frac{1}{\sqrt{2}}|0\rangle\left(|e_1 b_2\rangle + |b_1 e_2\rangle\right) \\ |\Psi\rangle_{t>\delta} &= \frac{1}{\sqrt{2}}\left(|\gamma_1\rangle + |\gamma_2\rangle\right)|b_1 b_2\rangle \end{aligned} \tag{3.56}$$

where $\delta > 0$ is a small time interval.

We now define the photon operator $\hat{\gamma}_i^\dagger$ given by the following property:

$$|\gamma_i\rangle = \hat{\gamma}_i^\dagger |0\rangle \tag{3.57}$$

so we can write the state of the system as:

$$|\Psi\rangle_{t>\delta} = \frac{1}{\sqrt{2}} \left(\hat{\gamma}_1^\dagger + \hat{\gamma}_2^\dagger\right) |0\rangle |b_1 b_2\rangle \tag{3.58}$$

For times $t > \delta$, the expectation value of the intensity measured at the point $(\mathbf{r}, t)$ in the screen is given by (dropping the "$t > \delta$" subindex):

$$\begin{aligned}
\langle \hat{I}(\mathbf{r}, t)\rangle &= \langle \Psi | \hat{\mathbf{E}}^{(-)}(\mathbf{r}, t) \cdot \hat{\mathbf{E}}^{(+)}(\mathbf{r}, t) | \Psi \rangle \\
&= \frac{1}{2} \langle 0 | (\hat{\gamma}_1 + \hat{\gamma}_2) \hat{\mathbf{E}}^{(-)}(\mathbf{r}, t) \cdot \hat{\mathbf{E}}^{(+)}(\mathbf{r}, t) (\hat{\gamma}_1^\dagger + \hat{\gamma}_2^\dagger) | 0 \rangle \\
&= \frac{1}{2} \left| \langle 0 | \, [\hat{\mathbf{E}}^{(+)}(\mathbf{r}, t), \ \hat{\gamma}_1^\dagger] + [\hat{\mathbf{E}}^{(+)}(\mathbf{r}, t), \ \hat{\gamma}_2^\dagger] \, | 0 \rangle \right|^2 \\
&= \frac{1}{2} \left| \Psi_\gamma^{(1)}(\Delta r_1, t) + \Psi_\gamma^{(2)}(\Delta r_2, t) \right|^2 \\
&= \frac{1}{2} \left(\left| \Psi_\gamma^{(1)}(\Delta r_1, t) \right|^2 + \left| \Psi_\gamma^{(2)}(\Delta r_2, t) \right|^2 + 2Re(\Psi_\gamma^{(1)}(\Delta r_1, t) \Psi_\gamma^{*(2)}(\Delta r_2, t)) \right)
\end{aligned} \tag{3.59}$$

where we have used the photon wave function Ψ_γ as defined in the previous chapter, and also:

$$\begin{aligned}
\langle 0 | \left[\hat{E}^{(+)}(\mathbf{r}, t), \hat{\gamma}_i^\dagger \right] | 0 \rangle &= \langle 0 | \left(\hat{E}^{(+)}(\mathbf{r}, t) \ \hat{\gamma}_i^\dagger - \hat{\gamma}_i^\dagger \ \hat{E}^{(+)}(\mathbf{r}, t) \right) | 0 \rangle \\
&= \langle 0 | \hat{E}^{(+)}(\mathbf{r}, t) \ \hat{\gamma}_i^\dagger | 0 \rangle \\
&= \langle 0 | \hat{E}^{(+)}(\mathbf{r}, t) | \gamma_i \rangle \\
&= \Psi_\gamma^{(i)}(\Delta r_i, t)
\end{aligned} \tag{3.60}$$

and:

$$\Psi_\gamma^{(i)}(\Delta r_i, t) = \frac{\mathcal{E}_0}{\Delta r_i} \Theta(t - \Delta r_i / c) \, e^{-(i\omega + \Gamma/2)(t - \Delta r_i / c)} \tag{3.61}$$

with:

$$\Delta r_i = |\mathbf{r} - \mathbf{r}_i| = S_i \tag{3.62}$$

the distance from the i^{th} atom to the point $\mathbf{r}$ in the detecting screen.

As before, the cross term can be rightfully identified as the rapidly oscillating term that causes the interference phenomena:

$$2Re(\Psi_\gamma^{(1)}(\Delta r_1, t) \Psi_\gamma^{*(2)}(\Delta r_2, t)) \ \propto \ \cos\left(\frac{\omega}{c}(S_1 - S_2)\right) \tag{3.63}$$

Therefore, the photon interacts with both scattering atoms in a quantum superposition. The experiment cannot resolve the atom that scattered the photon, and such uncertainty produces the interference pattern measured in the screen. This results in the exact same interference pattern as the one seen in the double slit experiment.

3.3.3 YOUNG'S MULTIPLE SCATTERER EXPERIMENT

We can easily generalize the previous results for the case of a Young's interference experiment with N scattering atoms (Figure 3.5). The expectation value of the intensity at $(\mathbf{r}, t)$ is given by:

$$\langle \hat{I}(\mathbf{r}, t) \rangle = \frac{1}{N} \left| \sum_{i=1}^{N} \Psi_{\gamma}^{(i)}(\Delta R_i, t) \right|^2 \tag{3.64}$$

where as before:

$$\Psi_{\gamma}^{(i)}(\Delta R_i, t) = \frac{\mathcal{E}_0}{\Delta r_{id}} \Theta(t - \Delta R_i/c)\, e^{-(i\omega + \Gamma/2)(t - \Delta R_i/c)} \tag{3.65}$$

and Δr_{id} is the distance from the i^{th} atom to the point $\mathbf{r}$ in the detecting screen, and ΔR_i is the *total interferometric distance* of the experiment:

$$\begin{aligned} \Delta R_i &= \Delta r_{si} + \Delta r_{id} \\ &= |\mathbf{r}_s - \mathbf{r}_i| + |\mathbf{r}_i - \mathbf{r}_d| \end{aligned} \tag{3.66}$$

and $\mathbf{r}_s$, $\mathbf{r}_d$, and $\mathbf{r}_i$ are the positions of the source, the detecting point, and the i^{th} atom, respectively.

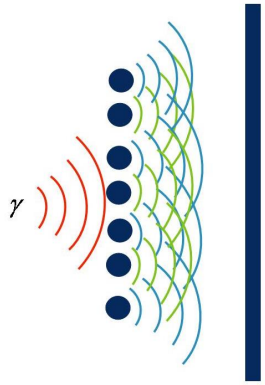

Figure 3.5: Young's interference experiment with N scattering atoms.

As before, the photon interacts simultaneously with all the atoms and the scattering is mathematically represented by a quantum superposition. The uncertainty of the specific atom that scatters the photon is what produces an interference pattern in the screen.

Notice that in this case, the photon wave functions require an extra phase factor. Indeed, for the case of two scatterers it is assumed that the photon source is symmetrically placed between the both of them. That is, it is presumed that the distance from the source to the first scatterer is the same as the distance from the source to the second scatterer. In the case of three or more scatterers, we cannot make such an assumption unless all of them are located in a circumference around the

source. The difference of distance from the source to each of the scatterers also contributes to the interference pattern. Therefore, the exponential and the step function require the extra phase factor to compensate for the right geometry of the scatterers. On the other hand, the amplitude term indicates the isotropic decay of the amplitude from its source (the scatterer) to the screen. As such, this term does not need to be corrected by the geometry of the scatterers[6].

3.3.4 SPECULAR REFLECTION AS A SCATTERING PROCESS

The preceding discussion suggests that we can describe specular reflections as a scattering process. As depicted in Figure 3.6, a light source emits a photon γ which is subsequently scattered by the N atoms that make the mirror's surface. Therefore, the detector in the right upper corner will measure an interference pattern similar to the one obtained by Young's experiment with multiple scattering atoms.

Figure 3.6: Specular reflection as a scattering process: a single photon is simultaneously scattered by all the atoms forming a quantum superposition (the shape and color of the radiated waves are for illustration purposes only, no physical meaning should be given to them).

In other words, *the incoming photon simultaneously interacts with all the atoms in the surface of the mirror*. This effect is mathematically described by a quantum superposition similar to the one used in the analysis of Young's interference experiment with multiple scattering atoms. Indeed, the photon is scattered by the atoms and the intensity of the photonic electromagnetic quantum field is measured by the detector. As in the previous examples, there is uncertainty in the actual atom that scattered the photon. Such an uncertainty ultimately leads to the interference pattern measured by the detector.

The mathematical description of specular reflection of a photon is the same as the one used in the previous subsection. We are only required to understand $\mathbf{r}_d$ as the position of the photodetector.

[6]The exact same argument holds true for the case of slits instead of scatterers.

As a consequence, for all means and purposes, the description of specular reflections boils down to a Young-type experiment with a large number of scattering centers and the photodetection screen is replaced by a photodetector on the same side as the light source. Thus, thinking about photons interacting with the atoms in a mirror as a sophisticated game of billiards is completely wrong.

Therefore, we have produced a consistent theoretical description of specular reflections solely based on fundamental QED scattering processes. That is, we have described specular reflections solely in terms of absorption and emission of photons by the mirror's constituent atoms.

3.3.5 THE CLASSICAL PATH OF THE PHOTON

The analogy with Young's scattering experiments has shown that a single photon is simultaneously scattered by all the atoms in a mirror. The scattered photon is described by a quantum superposition. The elements in the superposition correspond to the scattering events produced by each of the atoms. Uncertainty in the actual scattering event leads to quantum interference. Thus, the detector is really measuring an interference pattern similar to the one found in Young's experiments. In addition, in the previous chapter we proved that it is mathematically impossible to localize a photon. It was also mentioned that within QED and QFT it is not even possible to consider anything but the initial and final states of the system. But nevertheless, the law of reflections seems to require a very specific path for the light to travel, which appears to contradict our QED arguments.

We can reconcile both views by defining the *Classical Path of the photon*: the classical path of a photon traveling from a source to a detector is the *imaginary path* that results from demanding *maximum constructive interference* at the detection point.

Let us now calculate the classical path of the photon for a specular reflection experiment. Imagine the experimental setup shown in Figure 3.7. A single photon light source and a detector are located a distance a apart and a distance b over a mirror. Now consider only two of the many possible scattering events for a photon reflected off a mirror: the photon is scattered by the atom at $x-\delta$ and the photon is scattered by the atom at $x+\delta$. The straight lines in Figure 3.7 represent two of the many possible interferometric distances: they do not represent the paths of the photon. Indeed, as we discussed before, photon coordinates and photon paths are concepts that do not have meaning in the traditional context of QED.

As discussed in the previous sections, the intensity measured by the detector will have a rapidly varying interference term proportional to the cosine of the difference of the interferometric distances. That is:

$$\langle \hat{I}(\mathbf{r}_d) \rangle \propto \cos\left(\omega \frac{\Lambda_1 - \Lambda_2}{c}\right) \tag{3.67}$$

where $\mathbf{r}_d$ is the location of the detector and Λ_1 and Λ_2 are given by:

$$\begin{aligned} \Lambda_1 &\equiv l_1 + l_2 \\ \Lambda_2 &\equiv l_3 + l_4 \end{aligned} \tag{3.68}$$

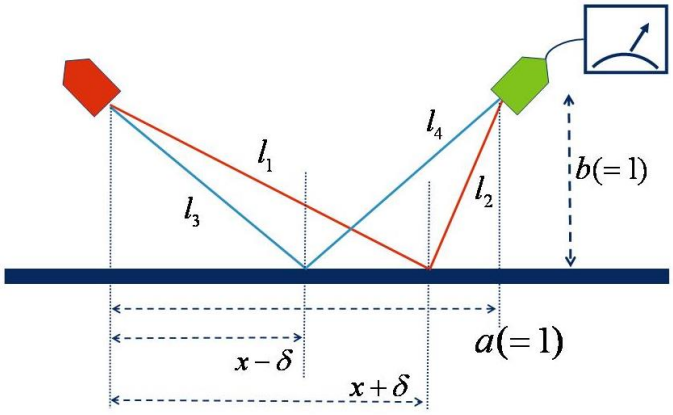

Figure 3.7: Two possible scattering events for a photon reflected off a mirror: the photon is scattered by the atom at $x-\delta$ and the photon is scattered by the atom at $x+\delta$. The straight lines represent interferometric distances and not photon paths.

and:

$$\begin{aligned} l_1^2 &= b^2+(x+\delta)^2 \\ l_2^2 &= (a-x-\delta)^2+b^2 \\ l_3^2 &= (x-\delta)^2+b^2 \\ l_4^2 &= (a-x+\delta)^2+b^2 \end{aligned} \tag{3.69}$$

Let us now assume that δ is very small, of the order of the inter-atomic distance. Then:

$$|\Lambda_1-\Lambda_2|\approx\mathcal{O}(\delta)\Rightarrow\langle\hat{I}(\mathbf{r}_d)\rangle\propto 1-\left(\frac{\omega}{c}\right)^2\tau(x) \tag{3.70}$$

where we have defined:

$$\tau(x)\equiv(\Lambda_1(x)-\Lambda_2(x))^2 \tag{3.71}$$

We need to determine the value of x which produces maximum constructive interference at $\mathbf{r}_d$. This happens when the variation of $\tau(x)$ is minimal, as this allows consecutive beams to increase the interference amplitude more rapidly. In other words, we need to find the point in the mirror for which $|d\tau/dx|$ is minimal.

Figure 3.8 shows the behavior of $\tau(x)$ and $d\tau/dx$ when $a=b=1$, and $\delta=10^{-4}$. The region for which $|d\tau/dx|$ is minimal corresponds to the region around $x\approx 0.5$:

$$\left|\frac{d\tau}{dx}\right|\approx 0\Longrightarrow x\approx\frac{1}{2} \tag{3.72}$$

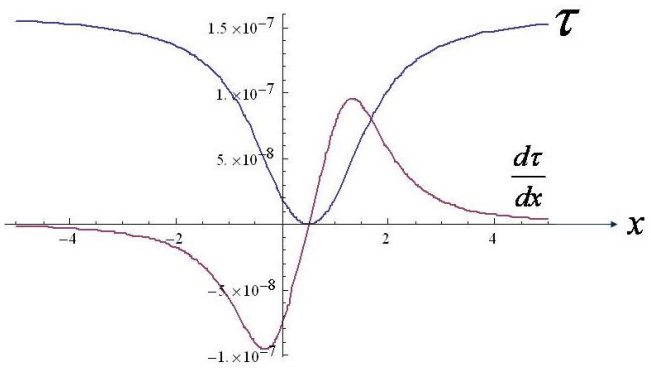

Figure 3.8: Maximum constructive interference in two photon scattering events occurs when $|d\tau/dx| \approx 0 \Rightarrow x \approx 0.5$.

Furthermore, the geometry of the experiment shown in Figure 3.7 implies that $x \approx 0.5$ is the exact same region of the mirror where:

$$\theta_i \approx \theta_r \tag{3.73}$$

Therefore, the classical path of the photon corresponds to an imaginary path where the incident and outgoing photons make equal angles with respect to the normal to the mirror. We have successfully recovered the law of reflection, specular reflections property **P1**, exclusively using quantum electrodynamical arguments involving the absorption and emission of photons[7].

While the previous example used a one-dimensional mirror, one could introduce another distance variable y orthogonal to x to represent the full two-dimensional extension of a flat mirror. In this case, the minimum of $|\nabla\tau(x, y)|$ is found in $(x, y) = (0.5, 0.0)$, which implies that the incident classical path of the photon **i**, the outgoing classical path of the photon **r**, and the normal to the mirror **n** are all contained in the same plane Π. This is specular reflections property **P2**.

Finally, it can be observed that the minimal value of $|d\tau/dx|$ is reached on a minimum of $\tau(x)$. In other words, the region $x \approx 0.5$ not only marks the region where $|d\tau/dx| \approx 0$, but it is also the region where the distance emitter-mirror-detector is minimal. Therefore, the classical path of the photon takes the path of least time. Therefore, Fermat's principle, specular reflection property **P3**, holds true.

[7] An alternative derivation requires the analysis of all the possible paths taken by the photon [30]. In the context of a path integral formulation of quantum mechanics [29], the interferometric distances can be safely interpreted as actual photon paths. Thus, Figure 7 would be showing two of the many possible paths that could have been taken by the photon. As discussed in Section 3.3.1, uncertainty about the traveled path leads to interference. Therefore, the fact that we do not know what atom scattered the photon leads to a path uncertainty and to an interference pattern in the detector.

3.4 FURTHER DEVELOPMENTS

In this final section we will address a few natural questions regarding the quantum nature of specular reflections. In particular, we will discuss why some materials are better reflectors than others, how big or how small a mirror can be, and what is the relevance of the inter-atomic distances and the number of incident photons in the specular reflection of light.

3.4.1 GOOD REFLECTORS

It is a well known fact from our daily lives that most materials will reflect light to a greater or to a lesser degree. However, metallic surfaces are often used to manufacture "good mirrors". Indeed, high quality mirrors are made by applying a reflective coating (silver), to a suitable substrate (glass). However, the substrate is only used to protect the reflective metallic coating from corrosion or any other type of physical damage. The unique physical characteristic that makes a metal an efficient reflecting material is that it has a good conduction band [8]. That is, metals have a partly empty electron energy band overlapping the valence band [3].

Let us recall that to derive the expressions for the Young's Scattering Experiments, we have assumed the scatterer to be a 2-level atom. Therefore, so far we have limited our discussion to reflecting surfaces made of atoms with only two energy levels. That is, these mirrors will only reflect light with a frequency near to the atom's resonant frequency:

$$\omega_i \approx \omega_{ab} \equiv \frac{E_a - E_b}{\hbar} \tag{3.74}$$

Therefore, so far we have described the quantum behavior of a good reflecting surface for light in the close neighborhood of ω_{ab}.

However, the scattering cross section for a photon-atom interaction given in Equation (3.20) holds for atoms with an infinite, but discrete number of energy levels ($n = 1, 2...$). We could extend these formulas to derive a Weisskopf-Wigner model for these types of atoms. The result would be a quantum description of a mirror that is a good reflector for light in the near neighborhood of the resonant frequencies ω_n. As a next step one could extend this model to the continuum of energies to represent the conductivity band of metals. Therefore, the conductivity band of a metal is ultimately responsible for the material to be a good reflector over a wide range of frequencies.

Furthermore, let us recall that the penetration distance d of an electromagnetic wave of frequency ω incident on a metallic object is given by:

$$d \approx \frac{c}{\sqrt{8\pi\,\mu\sigma\,\omega}} \tag{3.75}$$

where σ is the conductivity and μ the magnetic permeability of the material [8]. On the other hand, the reflectance of the material is:

$$\mathcal{R} \approx 1 - 2\sqrt{\frac{\omega}{2\pi\ \sigma}} \tag{3.76}$$

in the large σ regime [8]. Then, for a perfect conductor:

$$\begin{aligned} \lim_{\sigma \to \infty} d &= 0 \\ \lim_{\sigma \to \infty} \mathcal{R} &= 1 \end{aligned} \tag{3.77}$$

That is, a strong absorber is also a strong reflector [8]. In this situation, the incident photon is very likely to be absorbed and re-emitted by the atoms near the surface of the mirror. Very few atoms interact with the photon, even though they are strong absorbers. As a consequence, little energy is dissipated by the atoms and most of the energy reappears in the reflected light. Thus, for metallic surfaces which are good conductors, there is no need to look at the interferometric pattern on the "other side" of the mirror.

In addition, it is also important for a good mirror to be perfectly flat. Otherwise, the light will be reflected in many directions, creating the effect of diffuse light. In this case, the law of reflections is only valid on an infinitesimally small portion of the surface.

3.4.2 THE SIZE OF THE MIRROR

Let us consider the same setup as the one shown in Figure 3.7. What is the minimum size of the mirror so we can obtain the law of reflections? If the mirror is much smaller than λ_i, the wavelength of the incident photon, then a large portion of the incident light will be diffracted. The equations that describe the quantum nature of diffraction are exactly the same as the ones used in our discussion for reflections. However, in this situation we will not obtain the law of reflections because there is not an unique observation point characterized by maximum constructive interference [61].

A similar question comes to mind: how big can the mirror be to reflect a single photon? As previously discussed, the photon may interact with all the atoms that form an object forming a quantum superposition. The size of this range will depend on the optical aperture of the photon source. Thus, in principle, there is no upper bound on the size of the mirror.

3.4.3 INTER-ATOMIC DISTANCES

In the previous subsection we considered the overall size of the mirror. Here we will consider the inter-atomic distances between the atoms that make the reflective material. Let us consider first the case where the inter-atomic distance is larger than λ_i, the wavelength of the incident photon. In this situation, the light will be diffracted by each atom and the constructive interference on a privileged direction will be greatly reduced [61]. Such a phenomena is known as a *diffraction grating* and can be observed when looking at the surface of a CD or DVD from a low angle (the spiral grooves that encode the information form a diffraction grating) [43].

On the other hand, there is no lower limit to the size of the inter-atomic distances, and these can be as small as necessary (up to the limits imposed by the physical model of QED).

3.4.4 NUMBER OF PHOTONS

In the previous section we described how a single photon gets reflected off a mirror due to scattering processes. The law of reflections is recovered by considering the classical path of the photon, which is the imaginary line where the constructive interference is maximal. Of course, the interference pattern is not made of a discrete set of values, and the intensity has a natural width that goes from some minimal to maximal values.

In the case of two photons, the same ideas apply. However, it can be shown that in this case the width of the intensity is narrower [61]. As we continue to increase the number of photons, the intensity band becomes narrower and narrower, until it becomes very close to a thin straight line[8]. This is not surprising: as the number of photons increases, we approach the classical limit. In the limit of an infinitely large number of photons, the photons form well-defined rays of light that are reflected on a single direction. That is, the intensity of the field outside the established classical path of the photon goes to zero very rapidly.

3.5 SUMMARY

We have shown that all five physical properties that describe the specular reflection of light by a mirror can be deduced using only quantum electrodynamics and interferometric arguments. That is, the processes of emission and absorption of photons by atoms ultimately leads to the law of reflection, coplanarity, the Fermat Principle, frequency invariance between incident and outgoing radiation, and a quartic frequency dependence of the scattering cross section.

And no less important, the resulting equations are useful for some applications in quantum optics. For instance, as we will see in the following chapters, we can use these results towards the development of strategies and procedures to define and estimate quantum radar cross sections [61].

[8] We will discuss this behavior in Chapter 6.

CHAPTER 4

Classical Radar Theory

In this chapter we will discuss the theory behind the operation of a classical radar. We will derive the radar equation and discuss at some length the radar cross sections that characterize spherical and flat rectangular targets. As this is a classical system, we have to assume that the number of photons is very large, and as a consequence, classical radar can be perfectly described by Maxwell's equations without recurring to quantum theory.

4.1 THE RADAR EQUATION

Figure 4.1 describes the conceptual operation of a monostatic radar system[1]. A transmitter sends an electromagnetic pulse towards an airborne target located at a distance R. The power and gain of the transmitter are denoted by P_t and G_t, respectively. The target partially reflects the electromagnetic pulse back to the receiver. The power and aperture of the receiver are P_r and A_r, respectively. The pulse takes Δt from the moment it was transmitted to the moment its reflection is received.

From the knowledge of Δt it is possible to estimate the range to the target as:

$$R = c\frac{\Delta t}{2} \tag{4.1}$$

where c is the speed of light. However, this equation does not express how weak or how strong the measured signal will be.

The strength of the received radar signal is determined through *the radar equation* [31, 59, 95, 96]. It can be easily derived through an energetic analysis: if the outgoing power at the radar is $P_t G_t$, then the incident power density at the target is:

$$W_{i@T} = P_t G_t \times \frac{F^2}{4\pi R^2} \tag{4.2}$$

where $F \in [0, 1]$ is a form factor that measures the transparency of the space between the radar and the target. If this space is perfectly transparent to the radar pulse then $F = 1$, and if it is perfectly opaque then $F = 0$. For atmospheric attenuation due to fog and clouds, for instance, we can write F as:

$$F = e^{-\chi_c R/2} \tag{4.3}$$

where χ_c is the attenuation coefficient due to absorption and scattering.

[1] In a *monostatic radar*, the transmitter and the receiver are located in the same place. In a *bistatic radar*, the transmitter and the receiver are in different locations. In what follows, we will concentrate our discussion on monostatic radars.

Figure 4.1: Basic operation of a monostatic classical radar. An electromagnetic pulse is sent by the radar transmitter towards the target. The reflected pulse is measured by the radar receiver.

The $1/4\pi R^2$ term is the well known decrease of transmitted power of a spherical wave at a distance R from the source. We assume that the transmitter is isotropic and radiates uniformly in all directions. Thus, the radiated density in a sphere of radius R is given by the radiated power divided by the surface area ($4\pi R^2$).

Now let us assume that only a portion of this energy is scattered. Then, the scattered power at the target is:

$$P_{s@T} = W_{i@T} \times \sigma \tag{4.4}$$

where σ is called *the radar cross section* and will be discussed in detail in the following sections. Going back to our analysis, the scattered power density at the receiver is:

$$W_{s@r} = P_{s@T} \times \frac{F^2}{4\pi R^2} = \frac{P_t G_t \sigma F^4}{(4\pi)^2 R^4} \tag{4.5}$$

And finally, the scattered power at the receiver is:

$$P_r = P_{s@r} = W_{s@r} A_r \tag{4.6}$$

As a consequence, the radar equation is given by:

$$P_r = \frac{P_t G_t A_r \sigma F^4}{(4\pi)^2 R^4} \tag{4.7}$$

and it is the most fundamental equation in classical radar theory.

4.2 MAXIMUM DETECTION RANGE

The radar detector is sensitive to thermal noise [53, 95, 96]. The total amount of thermal power N_T can be written as:

$$N_T = k_B T_e B \tag{4.8}$$

where k_B is Boltzman constant, T_e is the "effective temperature", and B is the bandwidth of the receiver.

The signal-to-noise ratio (SNR) is given by:

$$\begin{aligned} SNR &= \frac{P_r}{N_T} \\ &= \frac{P_t G_t A_r \sigma F^4}{(4\pi)^2 R^4 k_B T_e B} \end{aligned} \tag{4.9}$$

Now, the aperture area A_r of the receiver can be written in terms of a "receiver gain" G_r as:

$$G_r = \frac{4\pi A_r}{\lambda^2} \tag{4.10}$$

and the SNR equation looks like:

$$SNR = \frac{P_t G_t G_r \lambda^2 \sigma F^4}{(4\pi)^3 R^4 k_B T_e B} \tag{4.11}$$

Clearly, there is a minimum value of SNR that allows the detection of a signal. This imposes a limit for the detection range of the radar system:

$$R_{max} \approx \left(\frac{P_t G_t G_r \lambda^2 \sigma F^4}{(4\pi)^3 k_B T_e B \;\; SNR_{min}} \right)^{1/4} \tag{4.12}$$

where in practice, SNR_{min} is in the order of 10 to 20 decibels [53].

4.3 RADAR JAMMING

Electronic countermeasures are often used in the modern battlefield to defeat the radar systems of the enemy [53, 80, 103]. There are passive and active countermeasures. The first kind involves the deployment of artificial clutter or chaff, which has a large return that hides the echo produced by the weapons systems. The second kind is jamming, which is an active countermeasure. This technique involves the active injection of noise to the enemy's radar.

The effectiveness of the jamming system can be described mathematically through the *jamming equation*. Let us assume the radar, target, and jammer system shown in Figure 4.2. The target is characterized by its radar cross section σ. The jammer emits electromagnetic waves with power P_j and gain G_j. The radar transmitter has power P_t and gain G_t. Finally, the radar receiver has a gain G_r that in general depends on the angular variables θ and ϕ.

Using similar expressions to the ones used to derive the radar equation, we have that the radar receives a jamming signal of power $P_r^{(j)}$ given by:

$$\begin{aligned} P_r^{(j)} &= W_{j@r} \, A_r \\ &= \left(\frac{P_j G_j}{4\pi R_j^2} \right) \times \left(\frac{\lambda^2 G_r(\theta_j, \phi_j)}{4\pi} \right) \end{aligned} \tag{4.13}$$

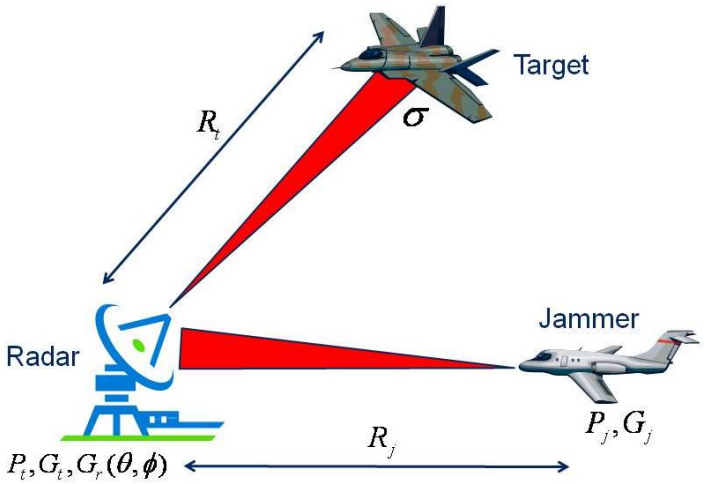

Figure 4.2: Jamming as an active radar countermeasure.

On the other hand, the target signal power is given by the radar equation:

$$P_r^{(t)} = \frac{P_t G_t \; G_r(\theta_t, \phi_t) \; \lambda^2 \sigma}{(4\pi)^3 R_t^4} \tag{4.14}$$

We can use these last two expressions to define a *signal-to-jam ratio* (SJR) as:

$$\begin{aligned} SJR &= \frac{P_r^{(t)}}{P_r^{(j)}} \\ &= \left(\frac{P_t G_t}{P_j G_j}\right) \times \left(\frac{R_j^2}{R_t^4}\right) \times \left(\frac{\sigma}{4\pi}\right) \times \left(\frac{G_r(\theta_t, \phi_t)}{G_r(\theta_j, \phi_j)}\right) \end{aligned} \tag{4.15}$$

The *burnthrough range* happens when SJR$\approx$ 1 and indicates when the jamming signal is able to mask the target's return. That is, the target will be hidden in the electric noise injected by the jammer when:

$$SJR < 1 \tag{4.16}$$

Finally, let us note that in general:

$$R_j \approx R_t \Longrightarrow \frac{R_j^2}{R_t^4} \ll 1 \tag{4.17}$$

which is a benefit for the jammer. But on the other hand, for directional radars pointing directly to the target:

$$G_r(\theta_t, \phi_t) \gg G_r(\theta_j, \phi_j) \Longrightarrow \frac{G_r(\theta_t, \phi_t)}{G_r(\theta_j, \phi_j)} \gg 1 \tag{4.18}$$

which gives an advantage to the radar system.

4.4 THE RADAR CROSS SECTION

The radar equation implies that the radar cross section σ is defined by:

$$\sigma = \frac{P_{s@T}}{W_{i@T}} \tag{4.19}$$

As already mentioned, σ represents the fraction of the incident power density that is reflected back to the receiver. As such, σ is a good measure of the "radar visibility" of the target. Indeed, the larger the value of σ for a given target, the easier it is to detect it. Similarly, a stealth vehicle is the one with a low σ.

An equivalent expression for σ is given by:

$$\sigma = \frac{4\pi R^2}{F^2} \times \frac{P_{s@T}}{P_t G_t} \tag{4.20}$$

This expression makes clear the fact that σ has units of area. A common interpretation of σ is the hypothetical area of a flat object required to reflect the same fraction of the incident power as the target in question. Note, however, that σ does not correspond to the projected area of the target, but depends on other factors as well.

A far more formal definition of the classical radar cross section is given by:

$$\sigma \equiv \lim_{R\to\infty} 4\pi R^2 \frac{|\mathbf{E}_{s@r}|^2}{|\mathbf{E}_{i@T}|^2} \tag{4.21}$$

where $\mathbf{E}_{i@T}$ is the incident electric field *at the target*, while $\mathbf{E}_{s@r}$ is the scattered electric field as measured *at the receiver* [53, 56].

Some important properties of σ include:

Strong Dependencies: It can be proved that σ strongly depends on the properties of the target. That is, it depends on the target's geometry (absolute and relative size, shape, and orientation), as well as its composition (material properties).

Weak Dependencies: It can be proved that σ is approximately independent on the properties of the radar system. That is, it depends very weakly on the strength and the position of the radar system. In particular, σ is independent of R, the range to the target[2].

As a consequence, it is clear that σ is a property that (approximately) characterizes a specific target, and not the radar system and/or its interaction with the target. Thus, σ emerges as a critical

[2]Even though there is an explicit R^2 term in the definition of σ, $|\mathbf{E}_{s@r}|^2$ depends implicitly on $1/R^2$. Indeed, $|\mathbf{E}_{s@r}|^2$ is the electromagnetic energy as measured at the receiver, which has decayed by the isotropic $F^2/4\pi R^2$ factor from its value at the target.

concept for the design of stealth vehicles [53, 56, 70]. In this case, the simulation of σ for the proposed design of a vehicle will provide a good estimate of its "radar invisibility". In addition, σ is also important to characterize the operational performance and capabilities of radar systems. That is, given a radar system, what is the minimum σ of a target that it can detect.

4.5 SCATTERING REGIMES

Depending on the value of the ratio of the characteristic size of the target a and the wavelength of the radar λ, three scattering regimes characterize the operation of radar [53, 56, 95, 96].

Rayleigh Regime ($a \ll \lambda$): This is the low-frequency case, and the incident electromagnetic wave shows little phase variation over the physical extent of the target. That is, at each instant of time, each portion of the target is affected by nearly the same electromagnetic field. In a sense, at each moment of time the electromagnetic field is approximately constant over the entire physical extension of the target. Then, the incident electromagnetic wave induces dipole moments which only depend on the size and orientation of the target.

Resonant Regime ($a \approx \lambda$): In this case, the phase of the incident electromagnetic field changes along the length of the target. This means that some of the energy of the electromagnetic field is "attached" to the target's surface, creating surface waves that travel over the spatial extent of the target.

Optical Regime ($a \gg \lambda$): In the high-frequency case, collective interactions are minimal and the body can be considered made of a collection of independent scattering centers. The total electromagnetic scattered field is the superposition of all the individual scattered fields. As a consequence, the geometry of the target plays a dominant role on the structure of the scattered fields.

4.6 THE RADAR X-BAND

The radar region includes the range of frequencies between 3 MHz and 300 GHz. In terms of λ, this region goes from 1 mm to about 100 m. The applications of radar of most interest, at least from a military perspective, are towards the detection and tracking of weapon systems and platforms such as missiles and aircrafts. These targets are usually large, ranging from one to a few dozen meters. The radar frequencies typically used for missile guidance as well as weather, aircraft, and ground surveillance belong to the X-band and range from 8-12 GHz (wavelengths between 2.5 and 3.75 cm) [95, 96]. For example, airport radar is usually found at 10.525 GHz. This range of frequencies is usually known as the Radar X-band because of its classified origins during World War II [85].

Then, for applications of interest, the characteristic size of the target a is much larger than the wavelength of a radar λ_X operating inside the X-band:

$$a \gg \lambda_X \tag{4.22}$$

and therefore, these radar systems operate in the optical regime.

4.7 SCATTERING MECHANISMS

Targets of interest, such as missiles or aircraft, are usually complex geometrical objects with inhomogeneous electric properties. Therefore, the specular reflection of an electromagnetic wave is only one of many possible scattering mechanisms that contribute to the accurate computation of the radar cross section.

Figure 4.3 shows some of the scattering mechanisms that play a role in the determination of σ for a hypothetical air vehicle [53, 56]. These include specular reflections, creeping and surface waves, as well as edge and corner diffraction. The complexity of the target also involves returns due to the bouncing of the electromagnetic waves inside cavities or around the shape of the vehicle (interaction echo). In addition, there are contributions produced by geometric discontinuities, such as changes in the curvature of the surfaces, as well as seam and surface discontinuities due to the physical ensemble of the airframe.

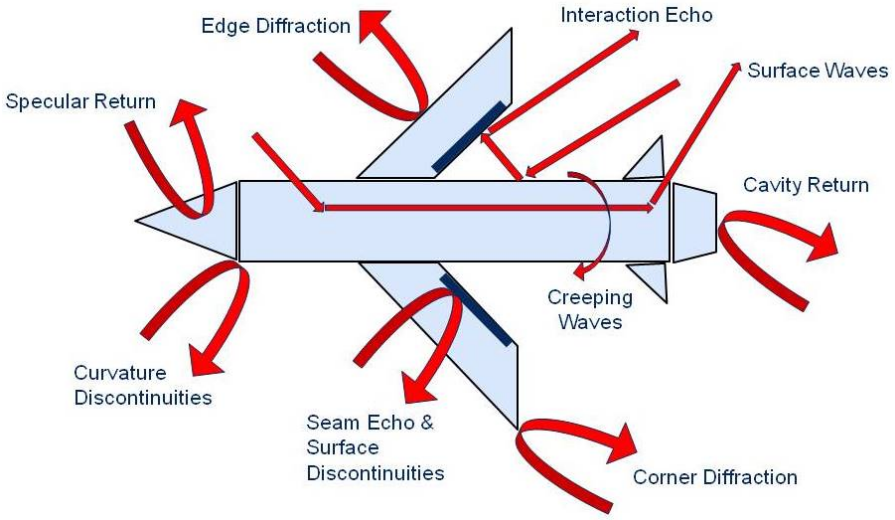

Figure 4.3: Principal scattering mechanisms for a hypothetical air vehicle [53, 56].

The most important contributions to the radar cross section for a smooth, continuous, and convex target are:

Specular Reflections: This is the mirror-like reflection of the radar pulse. This contribution follows the "Law of Reflections", that is, the incident and outgoing radiation form the same angle with respect to the normal of the surface.

End-Region Returns: This contribution is due to the finite size of targets, which often causes current discontinuities in the end regions of the body. The result is a sidelobe structure that contributes to the scattering away from the specular direction.

Absorption Effects: Depending on its composition and constitutive properties, the target may be able to absorb and dissipate a portion of the incident electromagnetic energy.

Diffraction Effects: Mostly due to tips, edges, and other discontinuities in the target's body.

In what follows, we will consistently ignore absorption and diffraction effects from all of our discussions, restricting ourselves to specular and end region returns.

4.8 SPECULAR AND END-REGION RETURNS

When an electromagnetic wave impacts a target, electric currents are formed on the surface of the body. In turn, these currents radiate electromagnetic energy that contributes to the scattered field. However, in practice, the currents that travel the target are unknown and are difficult to estimate due to the complexity of the body's geometry and composition.

The *physical optics approximation* can be used to simplify the computation of radar cross sections [53, 56]. This approximation provides good results as long as the interaction takes place in the optical regime; that is, the target is an electrically large body. In addition, this approximation breaks down as we increase the viewing angle away from the specular direction. As shown in Figure 4.4, using *geometric optics* we can assume that the current on the shadowed side of the target is zero, while it is nonzero in the illuminated portion. We have also assumed an incident plane electromagnetic wave.

The orthogonal area projection $A_\perp$ is the area of the shadow created by the target in a plane perpendicular to the wave vector of the incident radiation.

The current in the illuminated region of the target can be approximated as:

$$\mathbf{J} \approx 2\hat{\mathbf{n}} \times \mathbf{H}_i \tag{4.23}$$

where $\mathbf{H}_i$ is the incident magnetic field and $\hat{\mathbf{n}}$ is a surface normal [53].

The radiated field can be calculated using this current and the *Stratton-Chu Radiation Integrals*:

$$\begin{aligned} E_\theta(x, y, z) &= \frac{-ik\eta}{4\pi r} e^{-ikr} \int\int\int_V \mathbf{J} \cdot \hat{\theta}\, e^{ik\mathbf{r}'\cdot\hat{\mathbf{r}}} dV' \\ E_\phi(x, y, z) &= \frac{-ik\eta}{4\pi r} e^{-ikr} \int\int\int_V \mathbf{J} \cdot \hat{\phi}\, e^{ik\mathbf{r}'\cdot\hat{\mathbf{r}}} dV' \end{aligned} \tag{4.24}$$

where η is the field's impedance [53, 56]. Assuming a TEM (Transverse-Electro-Magnetic) wave, the electric and magnetic fields are related by:

$$\mathbf{H}(x, y, z) \approx \frac{\hat{\mathbf{r}} \times \mathbf{E}(x, y, z)}{\eta} \tag{4.25}$$

where it is understood that in the far-zone the radial component of the field is approximately zero.

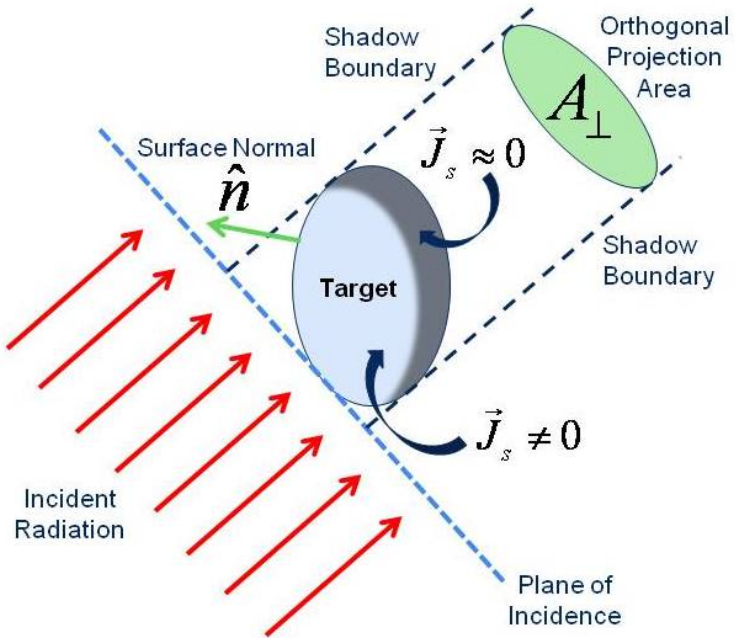

Figure 4.4: Interaction of a plane electromagnetic wave with a target in the physical optics approximation: using geometric optics we determine that the current in the shadowed area is zero, and non-zero in the illuminated portion of the body [53].

4.8.1 SPHERICAL TARGET

As a first example, let us consider a monostatic radar illuminating a spherical target of radius a as shown in Figure 4.5. The current created by an incident wave of amplitude H_0 and momentum k is:

$$\mathbf{J}_s = 2H_0 e^{-ik\Delta}(\hat{\mathbf{y}}w - \hat{\mathbf{z}}v) \tag{4.26}$$

where:

$$\begin{aligned} v &= \sin\theta \sin\phi \\ w &= \cos\theta \\ \Delta &= a(1-w) \end{aligned} \tag{4.27}$$

using the angles from standard spherical coordinates θ and ϕ [53].

Using the radiation integrals we can express the scattered electric field as:

$$\begin{aligned} \mathbf{E} &= \frac{-ik\eta H_0}{2\pi r} e^{-ikr} \int_0^{2\pi} \int_0^{\pi/2} (\hat{y}w - \hat{z}v) e^{-i2k\Delta} a^2 \sin\theta' d\theta' d\phi' \\ &= \frac{-i\eta H_0 a}{2r} e^{-ik(r+2a)} \hat{y} \left(1 - \frac{\sin(ka)}{ka}\right) \end{aligned} \tag{4.28}$$

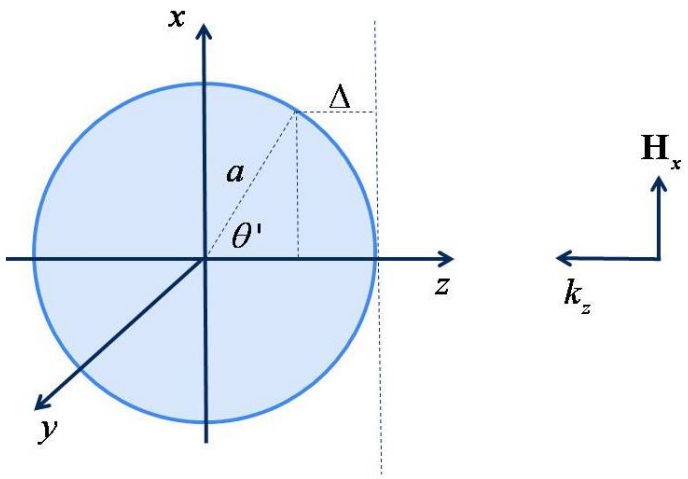

Figure 4.5: Geometry of a spherical target and an incident electromagnetic wave.

and therefore, the radar cross section is given by:

$$\sigma = \pi a^2 \left(1 - \frac{\sin(ka)}{ka}\right) \tag{4.29}$$

which clearly manifests a spherical symmetry (functionally independent of the angular variables θ and ϕ) [53].

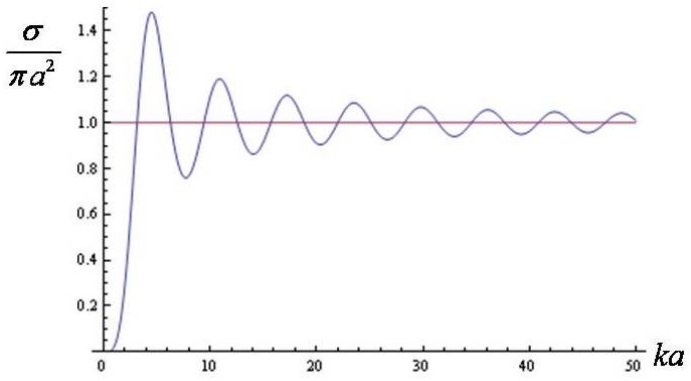

Figure 4.6: Radar cross section σ for a sphere of radius a and wave-vector k.

The dependence of σ on ka is shown in Figure 4.6. Two different regimes are observed. The low-frequency *Rayleigh Regime* for which:

$$ka \ll 1 \Rightarrow \sigma \approx \pi a^2 \frac{(ka)^4}{36} \propto \omega^4 \tag{4.30}$$

and the high-frequency *Optical Regime*:

$$ka \gg 1 \Rightarrow \sigma \approx \pi a^2 = A_\perp \tag{4.31}$$

Notice that in this regime, σ is equal to the projected area of the target $A_\perp$. This is a specific result for spherical bodies, and in general, for other geometric objects, this relation will not be true.

However, it is important to state that the Rayleigh regime solution is only an approximation, as we have used physical optics methods to derive σ. An exact solution involves a more sophisticated technique known as *Mie Theory* [8].

Furthermore, in the limit of the optical regime:

$$\lim_{\lambda \to 0} \sigma = \pi a^2 = A_\perp \tag{4.32}$$

which is independent of λ.

4.8.2 RECTANGULAR TARGET

Let us now consider a flat rectangular plate of size $A = a \times b$ as the one shown in Figure 4.7. If we only consider specular returns, then the radar cross section is zero everywhere except for $\theta = 0$. Therefore, avoiding specular reflections for the design of stealth vehicles simply requires that all surfaces should never be perpendicular to the propagation vector of the incoming radar pulse [70]. This is one of the reasons why the first stealth aircraft, the Lockheed Martin F117, resembles a diamond made of flat plates [86]. This design avoids specular returns in case an enemy ground radar is positioned in the forward direction.

Unfortunately, such a simple behavior of the radar cross section is correct only if the plate is of infinite size. Indeed, the finite size of the target introduces end-region returns. Let us consider an incident electromagnetic wave that generates a current in the surface of the target, as shown in Figure 4.7. Because the plate is a finite body, the current is discontinuous: the current is non-zero on the illuminated surface of the target, but it is zero on the dark side of the plate. Such a discontinuity is responsible for a contribution to the electromagnetic field that is radiated in all directions.

We can use the physical optics approximation and the Stratton-Chu radiation integrals to quantify the effect of the end-region returns on the radar cross section of the rectangular target [53]. First we assume an incident θ-polarized plane electromagnetic wave arriving from an angle (θ, ϕ):

$$\mathbf{E}_i = E_{0\theta}\, \hat{\theta}\, e^{-i\mathbf{k}_i \cdot \mathbf{r}} \tag{4.33}$$

If the plate is uniform and isotropic, the surface current $\mathbf{j}_s$ will be given by:

$$\mathbf{j}_s \approx -2\, \hat{\mathbf{z}} \times E_{0\theta}\, \hat{\phi}\, \frac{e^{-i\mathbf{k}_i \cdot \mathbf{r}}}{\eta} \tag{4.34}$$

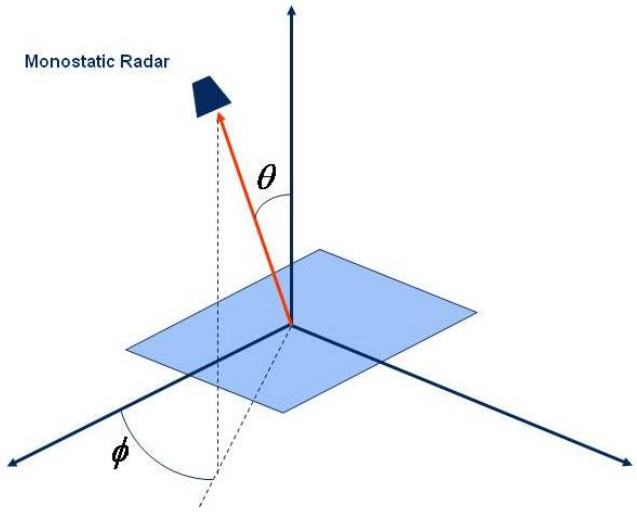

Figure 4.7: Sensor-target geometry for a rectangular 2D target.

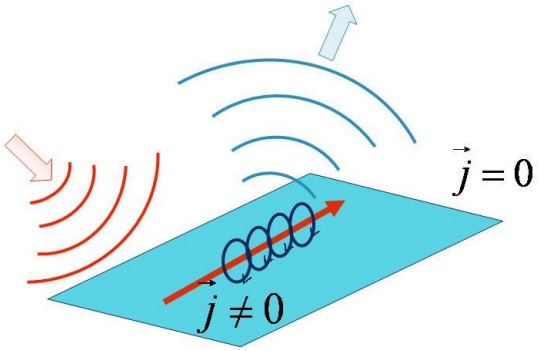

Figure 4.8: End-Region returns contribute to the σ_C. These returns are attributed to the current discontinuities due to the finite size of the target.

The far-zone scattered field will be given by:

$$E_\theta(r,\theta,\phi) = \frac{ik}{2\pi r}\, e^{-jkr}\, E_{0\theta}\, ab\, \cos\theta\, \frac{\sin kau}{kau}\, \frac{\sin kbv}{kbv} \tag{4.35}$$

where:

$$\begin{aligned} u &= \sin\theta\cos\phi \\ v &= \sin\theta\sin\phi \end{aligned} \tag{4.36}$$

and the radar cross section σ is calculated to be:

$$\sigma(\theta,\phi) = \frac{4\pi A^2}{\lambda^2}\cos^2\theta\left(\frac{\sin kau}{kau}\right)^2\left(\frac{\sin kbv}{kbv}\right)^2 \tag{4.37}$$

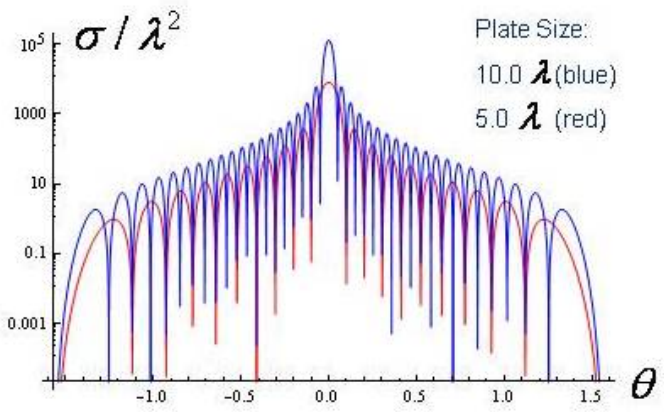

Figure 4.9: Simulation of σ_C vs. θ ($\phi = 0$) for a 2D flat rectangular plate. The highest value of σ_C is reached when the target is oriented in the specular direction ($\theta = 0$). The sidelobe structure is entirely due to end-region returns. Diffraction and absorption effects have been ignored.

Figure 4.9 shows the plot of σ/λ^2 for $\phi = 0$ and two plates of size ($a = 10\lambda, b = 10\lambda$) and ($a = 5\lambda, b = 5\lambda$). In both cases, the highest peak is found at $\theta = 0$ and corresponds to the return due to specular reflection:

$$\sigma(0,0) = \frac{4\pi A^2}{\lambda^2} \propto \omega^2 \tag{4.38}$$

Thus, the radar cross section has a quadratic dependency on the frequency of the incident electromagnetic wave. Furthermore, if we recall that we are working in the optical regime:

$$\sigma(0,0) \propto \frac{a^4}{\lambda^2} \gg a^2 \tag{4.39}$$

that is, in the specular direction, the radar cross section is much larger than the physical area of the target.

In addition, Figure 4.9 also makes evident a crucial property of end-region returns: they produce a *sidelobe structure* around the specular reflection region [53, 56]. This is a direct consequence

of the oscillatory behavior of the angular variables in the expression for the radar cross section, which in turn is due to the discontinuities in the surface currents.

The radar wavelength and size of the target determine how many lateral sidelobes are present in the radar cross section. Let us consider the $\phi = 0$ case. Then, the radar cross section is proportional to:

$$\sigma(\theta, 0) \propto \cos^2\theta \left(\frac{\sin(kau)}{kau}\right)^2 \tag{4.40}$$

The radar cross section reaches the value of zero on both sides of each sidelobe. This only happens when:

$$\sin(kau) = 0 \tag{4.41}$$

which means that:

$$kau = \frac{2\pi a}{\lambda}\sin\theta = 0, \pi, 2\pi, \ldots \tag{4.42}$$

However, the value of 0 corresponds to the maximum of σ. Then, the radar cross section is zero when:

$$\frac{2a}{\lambda}\sin\theta \in \mathbb{Z} - \{0\} \tag{4.43}$$

Then, for example, if $a = 2.5\lambda$, we have five zeroes in:

$$\sin\theta = \frac{1}{5}, \frac{2}{5}, \frac{3}{5}, \frac{4}{5}, \frac{5}{5} \tag{4.44}$$

and therefore, σ has four sidelobes on each side of the maximum. In general, the number of sidelobes per side is given by:

$$\lfloor 2a/\lambda - 1 \rfloor \tag{4.45}$$

It is important to remark that the sidelobe structure is the most important return after specular scattering. Indeed, the sidelobe structure can be used to detect targets even if the specular returns contribute in a negligible manner to the received radar signal [53, 56, 70]. Therefore, the sidelobe structure is crucial for the design of stealth vehicles (how to reduce it) and radar systems (how to exploit it).

4.8.3 GEOMETRY, FREQUENCY, AND SIDELOBES

As previously discussed, the sidelobe structure of σ can be exploited to enhance detection, even if the target avoids specular returns. However, the sidelobe structure can be reduced by smoothly tapering to zero the currents over several wavelengths [53]. For example, the sidelobe structure can be significantly reduced by changing the conductivity of the plate so that the induced current is linearly distributed in such a way that $\mathbf{j}_s = 0$ along the edges.

Furthermore, the sidelobe structure depends on the geometry of the target. Let us first consider the case of a flat rectangular target. Assume three targets of the same area but different proportions:

$$\begin{aligned} A_1 &= 2.5 \times 4.0\ \lambda^2 \\ A_2 &= 5.0 \times 2.0\ \lambda^2 \\ A_3 &= 10.0 \times 1.0\ \lambda^2 \end{aligned} \tag{4.46}$$

The cross section for these targets is shown in Figure 4.10. From these plots, it is evident that the three targets have the same maximum value of σ at $(\theta, \phi) = (0, 0)$, but their sidelobe structure is different. Therefore, on this specific orientation ($\phi = 0$), target A_1 is more likely to be detected by its sidelobe structure than target A_2.

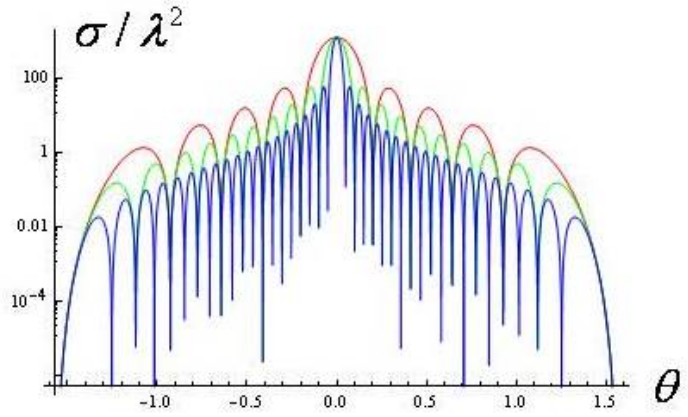

Figure 4.10: Radar cross section for a flat 2D plate of equal size, but different proportions (A_1:red; A_2:green; A_3:blue).

Another way to reduce the sidelobe structure is by changing the curvature of the surfaces that make the target. In double curved surfaces, for example, the currents smoothly taper to zero in the shadow regions [56]. The relationship between σ and geometry at the specular direction ($\theta = \phi = 0$) is illustrated in Table 4.1 [56].

It is important to note that the maximum value of the radar cross section has a different functional relationship with the frequency depending on the geometry of the target. It is only in the case of a doubly curved surface that the radar cross section is independent of the frequency.

We can use these values to compare the radar cross section of a spherical target:

$$\sigma_\circ = \pi a^2 \tag{4.47}$$

and a flat square target of similar size:

$$\sigma_\diamond = \frac{4\pi (2a)^4}{\lambda^2} \tag{4.48}$$

Table 4.1: Dependence of the radar cross section on target's geometry [56].

Surface	Example	Curvature Radii	$\sigma(0,0)$	ω Dependency
Flat	Plate	(∞, ∞)	$4\pi A^2/\lambda^2$	$\propto \omega^2$
Singly Curved	Cylinder	(a, ∞)	$2\pi a l^2/\lambda$	$\propto \omega$
Doubly Curved	Spheroid	(a_1, a_2)	$\pi a_1 a_2$	$\propto 1$

in the optical regime:

$$\frac{\sigma_\diamond}{\sigma_\circ} = 64\frac{a^2}{\lambda^2} \gg 1 \Rightarrow \sigma_\diamond \gg \sigma_\circ \tag{4.49}$$

That is, the radar cross section of a sphere is much smaller than the radar cross section of a flat plate of similar dimensions. This result is to be expected, as the plate will reflect most of the electromagnetic energy back to the radar, while the sphere will scatter a large part of it to other regions.

Let us consider a specific example. Assume a flat square plate of size $a = n\lambda$ with $\lambda = 0.1$ m and $n = 100$. That is, $a = 10$ m. Then, the area of the plate is $A = a^2 = 100\, m^2$. Then, the maximal value of its radar cross section at the specular direction is:

$$\sigma_\diamond = 4\pi\frac{A^2}{\lambda^2} \approx 1.3 \times 10^7\, m^2 \tag{4.50}$$

This means that:

$$\frac{\sigma_\diamond}{A} \approx 1.3 \times 10^5 \tag{4.51}$$

which means that the radar cross section at the specular direction is 100,000 times larger than the physical area of the plate.

We can now compare the radar cross section of this target with the one of a sphere of radius a with cross section given by:

$$\sigma_\circ = \frac{\pi}{a^2} \approx 314\, m^2 \tag{4.52}$$

As seen in Figure 4.11, the radar cross section of the plate is larger than the radar cross section of the sphere for a viewing angle of about 0.31 radians with respect to the specular direction.

The dependency of the radar cross section on the geometry of the target is one of the reasons as to why the new generation of stealth aircrafts does not have the diamond shape of the F117. For instance, the stealthier B2 Spirit features double curved surfaces across its fuselage [1, 86].

4.9 ENERGY CONSERVATION IN THE OPTICAL REGIME

If we ignore absorption effects, it is reasonable to require that energy is conserved during radar-target interactions. In the optical regime it is possible to find a simple equation that neatly describes this fact. Although it is not an important result in the context of classical radar theory, this equation will prove essential for the simplified description of a quantum radar cross section.

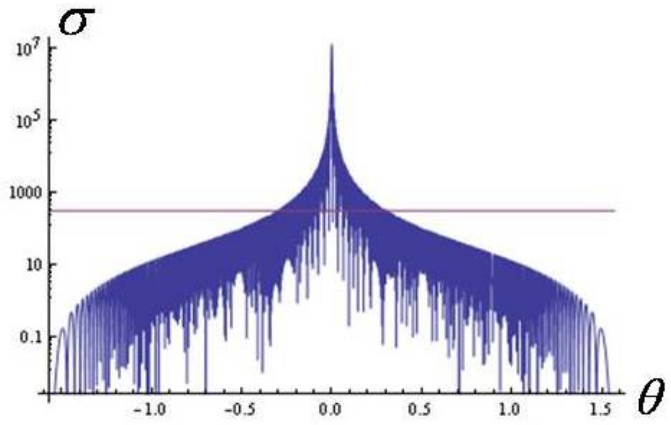

Figure 4.11: Radar cross section for a rectangular plate (blue) and a sphere (red) of similar dimensions. The former is larger than the second over an angle of about 0.31 radians around the specular direction.

Let us assume we have the expressions for the scattered fields under a bistatic radar. The coordinates of the transmitter are $\mathbf{r}_s$ and the coordinates of the receiver are $\mathbf{r}_d$ with respect to the target. If the energy is conserved, then the total incident energy on the target has to be scattered somewhere in space. That is:

$$\int_{T_\perp(\theta,\phi)} W_i(\mathbf{r}_s)\, dS \approx \lim_{r_d\to\infty} \int_{S_{r_d}\supset T} W_s(\mathbf{r}_s, \mathbf{r}_d)\, r_d^2\, d\Omega_d \tag{4.53}$$

where the first integral is taken over the orthogonal projected area of the target $T_\perp$, and the second integral over S_{r_d}, a sphere of radius r' that surrounds the target T. That is, we are integrating over all the possible positions of the radar receiver. In terms of the electric fields:

$$\int_{T_\perp(\theta,\phi)} |E_i(\mathbf{r}_s)|^2\, dS \approx \lim_{r_d\to\infty} \int_{S_{r_d}\supset T} |E_s(\mathbf{r}_s, \mathbf{r}_d)|^2\, r_d^2\, d\Omega_d \tag{4.54}$$

If we assume a harmonic field:

$$E_i \propto E_0\, e^{-i\vec{k}\cdot\vec{r}} \Rightarrow |E_i|^2 = E_0^2 \tag{4.55}$$

we get:

$$\int_{T_\perp(\theta,\phi)} |E_i(\mathbf{r}_s)|^2\, dS = E_0^2\, A_\perp(\theta,\phi) \tag{4.56}$$

where $A_\perp$ is the area of the orthogonal projection of the target and will depend on the orientation of the target. Energy conservation then implies that:

$$|E_i(\mathbf{r}_s)|^2 A_\perp(\theta,\phi) \approx \lim_{r_d\to\infty} \int_{S_{r_d}\supset T} |E_s(\mathbf{r}_s, \mathbf{r}_d)|^2\, r_d^2\, d\Omega_d \tag{4.57}$$

Using this expression for the conservation of energy we can rewrite the radar cross section for a monostatic radar as:

$$\sigma = \lim_{r\to\infty} 4\pi r^2 \frac{|E_s|^2}{|E_i|^2} \approx 4\pi A_\perp \lim_{r\to\infty} \frac{|E_s(\mathbf{r})|^2}{\int_{S_{r_d}\supset T} |E_s(\mathbf{r}_s, \mathbf{r}_d)|^2 \, d\Omega_d} \tag{4.58}$$

where we have set:

$$\mathbf{r} = \mathbf{r}_s = \mathbf{r}_d \tag{4.59}$$

on the numerator. Notice that, in general, the projected area is a function of the angular coordinates $A_\perp = A_\perp(\theta, \phi)$.

This expression for the radar cross section is only valid in the optical regime. Indeed, all the incident radiation is absorbed and scattered by a target only if the target's dimensions are greater than the wave length of the incident electromagnetic wave. One way to think about the physics behind this fact is to consider the radar as a diffraction limited optical sensor. The angular resolution θ is given by the Rayleigh criterion:

$$\sin\theta \approx 1.220 \frac{\lambda}{D} \tag{4.60}$$

where D is the diameter of the lens' aperture and the numerical factor is derived from the position of the first dark ring surrounding the central Airy disc [8, 43]. In the optical regime, λ and θ are very small, which means that the device can resolve small variations in the geometry of the target. On the other hand, if λ is large, then the angular resolution is large and may even be larger than the target itself. In this case, not all the incident radiation is being scattered, as a portion of it is "passing through" the object.

As an example, let us consider a spherical target S_T of radius a. Then, integrating the above expression for σ we get:

$$\int_{S_r\supset S_T} \sigma \, d\Omega \approx 4\pi A_\perp \tag{4.61}$$

In addition, because of the spherical symmetry of the target, we also know that:

$$\int_{S_r\supset S_T} \sigma \, d\Omega = \sigma 4\pi \tag{4.62}$$

and therefore:

$$\sigma \approx A_\perp = \pi a^2 \tag{4.63}$$

which is the value we had already estimated for the spherical target in the optical regime.

Let us consider now the case of a flat square target of area $A = a^2$. From the previous section we know that the scattered field is given by:

$$|E_s(r, \theta, \phi)|^2 = A^2 \frac{k^2}{4\pi^2 r^2} E_i^2 \cos^2\theta \left(\frac{\sin(kau)}{kau}\right)^2 \left(\frac{\sin(kbv)}{kbv}\right)^2 \tag{4.64}$$

and as a consequence, using the traditional expression for the cross section at $\phi = 0$ we obtain:

$$\sigma(\theta, 0) = \frac{4\pi A^2}{\lambda^2} \cos^2\theta \left(\frac{\sin(kau)}{kau}\right)^2 \tag{4.65}$$

On the other hand, using the expression for the scattered field in the new expression for the cross section we have:

$$\tilde{\sigma}(\theta, 0) = \frac{4\pi A_\perp}{2} \frac{\cos^2\theta \left(\frac{\sin(kau)}{kau}\right)^2}{\int \cos^2\theta \left(\frac{\sin(kau)}{kau}\right)^2 \left(\frac{\sin(kbv)}{kbv}\right)^2 d\Omega} \tag{4.66}$$

As we are interested in comparing the accuracy of our approximation, we have added a "tilde" symbol to distinguish between both of them. Furthermore, recalling that the maximum value of the cross section is reached at $\theta = 0$, we define the normalized error between both expressions as:

$$\epsilon(\theta) = \frac{\tilde{\sigma}(\theta) - \sigma(\theta)}{\sigma(0)} \tag{4.67}$$

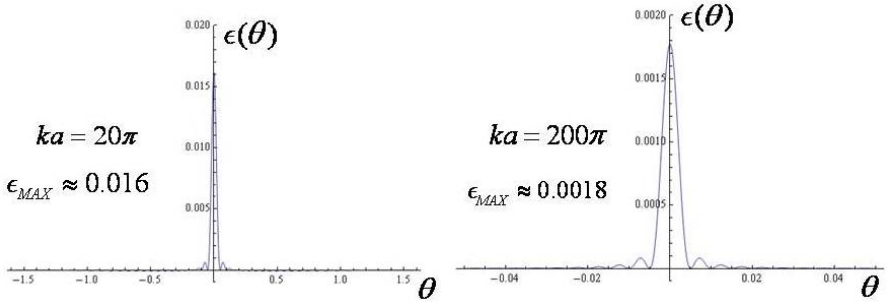

Figure 4.12: Relative error using the expression for σ based on energy conservation on the optical regime. The error diminishes as we get further inside the optical regime.

Figure 4.11 shows the behavior of $\epsilon(\theta)$ for a plate of size $ka = 20\pi$ and for a larger plate of size $ka = 200\pi$. As the value of ka increases, the error decreases. As expected, the error decreases as we penetrate the optical regime ($ka \gg 1$).

4.10 RADAR AS AN INFORMATION CHANNEL

Formally, we can describe radar performance as an information channel. The target information produced by the radar system includes [53, 56, 95, 96]:

Range: The range to the target is obtained through a measurement of the time interval for the echo signal Δt.

Speed: The speed of the target can be obtained by analyzing the Doppler shift or changes in the target's range.

Direction: A directional antenna can provide information about the target's direction.

Size: The size of the target has an influence on the magnitude of the returned signal due to the radar cross section.

Shape: The shape and geometry of the target determine its radar cross section.

Components: The components of the target, such as moving parts in the case of a propeller, can be determined by analyzing the frequency components of the Doppler signal.

The fidelity of the information depends on the amount of noise in the signal, but also on the value of the radar cross section of the target. Therefore, the process of obtaining information from a target using radar, can be described as a noisy communication channel. Furthermore, the radar cross section could be treated as a form of "geometric noise".

4.11 SUMMARY

The radar equation describes the strength of the electromagnetic signal that arrives to the receiver. This equation depends on the radar cross section, which is an important quantity that characterizes the visibility of the targets as seen under a radar. Due to the finite size of the targets, a sidelobe structure is observed on the angular dependence of the radar cross section. Strongly dependent on geometry, these sidelobes enable the detection of targets that avoid specular returns, and therefore, they are crucial for the optimal design of stealth vehicles and radar systems.

CHAPTER 5

Quantum Radar Theory

As discussed in the previous chapter, traditional radar systems employ classical electromagnetic waves to detect targets. That is, the traditional radar signal is made of a large number of photons. Quantum radar generalizes the concept of radar, but this novel device operates with a relatively small number of photons. As such, its theoretical description has to be done using quantum electrodynamics.

The motivation for developing the concept of quantum radar is the potential use of quantum phenomena to increase the sensitivity of the sensing system. As we will see in this chapter, entangled-photons quantum radar appears to offer higher sensitivity. Furthermore, it seems that it is much more difficult to conduct jamming on a quantum radar system. In addition, quantum radar inherits some of the advantages of traditional radar systems. For instance, microwaves photons are able to penetrate clouds and fog, while photons in the visible regime are most likely to be absorbed or scattered by the environment.

In this chapter we will present the theory behind quantum radar. We will place emphasis on the two major standoff sensing techniques proposed to date: the interferometric quantum radar and quantum illumination. Even though it does not operate on the microwave regime that characterizes radar, we will briefly discuss quantum LADAR. In addition we will overview the state-of-the-art on the technologies required for the construction of quantum radar transmitters and receivers.

5.1 STANDOFF QUANTUM SENSORS

In general, we can define a quantum radar as a standoff detection system that uses microwave photons and exploits some form of quantum phenomena to enhance its capabilities to detect, identify, and resolve targets of interest.

The targets are assumed to posses a low reflectivity and are far away from the detector. Furthermore, the radar-target system is presumed to be immersed in a noisy and lossy environment. That is, the radar signal may be attenuated through absorption or scattering processes, and the overall performance of the system is affected by the presence of noise.

Furthermore, as its name suggests, these devices operate in the microwave regime that characterizes classical radar signals. This is an important feature that inherits the advantages of traditional radar pulses such as being able to penetrate clouds and fog.

5.1.1 THE FUNDAMENTAL LIMITS OF QUANTUM METROLOGY

The measurement process in quantum mechanics is restricted by Heisenberg's uncertainty principle [44, 60]. Suppose we have a quantum system made of N photons and the quantum state has a

relative phase ϕ. Then, in terms of the state phase ϕ and the number of photons N, the Heisenberg principle leads to the inequality:

$$\Delta\phi \, \Delta N \geq 1 \tag{5.1}$$

where $\Delta\phi$ and ΔN represent the phase and photon number fluctuations, respectively [68].

Let us also assume we have a monochromatic *coherent state* of the form[1]:

$$|\alpha\rangle = e^{-|\alpha|^2/2} \sum_{N=0}^{\infty} \frac{\alpha^N}{(N!)^{1/2}} |n\rangle \tag{5.2}$$

where $|n\rangle$ represents the state of n photons with frequency ω [68, 73, 92]. Then, the probability of finding N photons is:

$$\begin{aligned} P(N) &= |\langle N|\alpha\rangle|^2 \\ &= \frac{e^{-\langle N\rangle}\langle N\rangle^N}{n!} \end{aligned} \tag{5.3}$$

which clearly obeys a Poisson distribution law [68]. Furthermore:

$$\langle N\rangle = \langle\alpha|N|\alpha\rangle = \langle\alpha|\hat{a}^\dagger\hat{a}|\alpha\rangle = |\alpha|^2 \tag{5.4}$$

and:

$$\langle N^2\rangle = \langle\alpha|\hat{a}^\dagger\hat{a}\hat{a}^\dagger\hat{a}|\alpha\rangle = \langle N\rangle^2 + \langle N\rangle \tag{5.5}$$

And therefore:

$$(\Delta N)^2 = \langle N^2\rangle - \langle N\rangle^2 = \langle N\rangle \tag{5.6}$$

which means that:

$$\Delta N = \sqrt{\langle N\rangle} \tag{5.7}$$

This is known as *shot noise* and it is due to the discrete nature of light in the quantum realm [10, 57, 68].

In the case of shot noise, the Heisenberg inequality takes the form:

$$\Delta\phi \geq \frac{1}{\sqrt{\langle N\rangle}} \tag{5.8}$$

This expression for the limit on the sensitivity for a phase measurement is known as the *Standard Quantum Limit*[2] [10, 35, 57].

The standard quantum limit is a consequence of the discrete nature of the electromagnetic field, as well as the Poissonian statistics of classical light [57, 68]. These properties of quantum light translate into vacuum fluctuations that affect the measurement of the amplitude of an electromagnetic field [14, 15]. In a sense, these features of the quantum electromagnetic field tend to prevent the cooperative behavior of the photons [35].

[1] Coherent states of light represent quite well the light emitted by a laser.
[2] This limit is also known as the *shot-noise limit* or *coherent state limit*.

On the other hand, one could argue that the basic principles of quantum theory do not impose a specific value on the fluctuations on the number of photons. The standard quantum limit is a consequence of the use of non-optimal measurement strategies, and in principle, it could be avoided:

$$\langle \Delta^2 N \rangle \approx \mathcal{O}\left(\langle N \rangle^2\right) \tag{5.9}$$

That is, the true fundamental limit is the one given by Heisenberg's principle, which leads to the *Heisenberg Limit*:

$$\Delta\phi \geq \frac{1}{\langle N \rangle} \tag{5.10}$$

The Heisenberg limit does not depend on the measurement strategies and it is unavoidable [35, 57].

The sensitivity of most of our modern sensors is bounded by the standard quantum limit. However, there is reason to believe that it is possible to build sensors that can beat the standard quantum limit but are limited by the Heisenberg limit [35, 36]. A regime of variables for which the sensitivity of a sensor exceeds the value imposed by the standard quantum limit is called the *Supersensitivity Regime*, and the sensor is said to be *Supersensitive*.

In particular, it has been shown that entanglement offers a way to bypass the barrier imposed by the standard quantum limit [35, 36]. But nevertheless, it is important to note that entanglement is not strictly necessary to achieve the Heisenberg limit. To date some other alternatives have been proposed in the literature. These include, for example, the injection of squeezed states [7, 104] or the injection of Fock states into the measurement system [46].

In any event, most strategies are based on the exact same principle: perform collective measurements after highly correlated states have been injected into the system [35, 36]. Such is the case of the interferometric quantum radar that uses highly entangled states to reach the Heisenberg limit.

Finally, it is important to remark that Heisenberg limit metrology is very challenging to accomplish [35, 36]. At these high precision scales, there is a large number of factors that have important contributions and cannot be neglected. For instance, it is crucial to estimate the effect of thermal noise and other dissipative processes on the signal, as well as any other sources of noise that may limit the performance of the detector and the transmitter.

5.1.2 CLASSIFICATION OF STANDOFF QUANTUM SENSORS

Standoff quantum sensing architectures can be classified according to the type of quantum phenomena exploited by the system [42]. The three basic categories are the following:

Type 1: The quantum sensor transmits un-entangled quantum states of light.

Type 2: The quantum sensor transmits classical states of light, but uses quantum photo-sensors to boost its performance.

Type 3: The quantum sensor transmits quantum signal states of light that are entangled with quantum ancilla states of light kept at the transmitter.

The principal examples of quantum radar systems are the single photon quantum radar and the entangled photon quantum radar. These are Type-1 and Type-3 sensors, respectively. On the other hand, quantum LADAR is an example of a Type-2 sensor. The major features of these examples will be described next.

5.1.3 SINGLE-PHOTON QUANTUM RADAR

Single photon quantum radars are Type-1 sensors. These systems operate in a similar fashion as a classical radar. As shown in Figure 5.1, a quantum radar transmitter sends a single photon pulse towards a target. The target reflects the photon which is subsequently detected by the radar receiver.

One of the advantages of quantum radar is the fact that some targets appear to look bigger when looked with low photon number pulses. That is, as we will see in Chapter 6, the radar cross section near the specular region of some targets is larger than its classical counterpart when the targets are illuminated with individual photons (entangled or not).

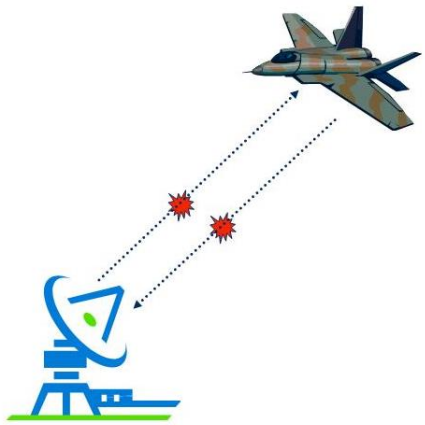

Figure 5.1: The basic concept of a single photon quantum radar: a single photon is emitted towards a target, and subsequently the photon is reflected back to the receiver.

5.1.4 ENTANGLED-PHOTONS QUANTUM RADAR

The greatest benefit of quantum radars is obtained with the use of entangled states of light. These are Type-3 sensors. As shown in Figure 5.2, an entangled pair of photons is generated. One of these photons is sent towards the target and the other kept in the radar system. The outgoing photon is reflected by the target and subsequently received by the radar. At this point the correlations embedded in the entangled states are exploited to increase detection performance.

Examples of these systems are the *Interferometric Quantum Radar* and *Quantum Illumination*. Both of these are discussed in some detail in the following sections.

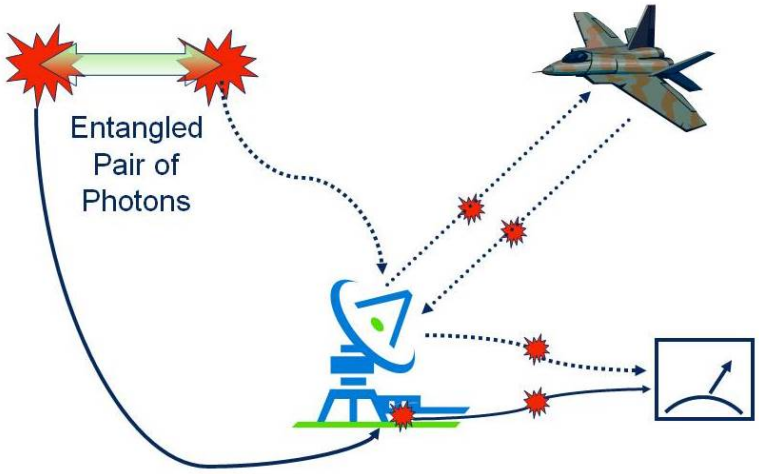

Figure 5.2: An entangled-photons quantum radar system: an entangled pair is produced, one of the photons is sent towards the target while the other is kept in the system. The correlation between these photons can be exploited to increase the performance of the device.

5.1.5 QUANTUM LADAR

Quantum LADAR is a Type-2 standoff quantum sensor that operates in the visible and near-visible regimes[3] [22, 23, 41, 58, 79, 93]. As such, quantum LADAR does not count as a form of quantum radar technology. Nevertheless, it is important to mention that this is another promising quantum sensor which theory is well understood and the development of an operational prototype is currently underway. The advantages of LADAR over radar resides on the small wavelengths of the former, which allows it to resolve small spatial information [76]. On the other hand, LADAR cannot penetrate fog or clouds as radars do, and as a consequence, the operational range of a LADAR is usually restricted within 100 km [76]. The use of squeezed vacuum injection to reduce the noise due to vacuum fluctuations is one way in which quantum effects can be harnessed to improve the performance of LADAR [58].

[3]LADAR stands for Laser Detection And Ranging, and it is the exact same technology as LIDAR (Light Detection And Ranging). However, in the military context, the former is the preferred acronym.

5.2 INTERFEROMETRIC QUANTUM RADAR

The quantum radar systems described in Figure 5.1 and 5.2 resemble an interferometer with a very long arm (as big as the range to the target R). This suggests that one way to analyze the performance of a quantum radar is to describe it as a quantum interferometer.

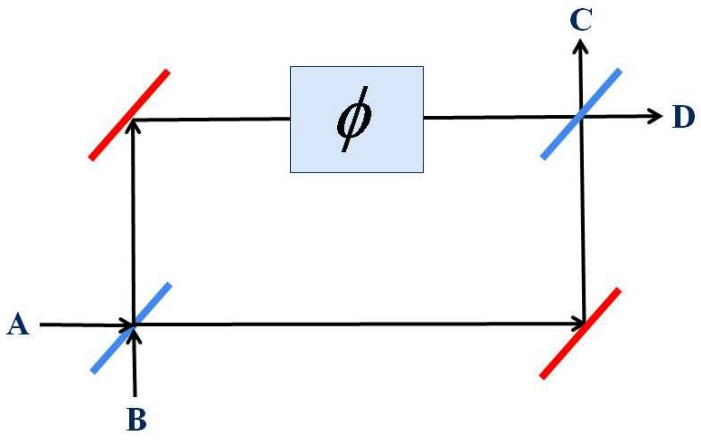

Figure 5.3: Mach-Zender interferometer with input ports A and B, output ports C and D, and a phase delay ϕ in one of the arms.

Let us consider the Mach-Zender interferometer made of two mirrors and two beam splitters as shown in Figure 5.3. One of the arms of the interferometer introduces a delay phase ϕ. The value of ϕ can be estimated by measuring the intensity (i.e., number of photons) of the two output beams. In agreement with our previous discussion, it can be shown that, after measuring the output for a beam with N non-entangled photons, one can estimate the value of ϕ with a statistical error proportional to $1/\sqrt{N}$ [20, 66]. That is, this interferometric measurement is bounded by the standard quantum limit.

Similarly, let us assume we want to use an interferometer-like sensor to determine the range of a target. The best classical strategy to perform a range estimation is the one currently exploited by traditional radar systems. That is, the direct calculation of the average travel time measured for N non-entangled photons. It can be shown that in this case the error is given by:

$$\delta R \approx \mathcal{O}\left(\frac{1}{\Delta\omega\sqrt{N}}\right) \tag{5.11}$$

where $\Delta\omega$ is the bandwidth of the radar signal [35].

However, as we will see next, entangled photons can be used to beat the standard quantum limit and reach the Heisenberg limit.

5.2.1 QUANTUM INTERFEROMETRY

Let us assume we have a NOON state:

$$|\Psi_{NOON}\rangle = \frac{1}{\sqrt{2}}\left(|N0\rangle + |0N\rangle\right) \tag{5.12}$$

which is a highly entangled state of two photonic modes in an interferometer [9]. These states are often proposed for a variety of quantum sensing applications. Each half of the entangled state passes through a different arm of the interferometer, so we can write the state as:

$$|\Psi_{NOON}\rangle = \frac{1}{\sqrt{2}}\left(|N\rangle_1|0\rangle_2 + |0\rangle_1|N\rangle_2\right) \tag{5.13}$$

where the subindex identifies the arms of the interferometer. Furthermore, we assume that we are interested in measuring a phase difference ϕ that arises when photons are sent through the second arm of the interferometer [20, 66]. The effect of a phase shift ϕ on the NOON state is given by:

$$|\Psi^{(\phi)}_{NOON}\rangle = \frac{1}{\sqrt{2}}\left(|N\rangle_1|0\rangle_2 + e^{iN\phi}|0\rangle_1|N\rangle_2\right) \tag{5.14}$$

We can write the NOON state in terms of the creation and annihilation operators as:

$$\begin{aligned} |\Psi^{(\phi)}_{NOON}\rangle &= \frac{1}{\sqrt{2}}\left(\frac{(\hat{a}_1^\dagger)^N}{\sqrt{N!}}|0\rangle_1|0\rangle_2 + e^{iN\phi}\frac{(\hat{a}_2^\dagger)^N}{\sqrt{N!}}|0\rangle_1|0\rangle_2\right) \\ &= \frac{1}{\sqrt{2N!}}\left((\hat{a}_1^\dagger)^N + e^{iN\phi}(\hat{a}_2^\dagger)^N\right)|0\rangle_1|0\rangle_2 \end{aligned} \tag{5.15}$$

In order to measure the phase shift ϕ, the detector has to implement a measurement of the following observable:

$$\begin{aligned} \hat{A}_D &= |N0\rangle\langle 0N| + |0N\rangle\langle N0| \\ &= \frac{1}{N!}\left((\hat{a}_1^\dagger)^N|0\rangle\langle 0|(\hat{a}_2^\dagger)^N + (\hat{a}_2^\dagger)^N|0\rangle\langle 0|(\hat{a}_1^\dagger)^N\right) \end{aligned} \tag{5.16}$$

With this setup, the amount of "noise" is given by:

$$\begin{aligned} \Delta^2 A_D &= \left(\langle \hat{A}_D^2\rangle - \langle \hat{A}_D\rangle^2\right) \\ &= \sin^2 N\phi \end{aligned} \tag{5.17}$$

while the phase responsivity is:

$$\frac{d\langle \hat{A}_D\rangle}{d\phi} = -N\sin N\phi \tag{5.18}$$

Then, the phase estimation error is approximately given by:

$$\delta\phi \approx \frac{\Delta A_D}{|\frac{d\langle \hat{A}_D\rangle}{d\phi}|} = \frac{1}{N} \tag{5.19}$$

That is, this interferometric phase measurement procedure using highly entangled states can reach the Heisenberg limit [20, 66].

5.2.2 ATTENUATED QUANTUM INTERFEROMETRY

Let us assume now the exact same interferometric experiment described above, but the interferometer is immersed in an attenuating medium [32, 33]. The expression for the propagation of an attenuated NOON state was given in Chapter 2 and is repeated here for convenience:

$$|\Psi_{NOON}\rangle = \frac{1}{\sqrt{2N!}} e^{-i\omega\eta_1/c - \chi_{c1}(\omega)/2)(NL_1)} \left(\hat{a}_1^\dagger\right)^N |0\rangle_1 |0\rangle_2 \tag{5.20}$$

$$+ \frac{1}{\sqrt{2N!}} e^{-i\omega\eta_2/c - \chi_{c2}(\omega)/2)(NL_2)} \left(\hat{a}_2^\dagger\right)^N |0\rangle_1 |0\rangle_2 \tag{5.21}$$

$$+ |\Phi\rangle$$

where each component travels across distances L_1 and L_2 over two different media characterized by refraction indices η_1 and η_2, and attenuation coefficients χ_{c1} and χ_{c2}. Also, $|\Phi\rangle$ is a state that represents those states scattered outside the NOON basis.

In the case of the interferometric experiment described above, the amount of noise is given by:

$$\Delta^2 A_D = \frac{1}{2}\left(\alpha_1^N - 2\alpha_1^N\alpha_2^N + \alpha_2^N + (\alpha_1\alpha_2)^N \sin^2 N(\phi - \phi_0)\right) \tag{5.22}$$

while the phase responsivity is:

$$\frac{d\langle \hat{A}_D\rangle}{d\phi} = -N(\alpha_1\alpha_2)^{N/2} \sin N(\phi - \phi_0) \tag{5.23}$$

and we have defined the transmittance of the medium as:

$$\alpha_i \equiv e^{-\chi_{ci} L_i} \tag{5.24}$$

and the dispersion phase shift as:

$$\phi_0 \equiv \frac{\omega}{c}(\eta_2 L_2 - \eta_1 L_1) \tag{5.25}$$

Then, the phase estimation error is given by:

$$\delta\phi = \frac{\sqrt{\frac{1}{2\alpha_1^N} + \frac{1}{2\alpha_2^N} - 1 + \sin^2 N(\phi - \phi_0)}}{N\,|\sin N(\phi - \phi_0)|} \tag{5.26}$$

It is only in the limit of no attenuation:

$$\lim_{\alpha_1 \to 1} \lim_{\alpha_2 \to 1} \delta\phi = \frac{1}{N} \tag{5.27}$$

that the Heisenberg limit can be achieved.

5.2.3 SEPARABLE STATES

For comparison purposes it is useful to know the phase estimation error in the case where one uses separable states instead of entangled NOON states [32, 33]. The state (without attenuation) is taken to be:

$$|\Psi_S\rangle = \frac{1}{\sqrt{2^N}} \left(|10\rangle + |01\rangle\right)^{\otimes N} \tag{5.28}$$

which can be rewritten as:

$$|\Psi_S\rangle = \frac{1}{\sqrt{2^N}} \prod_{j=1}^{N} \left(\hat{a}_1^{\dagger(j)} + \hat{a}_2^{\dagger(j)}\right) |0\rangle_1 |0\rangle_2 \tag{5.29}$$

The observable for separable states is:

$$\hat{A}_S = \bigoplus_{j=1}^{N} \left(|01\rangle^{(j)(j)}\langle 10| + |10\rangle^{(j)(j)}\langle 01|\right) \tag{5.30}$$

Introducing the attenuation of the states as we did before, we obtain the following variance on the phase measurement:

$$\Delta^2 A_S = \frac{N}{2} \left(\alpha_1 - 2\alpha_1\alpha_2 + \alpha_2\right) + N\, \alpha_1\alpha_2\, \sin^2(\phi - \phi_0) \tag{5.31}$$

and a phase responsivity:

$$\frac{d\langle \hat{A}_D\rangle}{d\phi} = -N\sqrt{\alpha_1\alpha_2}\, \sin(\phi - \phi_0) \tag{5.32}$$

As a consequence, the phase estimation error is:

$$\delta\phi = \frac{\sqrt{\frac{1}{2\alpha_1} + \frac{1}{2\alpha_2} - 1 + \sin^2(\phi - \phi_0)}}{\sqrt{N}\, |\sin(\phi - \phi_0)|} \tag{5.33}$$

which in the no-absorption limit takes the value:

$$\lim_{\alpha_1 \to 1} \lim_{\alpha_2 \to 1} \delta\phi = \frac{1}{\sqrt{N}} \tag{5.34}$$

As expected, separable states cannot be used to beat the standard quantum limit even in the absence of attenuation.

5.2.4 ATMOSPHERIC QUANTUM INTERFEROMETRY

Typical examples of atmospheric attenuation caused by fog or clouds are given in Table 5.1 for different wavelengths in the radar region [95, 96]. In particular, $\lambda = 3.2$cm is inside the radar X-band (2.5-3.75 cm; 8-12 GHz). It can be observed that in this regime, the attenuation coefficient

increases as we decrease the wavelength. Therefore, it is convenient to be on the higher-end of the radar X-band.

As a comparison, the average atmospheric attenuation for visible light at 550 nm is of about 0.87 dB/km, much higher than the attenuation suffered by X-band radar in the cases considered in Table 5.1 [91]. This is to be expected, the ability of radar waves to penetrate fog and clouds is the reason as to why radar is so important in the military and civilian worlds.

Table 5.1: Attenuation (dB/Km) caused by fog and clouds on different wavelengths in the radar region [95, 96].

Visibility (m)	$\lambda = 1.25$ cm	$\lambda = 3.2$cm	$\lambda = 10$cm
30	1.25	0.20	0.02
90	0.25	0.04	0.004
300	0.045	0.007	0.001

In general, the dielectric constant of a medium varies with temperature, and as a consequence, the attenuation coefficient varies with the temperature [95, 96]. The values reported in Table 5.1 for the attenuation coefficient are taken at 0°C. Approximately, the values for 15°C and 25°C can be obtained by multiplying the coefficient in the table by 0.6 and 0.4, respectively. That is, in this specific regime, the attenuation coefficient decreases as the temperature increases.

Let us analyze the behavior of the quantum interferometer in the case where $\lambda = 3.2$ cm. We consider two of the scenarios shown in Table 5.1: a visibility of 300 m which is equivalent to an attenuation constant of $\chi_c = 0.0016/km$, and a visibility of 30 m equivalent to an attenuation constant of $\chi_c = 0.046/km$.

The behavior of the phase error for both cases can be observed in Figure 5.4 for two range distances using $N = 2$ entangled NOON states. The phase estimation error depends on the value of ϕ and it never reaches the Heisenberg limit (the vertical line at $\delta\phi = 0.5$). Furthermore, as the range increases, the minimum phase error moves away from the Heisenberg limit.

The behavior of the phase estimation error when one changes the atmospheric attenuation by 1 dB/km is shown in Figure 5.5. As can be observed, the effect of this change on the phase estimation error is substantial.

But perhaps more dramatic, it can be observed that the phase estimation error diverges when the sine function in the denominator of Equation (5.26) is close to zero. The number of divergent points in a range of values of ϕ depends on the number of photons N. Figure 5.6 compares the case of 2, 4, and 8 photons. The reason for these divergences is not physical, but simple a consequence that the approximation used for the phase estimation error:

$$\delta\phi \approx \frac{\Delta A_D}{|\frac{d\langle \hat{A}_D \rangle}{d\phi}|} = \frac{\sqrt{\frac{1}{2\alpha_1^N} + \frac{1}{2\alpha_2^N} - 1 + \sin^2 N(\phi - \phi_0)}}{N\,|\sin N(\phi - \phi_0)|} \tag{5.35}$$

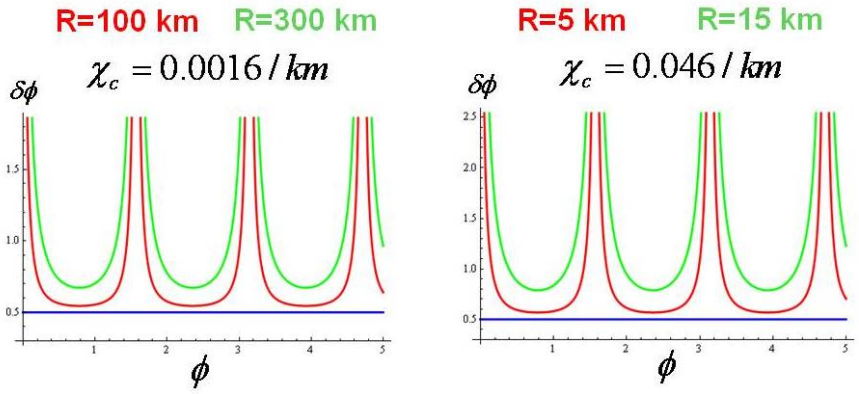

Figure 5.4: Phase estimation error as a function of the phase ϕ using $N = 2$ NOON states. Notice that, due to atmospheric attenuation, $\delta\phi$ never reaches the Heisenberg limit.

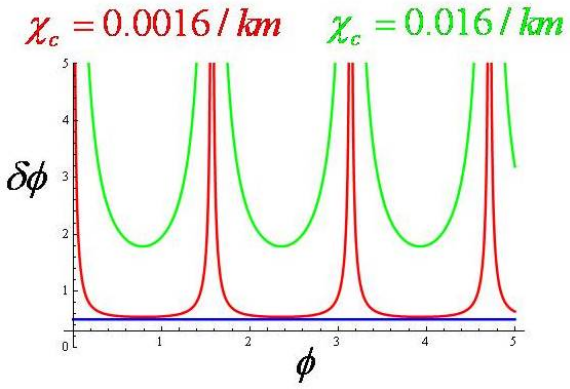

Figure 5.5: A change of 1 dB/km in the atmospheric attenuation constant produces a significant effect on the minimum value achievable by the phase estimation error.

does not hold well in the regions where the sine function in the denominator becomes zero. That is, the approximation does not hold for those points near:

$$N\,(\phi - \phi_0) \approx 0, \pi, 2\pi, ..., (2n)\pi \tag{5.36}$$

where n is an integer number.

In any event, one can see that the phase estimation error is minimal when the sine function in the denominator is 1. That is:

$$\delta\phi_{min}^{(e)} \approx \frac{1}{N}\sqrt{\frac{1}{2\alpha_1^N} + \frac{1}{2}} \tag{5.37}$$

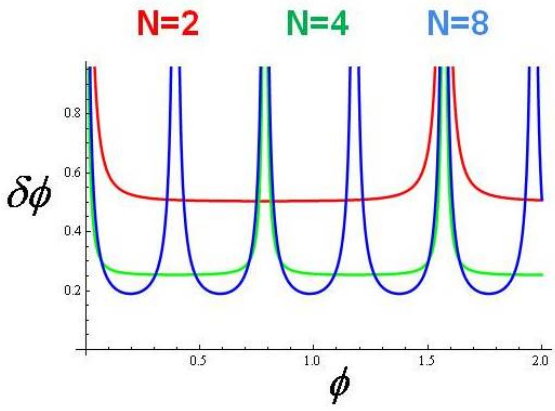

Figure 5.6: Phase estimation error for 2, 4, and 8 photons at 10 km range and 300 km visibility. The higher the number of photons, the more divergent points are found.

where we have ignored the contribution from the second arm, assuming it is in a well controlled environment inside the sensing apparatus.

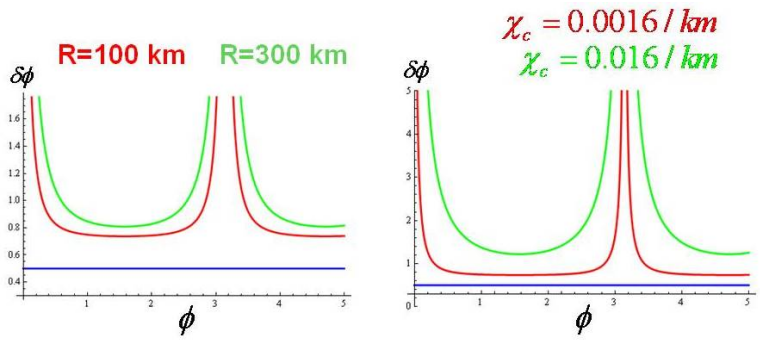

Figure 5.7: Phase estimation error for non-entangled states.

As shown in Figure 5.7, a similar behavior is observed in the case of quantum interferometry using separable states. In this case, however, the minimum value of the phase estimation error is given by:

$$\delta\phi_{min}^{(ne)} \approx \frac{1}{\sqrt{N}} \sqrt{\frac{1}{2\alpha_1} + \frac{1}{2}} \tag{5.38}$$

Notice that in the limit of no attenuation, these last two expressions reduce to the standard quantum limit and the Heisenberg limit, respectively.

Now let us assume that somehow we reach the minimum phase estimation error. The range of the detection system for the entangled (Ψ_e) and non-entangled (Ψ_{ne}) cases are shown in Figure 5.8. As expected, the entangled system is able to reach the Heisenberg limit (HL) at very small distances, while the separable state merely reaches the standard quantum limit (SQL). For an attenuation corresponding to a visibility of 300 m the estimation process using entangled states exceeds the standard quantum limit up to about 350 km. On the other hand, supersensitivity is restricted to about 12 km when the visibility is close to 30 km.

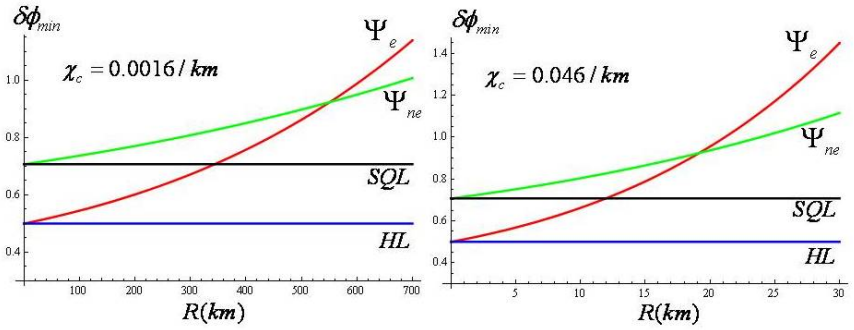

Figure 5.8: Phase estimation error as a function of the range to the target for a $N = 2$ entangled Ψ_e and non-entangled Ψ_{ne} sensors. The extent of the supersensitivity regime, where $HL \leq \delta\phi \leq SQL$, depends on the atmospheric attenuation constant.

It is important to observe that, for large ranges the sensitivity of the entangled system becomes worse than that for the non-entangled system. This is observed to happen at about 550 km in Figure 5.8 for the scenario corresponding to 300 m visibility, and at about 19 km for the scenario with a 30 m visibility. That is, for the high visibility case, the use of entanglement brings an improvement in phase measurement up to about 550 km.

In Figure 5.9 we can observe the performance of the system when we use a larger number of entangled states in the NOON state. The case for $N = 10$ is shown. It can be observed that in the high visibility scenario, supersensitivity is achieved up to about 180 km, and at about 7 km for the low visibility scenario.

Figure 5.10 compares the phase estimation error for $N = 2$ and $N = 10$. As expected, the phase estimation error is reduced as N increases. However, the performance of the highly entangled states degrades more quickly than for the simpler entangled state.

Finally, it is worth comparing the performance of quantum interferometry in the radar and visible wavelengths. In Figure 5.11 we show the phase estimation error for an attenuation coefficient of 0.87 dB/km, which corresponds to $\lambda = 550$ nm light traversing average atmospheric conditions. It can be observed that the phase estimation error is severely compromised by the atmospheric attenuation, and the range of super-sensitivity is of about 0.6 km.

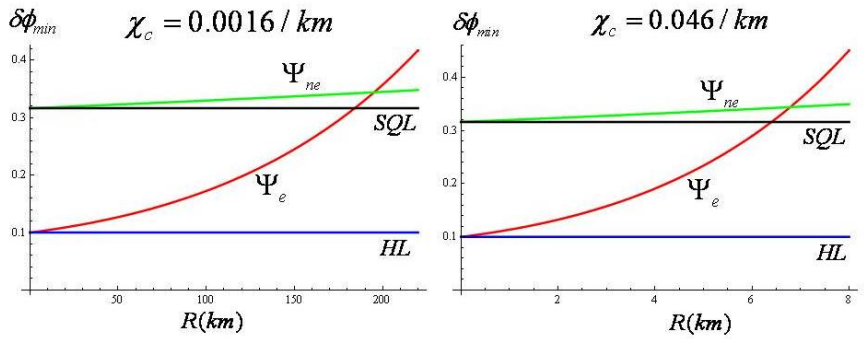

Figure 5.9: Phase estimation error as a function of the range to the target for a $N = 10$ entangled Ψ_e and non-entangled Ψ_{ne} sensors. The minimum value of the phase estimation error is smaller than for the $N = 2$ case, but the range of super-sensitivity is also smaller than for the $N = 2$ case.

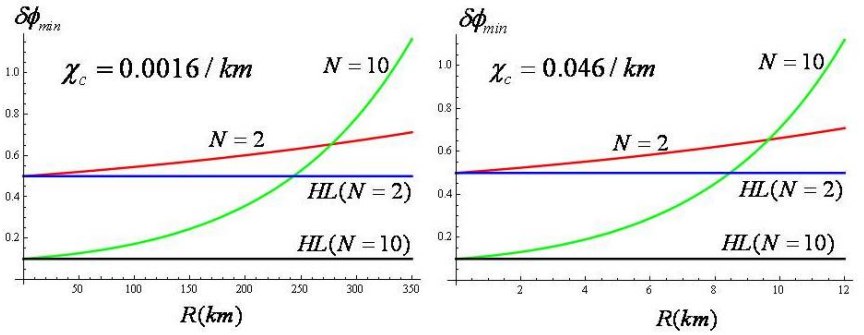

Figure 5.10: Phase estimation error for $N = 2$ and $N = 10$.

All these effects are a consequence of atmospheric attenuation. If the quantum interferometer systems could operate in a perfect vacuum for which $\chi_c = 0$, then the sensors using NOON states would operate at their Heisenberg limit regardless of the range to the target (and the sensors operating with non-entangled states would operate at their standard quantum limit at all values of R).

So far we have been talking about phase estimation, but these results can be easily generalized for the case of range-to-target estimation, the natural function of a radar system. The range-to-target estimation error can be approximated by:

$$\delta R \approx \frac{\lambda}{2\pi}\,\delta\phi \tag{5.39}$$

where λ is the wavelength of the photons. Therefore, all our observations for the behavior of $\delta\phi$ hold the same for δR.

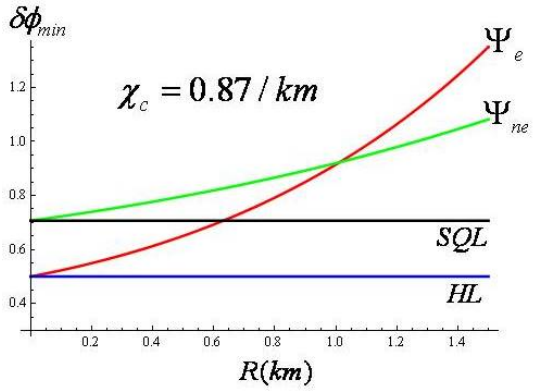

Figure 5.11: Atmospheric attenuation for the phase estimation error using visible light ($\lambda = 550$ nm) instead of microwaves.

One may find it surprising that if we use $\lambda = 3.2$ cm, then the range error in the supersensitivity regime will also be in the order of cm. It is not expected that a quantum radar will operate at this sensitivity when detecting incoming targets. Indeed, this analysis has considered the target as a perfectly reflective and static object, which allows for a very sensitive measurement. In a sense, the scenario discussed so far resembles the situation with the Lunar Laser Ranging Experiment, which is able to measure the distance from the Earth to the Moon with milimetric accuracy [109].

The fact that the super-sensitivity regime may reach up to 350 km suggests that long-range phase estimation may be *feasible* using quantum interferometry with NOON states. However, many issues remain problematic. For instance, we have assumed that the detectors have perfect sensitivity. In reality this is not the case, and the imperfect performance of the sensors involved will diminish the supersensitivity regime achievable by the system. In addition, the expressions derived present periodic divergences.

As a consequence, these observations make evident that long-range phase estimation using basic quantum interferometry with NOON states may be severely restricted due to the attenuating effects of the atmosphere. However, this only means that NOON states alone are not enough to build a robust interferometric quantum radar for practical applications.

5.2.5 ADAPTIVE OPTICS CORRECTION

As we have seen, because of atmospheric attenuation, the use of NOON states is not enough to guarantee supersensitivity on a quantum radar. To circumvent this problem, James Smith from the US Naval Research Laboratory developed an adaptive optics correction method that allows supersensitivity over ranges up to 5000 km and for atmospheres with significant variation in their electromagnetic properties [97].

The proposed atmospheric correction method is inspired by the *guide stars* correction technique, which is widely used in adaptive optics to improve the performance of telescopes [101]. In general, a turbulent atmosphere is not a homogeneous medium. This causes fluctuations on electromagnetic properties such as the optical refractive index. These variations are responsible for wavefront distortions that produce loss mechanisms such as beam spreading, beam wandering, and intensity fluctuations (scintillations). In astronomy, the correction of images of dim stars is accomplished using a nearby bright star as a reference to determine the shape of the distorted optical wavefronts. It is assumed that the light from both sources pass through the same portion of the atmosphere. The telescope uses a wavefront sensor to measure the distortions that the atmosphere has introduced to the incoming stellar light. Subsequently, a computer determines the optimal shape of an mirror that can correct for these distortions, and a flexible mirror is shaped accordingly.

This atmospheric correction technique can also be used to improve the performance of RF and laser radar [110, 111]. In the former case, the "guide stars" could be implemented using small electronic devices that produce electromagnetic radiation of fixed frequency and amplitude. These devices can be fired by artillery and could provide a mean to measure the refraction, attenuation, and other electromagnetic properties of the atmosphere along the line-of-sight path between the source and the detector. These values can be extrapolated over time and space to provide an approximate electromagnetic map of the atmosphere that surrounds the radar and the target. In addition, the adaptive optics system may be fed with historical information as well as with data measured from electromagnetic sources of opportunity.

The adaptive optics technique in a quantum radar introduces a phase shift ϕ_{ao} that can be controlled by the user. Then, neglecting the contribution from the small interferometer arm L_1, the corrected phase estimation error is given by:

$$\delta\phi^{(c)} \approx \frac{\sqrt{\frac{1}{2(\alpha_2^{(c)})^N} - \frac{1}{2} + \sin^2 N(\phi + \phi_{ao} - \phi_0^{(c)})}}{N\,|\sin N(\phi + \phi_{ao} - \phi_0^{(c)})|} \tag{5.40}$$

where the corrected dispersion phase shift is:

$$\phi_0^{(c)} \approx \frac{\omega}{c}\,\eta^{(c)}\,L_2 \tag{5.41}$$

the corrected transmittance of the medium is:

$$\alpha_2^{(c)} = e^{-\chi^{(c)} L_2} \tag{5.42}$$

and the parameters $\eta^{(c)}$ and $\chi^{(c)}$ are the corrected refractive and attenuation constants of the medium, respectively.

As made evident in the analysis of atmospheric quantum interferometry, the phase estimation error diverges when the sine function in the denominator becomes zero. Therefore, the adaptive optics technique also requires for the user to implement a controlled phase delay ϕ_{ao} in a way such

that $\delta\phi^{(c)}$ is minimum when we estimate the range to the target L_2. That is, ϕ_{ao} has to be chosen in a way such that the sine function in the denominator becomes 1 or -1:

$$N(\phi + \phi_{ao} - \phi_0^{(c)}) = \frac{\pi}{2}, \frac{3\pi}{2}, ..., \frac{(2n+1)\pi}{2} \tag{5.43}$$

Therefore:

$$\delta\phi^{(c)} \approx \frac{1}{N}\sqrt{\frac{1}{2(\alpha_1^{(c)})^N} + \frac{1}{2}} \tag{5.44}$$

and similarly for the non-entangled case:

$$\delta\phi_{ne}^{(c)} \approx \frac{1}{\sqrt{N}}\sqrt{\frac{1}{2\,\alpha_1^{(c)}} + \frac{1}{2}} \tag{5.45}$$

Unfortunately, the adaptive optics technique for quantum interferometry requires of estimated values for several parameters, including the range to target L_2. In a sense, the adaptive optics technique for quantum interferometry implements an information fusion and filtering process that improves the values of the estimated variables. This means that adaptive-optics interferometric quantum radar may be better suited to discriminate or identify targets that have already been detected by other means.

In any event, it is expected that the use of adaptive optics in an interferometric quantum radar will be able to increase the supersensitivity regime to well over 1000 km [97].

5.3 QUANTUM ILLUMINATION

Quantum Illumination is a revolutionary photonic standoff quantum sensing technique developed by Seth Lloyd at MIT [67]. This technique enhances the sensitivity of photodetection of light in noisy and lossy environments. By design, quantum illumination is not restricted to any specific frequency, so in principle, it could work in the radar X-band regime.

The setup is similar to the case of single-photon and entangled-photons quantum radar discussed above. We assume a target that is illuminated by a quantum illumination device. The goal is to detect the presence of the target even in a noisy and lossy environment. As we will see, entanglement increases the sensitivity of the detection system. Quite amazingly, the enhancement provided by quantum illumination using entangled photons is only observed in a noisy and lossy environment.

Quantum illumination has a different detection strategy than an interferometric quantum radar. In the present case, one does not perform phase measurements, but simple photon detection counts are enough. Nevertheless, this is not an easy task. As we will discuss later, although the measurement of entangled photons is physically realizable, it is a very challenging procedure.

The interaction between the signal photons and the target can be modeled as a beam splitter with small reflectivity η. Noise is injected into the system with average photon number b into each

optical mode (frequency or polarization). Although it is not necessary, we can assume that $b \ll 1$ to simplify the mathematical formalism, but the general results remain valid for arbitrary b. The $b \ll 1$ case corresponds to the scenario where the thermal radiation is substantially below the signal photon energies.

If the photodetector is characterized by a bandwidth W and a temporal detection window T, then, in principle, the device can distinguish between d different radiation modes:

$$d \approx W \times T \tag{5.46}$$

Furthermore, we assume that T is small enough so that at most one noise photon is observed per detection event, that is:

$$d \times b \ll 1 \tag{5.47}$$

We consider two modes of operation, when the signal photons are not entangled and when they are entangled. These two modes will be analyzed and compared in what follows.

5.3.1 NON-ENTANGLED PHOTONS

Let us first assume the case of non-entangled signal photons. Two cases are possible: (1) the target is not within range, so it will be undetectable by the system (but it is possible that the system will record a false positive), and (2) the target is within range, and there is some probability that the system will succeed in detecting it. To analyze the performance of quantum illumination we need to compute the probabilities for all these events.

Case (1): No Target Within Range

If the target is not within range then the signal photon will be lost. The only photons detected by the system are noise photons which can be described by:

$$\rho_1 = \underbrace{\rho_b \otimes \rho_b \otimes \ldots \otimes \rho_b}_{\text{d states}} \tag{5.48}$$

Indeed, there is one possible noise photon state with b photons on average (ρ_b) for each of the d possible optical modes. We can rewrite ρ_1 as:

$$\rho_1 = \bigotimes_{k=1}^{d} \rho_b^{(k)} \tag{5.49}$$

where:

$$\rho_b^{(k)} = |k\rangle\langle k| \tag{5.50}$$

is the density operator for a single noise photon in the mode k.

Because the average number of photons per detection event is small, $db \ll 1$, we can approximate ρ_1 as:

$$\rho_1 \approx (1 - db)|0\rangle\langle 0| + b\sum_{k=1}^{d}|k\rangle\langle k| \tag{5.51}$$

where $|k\rangle$ is a single-photon state in the mode k and the vacuum state is represented by $|0\rangle$. That is, there is a probability $(1 - db)$ that we will not measure any signal, and a probability b that we will measure one out of d possible noise photons.

The accuracy of the approximation can be computed through the norm distance, which results in:

$$\left\|\rho_1^{approx} - \rho_b \otimes \rho_b \otimes ... \otimes \rho_b\right\|_1 \approx d^2b^2 + \mathcal{O}(b^3) \tag{5.52}$$

and therefore, the approximate expression is correct as long as we remain in the lowest order of b.

Case (2): Target Within Range

If the target is within range of the quantum illumination system, then there is a probability η that we will measure a thermalized signal photon $\tilde{\rho}$, and a probability $(1 - \eta)$ that we will just measure noise ρ_1. That is:

$$\rho_2 = (1 - \eta)\rho_1 + \eta\tilde{\rho} \tag{5.53}$$

where ρ_1 is given by Equation (5.51). However, it can be shown that:

$$\eta\left\|\rho - \tilde{\rho}\right\|_1 \approx \eta db + \mathcal{O}(\eta b^2) \tag{5.54}$$

where ρ is the signal photon state. In the regimen of interest we can ignore terms $O(\eta b)$ and as a consequence:

$$\tilde{\rho} \approx \rho \tag{5.55}$$

which leads to:

$$\rho_2 \approx (1 - \eta)\rho_1 + \eta\rho \tag{5.56}$$

Detection Probability

We have a probabilistic problem with two possible hypothesis: (TR) there is a target within range or (NTR) there is no target within range. To discriminate between these two hypothesis we need to repeat the probabilistic experiment several times. That is, we need to repeatedly send signal photons towards a region of space to determine if there is a target.

Using the expressions for ρ_1 and ρ_2 we can determine the probabilities of detecting a target within range, measuring a false positive (detecting a target that is not there), or the probability that no target is present in the region of interest.

Thus, for instance, the probability of a false positive is the probability of positive detection "+" of a target that is not within range, NTR. This is obtained from ρ_1 by computing the probability of measuring one of the d noise photons in the mode k. This probability is given by:

$$p(+|NTR) = b \tag{5.57}$$

On the other hand, the probability of getting a negative detection "−" (that is, the probability of successfully concluding that there is no target within range) is given by:

$$p(-|NTR) = 1 - b \tag{5.58}$$

A similar analysis follows for the case where there is a target within range, TR, and the entire set of probabilities are:

$$\begin{aligned} p(-|NTR) &= 1 - b \\ p(+|NTR) &= b \\ p(-|TR) &= (1-b)(1-\eta) \\ p(+|TR) &= b(1-\eta) + \eta \end{aligned} \tag{5.59}$$

which clearly satisfy the probability normalization conditions:

$$\begin{aligned} NTR: &\quad p(-|NTR) + p(+|NTR) = 1 \\ TR: &\quad p(-|TR) + p(+|TR) = 1 \end{aligned} \tag{5.60}$$

The number of times we need to repeat the probabilistic experiment is the number of photons that we need to send towards a region of space to determine if a target is within range. This number depends on the signal-to-noise ratio (SNR) of the quantum illumination system and can be estimated to be:

$$\begin{aligned} SNR &\approx \frac{p(+|TR)}{p(+|NTR)} \\ &\approx \frac{b(1-\eta)+\eta}{b} \\ &\approx 1 - \eta + \frac{\eta}{b} \\ &\approx \mathcal{O}(\eta/b) \end{aligned} \tag{5.61}$$

Depending on the value of SNR, two regimes of interest have to be considered: (H) a High SNR regime in which SNR>1, and (L) a low SNR regime in which SNR<1. For the first case, the number of photons required to discriminate between the two possible hypotheses is given by N_H and is approximated by:

$$N_H \approx \mathcal{O}(1/\eta) \tag{5.62}$$

On the other hand, for the low SNR regime, the number of photons necessary to discriminate between the hypotheses is denoted by N_L and given by:

$$N_L \approx \mathcal{O}(8b/\eta^2) \tag{5.63}$$

As expected, N_H is smaller than N_L:

$$N_L \approx \mathcal{O}(8b/\eta^2) \approx \mathcal{O}(b/\eta) \times \mathcal{O}(1/\eta) \approx \mathcal{O}(b/\eta) \times N_H > N_H \tag{5.64}$$

in the low SNR regime ($b > \eta$).

5.3.2 ENTANGLED PHOTONS

Let us now consider quantum illumination using entangled photons. As usual, we need to generate entangled signal and ancilla photon states. The signal photon (S) is sent towards a target and the ancilla photon (A) is kept within the radar system. Both photons are entangled in their momentum degrees of freedom over all possible modes d:

$$|\Psi\rangle^{(e)} = \frac{1}{\sqrt{d}} \sum_{k=1}^{d} |k\rangle_S |k\rangle_A \tag{5.65}$$

Recall that $|k\rangle$ represents single photon states in the mode k. As a consequence, $|\Psi\rangle^{(e)}$ represents a 2 photon system. The associated density matrix for the entangled state is:

$$\rho^e = |\Psi\rangle^{(e)(e)}\langle\Psi| \tag{5.66}$$

As in the case for non-entangled photons, we have two cases to consider: (1) when a target is not within range and (2) when the target is within range.

Case (1): No Target Within Range

If there is no target within range, then the system will just be able to detect noise photons. The signal state is considered lost and then it can be approximated by ρ_1 as described in the case for non-entangled photons. At the same time, the ancilla state goes to the completely mixed state:

$$\begin{aligned} \rho_1^e &\approx \rho_1 \otimes \frac{I_A}{d} + \mathcal{O}(b^2) \\ &\approx \left[(1 - db)|0\rangle_S\langle 0| + b \sum_{k=1}^{d} |k\rangle_S\langle k| \right] \otimes \frac{I_A}{d} + \mathcal{O}(b^2) \\ &\approx [(1 - db)|0\rangle_S\langle 0| + bI_S] \otimes \frac{I_A}{d} + \mathcal{O}(b^2) \end{aligned} \tag{5.67}$$

and I_S and I_A are the identity operators on the single photon Hilbert space for the system and ancilla photons, respectively:

$$I_X = \sum_{k=1}^{d} |k\rangle_X\langle k| \tag{5.68}$$

for $X = S, A$.

Case (2): Target Within Range

If the target is within range, the system will detect the original entangled state with probability η, and it will detect a noise photon ρ_1^e with probability $(1 - \eta)$. As before, the signal state will be thermalized, but it can be represented by the original state if we are kept within terms of the order of $\mathcal{O}(b, b^2)$. That is:

$$\rho_2^e = (1 - \eta)\rho_1^e + \eta\rho^e + \mathcal{O}(\eta b, \eta b^2) \tag{5.69}$$

where once again we have replaced the thermalized density operator $\tilde{\rho}^e$ by ρ^e, an operation that can be done in the approximation regime under consideration.

Detection Probability

As in the case with non-entangled photons, we need to discriminate between two hypothesis. The associated probabilities can be computed from ρ_1^e and ρ_2^e. Then, the probability of positive detection "+" of a target that is not within range, NTR, is obtained from ρ_1^e and is given by:

$$p_e(+|NTR) = \frac{b}{d} \tag{5.70}$$

Similarly, the probability for a negative detection "−" (that is, correctly concluding that there is no target within range) is:

$$p_e(-|NTR) = 1 - \frac{b}{d} \tag{5.71}$$

These two equations make clear the effect of entanglement, as they are the same for the case of non-entangled photons but making the replacement:

$$b \longrightarrow \frac{b}{d} \tag{5.72}$$

In other words, the noise b is effectively reduced by a factor d.

A similar conclusion follows for the case where the target is within range. The entire set of probabilities is then given by:

$$\begin{aligned} p_e(-|NTR) &= 1 - \frac{b}{d} \\ p_e(+|NTR) &= \frac{b}{d} \\ p_e(-|TR) &= \left(1 - \frac{b}{d}\right)(1-\eta) \\ p_e(+|TR) &= \frac{b}{d}(1-\eta) + \eta \end{aligned} \tag{5.73}$$

which clearly satisfy the probability normalization conditions:

$$\begin{aligned} NTR: &\quad p_e(-|NTR) + p_e(+|NTR) = 1 \\ TR: &\quad p_e(-|TR) + p_e(+|TR) = 1 \end{aligned} \tag{5.74}$$

For the entangled-photons case, the signal-to-noise ratio is given by:

$$SNR^e \approx \mathcal{O}(\eta/b \times d) \tag{5.75}$$

which reflects the fact that the entanglement has increased the SNR by a factor of d.

Once again, two regimes appear, a (H) high SNR regime where SNR$>$ 1 and a (L) low SNR regime in which SNR$<$ 1. The number of photons necessary to determine the presence of a target in the high SNR regime is given by:

$$N_H^e \approx \mathcal{O}(1/\eta) \tag{5.76}$$

On the other hand, for the low SNR regime, the number of photons necessary to discriminate if a target is within range is:

$$N_L^e \approx \mathcal{O}(8b/d\eta^2) \tag{5.77}$$

5.3.3 SENSITIVITY COMPARISON

All the relevant results for quantum illumination are condensed in Table 5.2. We can conclude that the use of entangled states increases the signal-to-noise ratio by a factor d:

$$\frac{SNR^e}{SNR} \approx d > 1 \implies SNR^e > SNR \tag{5.78}$$

The advantage of a higher SNR is its effect on the number of photons necessary to elucidate the presence or absence of a target in a given region of space. As seen in the table, for the high SNR regime, entanglement does not improve the performance of the system. It is only in the low SNR regime where entanglement provides an advantage over single-photon pulses. Indeed:

$$\frac{N_L^e}{N_L} \approx \frac{1}{d} < 1 \implies N_L^e < N_L \tag{5.79}$$

Table 5.2: Sensitivity of Quantum Illumination for Entangled and Non- Entangled States.

	Non-Entangled Photons	Entangled Photons
$p(-\|NTR)$	$1-b$	$1-b/d$
$p(+\|NTR)$	b	b/d
$p(-\|TR)$	$(1-b)(1-\eta)$	$(1-b/d)(1-\eta)$
$p(+\|TR)$	$b(1-\eta)+\eta$	$(1-\eta)b/d+\eta$
SNR	$\mathcal{O}(\eta/b)$	$\mathcal{O}(\eta d/b)$
High SNR	$\eta/b > 1$	$\eta d/b > 1$
N_H	$\mathcal{O}(1/\eta)$	$\mathcal{O}(1/\eta)$
Low SNR	$\eta/b < 1$	$\eta d/b < 1$
N_L	$\mathcal{O}(8b/\eta^2)$	$\mathcal{O}(8b/\eta^2 d)$

Let us recall that an *ebit* is one unit of bipartite entanglement. In other words, an ebit is the amount of entanglement that characterizes a maximally entangled state made of 2 qubits. Thus, a 2-qubit Bell state contains 1 ebit of entanglement. And in general, a maximally entangled state made of two systems of dimension d has $m = \log_2 d$ ebits of bipartite entanglement. Therefore,

quantum illumination in the low SNR regime increases the sensitivity of the detector by a factor 2^m. That is, considering entanglement as a resource, quantum illumination offers an exponentially large improvement on the sensitivity of the detection system.

It is also important to observe that, within the approximation considered, the reflected signal photon can be considered as fully thermalized. In other words, any possible level of entanglement between the signal and ancilla photons is annihilated by thermal effects. But even so, quantum illumination is able to extract the correlation between these states to enhance detection. By any means, this is a rather surprising and unexpected result.

As previously mentioned, the treatment presented here is limited to the low-temperature regime which corresponds to a small number of noise photons per mode ($b \ll 1$). However, quantum illumination has been shown to work even in the high-temperature case [67]. The final result is the same: sensitive performance is enhanced in the low SNR limit by a term exponentially large in the number of ebits of entanglement used for the photon states.

Finally, it is worth noticing that the calculation of detection probabilities presented here was limited to the use of optimal single-shot measurements [44]. That is, we just computed the projection of the desired outcome over the quantum state. However, a formal treatment has to involve the *Chernoff Quantum Bound* which determines the optimal strategy that minimizes the total probability of error during the discrimination of two different quantum states when one can access an asymptotically large number of copies [4, 12]. A formal estimation of the probabilities using the Chernoff bound can be found in Lloyd's paper and leads to the same results presented here [67].

5.3.4 GAUSSIAN STATES

The study of quantum illumination can be extended for the case of entangled Gaussian or coherent states [48, 94]. In the number-ket representation, a two-mode (system S + ancilla A) monochromatic Gaussian states takes the form:

$$|\Psi\rangle_{SA} = \sum_{n=0}^{\infty} \sqrt{\frac{N_S^n}{(N_S+1)^{n+1}}} |n\rangle_S |n\rangle_A \tag{5.80}$$

where N_S is the average number of photons per mode [73, 92]. The above expression is given in terms of the number-ket representation. That is, the states $|j\rangle$ and $|i\rangle$ represent states of j and i photons, respectively, with some common momentum k.

It can be shown that by making an optimal joint measurement on the entangled Gaussian state, quantum illumination offers a 6 dB improvement in the error probability over a coherent state system in the lossy, noisy, low-brightness scenario [48, 94].

In addition, it has been found that quantum illumination with entangled Gaussian states brings increased performance in the angular resolution for the reliable discrimination between one or two possible targets sustaining a small angle as viewed by the transmitter [37].

5.3.5 ENTANGLED MEASUREMENTS

Arguably, the most challenging aspect of implementing a quantum illumination radar system is the ability to perform detection of entangled states. These types of measurements have been successfully performed in the laboratory, but they are difficult to accomplish [18, 28]. Indeed, the detector has to verify that the signal and ancilla photons are correlated in their frequency and time of arrival [67].

The correlation on their time of arrival may be difficult if the range to the target is unknown. In such a case, the quantum illumination system has to delay the ancilla photon across a large number of times until it can find a match. This added complexity suggests that perhaps quantum illumination is best suited to discriminate the number of possible targets once a positive detection has been established using traditional radar or other sensing systems.

Furthermore, the detector has to verify the energy correlation without distinguishing between the different possible modes k:

$$\omega_k^S + \omega_k^A = \omega \tag{5.81}$$

where ω is the frequency of the original photon used to create the entangled pair through parametric down-conversion.

In spite of these challenges, a feasible quantum illumination detector has been recently proposed in the scientific literature [38, 39].

5.4 QUANTUM RADAR JAMMING

As we discussed in Chapter 4, active radar countermeasures include the use of jamming to hide the presence of a target. In this regard, it is important to mention that quantum radar appears to be more robust against the effects of a jamming signal. Indeed, let us recall that both quantum radar proposals, the interferometric quantum radar and quantum illumination, take advantage of the same principle to achieve higher performance. That is, these systems perform collective measurements after highly correlated states have been injected into the system. These correlations can be exploited to prevent signal photons to get lost in noise or jamming signals.

Let us consider, for example, the case of quantum illumination using non-entangled photons. The signal-to-jam ratio will be approximately given by:

$$SJR_{ne} \approx \mathcal{O}(\eta/j) \tag{5.82}$$

where η is the reflectivity of the target and j is the average number of photons injected by the jammer into the system.

On the other hand, if we use entangled photons, the signal-to-jam ratio is now given by:

$$SJR_e \approx \mathcal{O}(\eta/j \times 2^m) \tag{5.83}$$

where m is the number of ebits of entanglement in the photon states.

As a consequence, entangled quantum illumination is less likely to be jammed than a quantum radar operating with non-entangled photons. That is, in terms of entanglement as a resource, a quantum radar is exponentially less likely to be jammed than a classical radar.

5.5 PHYSICAL REALIZATION OF A QUANTUM RADAR

To date, quantum radar remains an intriguing theoretical proposal. The hardware that enables quantum radar transmission and reception remains to be implemented. While the generation and detection of entangled photons in the visible regime is done quite easily with today's technology, it is not yet possible to perform these operations with photons in the microwave range.

However, some ideas have been proposed towards the generation and detection of photons in the radar region. Some of these will be briefly discussed in what follows.

5.5.1 TRANSMITTER

The key element in the quantum radar transmitter is the generation of entangled photons in the microwave regime. Parametric down-conversion is the most widely known technique to entangle photons in the visible regime [84]. This entanglement generation technique uses a non-linear crystal that splits an incoming photon into two entangled photons.

A less known entanglement generation strategy is the use of semiconductor nanostructures. In particular, the decay of bi-excitonic states in quantum dots involve *inter-band transitions* between valence and conduction bands that generate entangled photons with frequencies in the visible range [5, 99].

However, a similar technique has been proposed for the generation of entangled photons in the microwave regime [27]. This strategy produces entangled photons produced by *intra-band transitions* of conduction band electrons. Photon-assisted tunneling experiments have shown that these transitions couple to microwave photons [108]. As a consequence, microwave photons are produced from spontaneous downward transitions between single-particle levels in a quantum dot.

This entanglement generation scheme can be accomplished by using an array of four quantum dots connected to two electron reservoirs and inserted inside a cylindrical microwave resonator as shown in Figure 5.12 [27]. For convenience, the dots are labeled (T) top, (B) bottom, (L) left, and (R) right. The two lateral dots, L and R, are used to provide unique initial and final states for an electron in the conduction band. On the other hand, the T and B dots provide two decay paths.

The electron transitions are shown in Figure 5.13. The electron begins in the quantum dot L and tunnels into excited states of the dots T and B. The state at this stage can be assumed to be symmetric and given by:

$$|\psi\rangle = \frac{1}{\sqrt{2}}\left(|T_1\rangle + |B_1\rangle\right) \tag{5.84}$$

That is, the electron can be in the excited state of T or B with equal probability. Then, the electron state decays into the ground states of T or B and in the process emits two photons. If the electron decays from T, then both photons have left-handed circular polarization states. On the other hand, if the electron decays from B, then both photons have right-handed circular polarization states. Then, the quantum state at this stage can be described as:

$$|\Psi\rangle = \frac{1}{\sqrt{2}}\left(|T_0\rangle \otimes |++\rangle + |B_0\rangle \otimes |--\rangle\right) \tag{5.85}$$

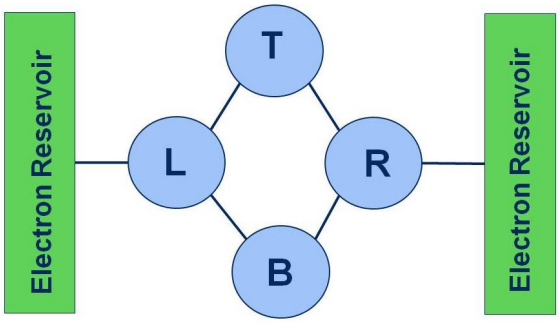

Figure 5.12: Arrangement of four quantum dots for a microwave photon entangler [27].

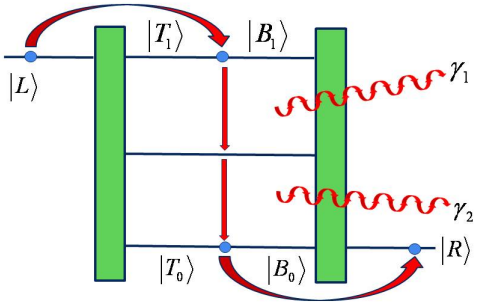

Figure 5.13: Electron transitions in the quantum dots that generate a pair of entangled microwave photons [27].

which can be rewritten as:

$$|\Psi\rangle = \frac{1}{\sqrt{2}}\left(|\psi_+\rangle|\Phi_+\rangle + |\psi_-\rangle|\Phi_-\rangle\right) \tag{5.86}$$

where the electron states are:

$$|\psi_\pm\rangle = \frac{1}{\sqrt{2}}\left(|T_0\rangle \pm |B_0\rangle\right) \tag{5.87}$$

and the photonic states are:

$$|\Phi_\pm\rangle = \frac{1}{\sqrt{2}}\left(|++\rangle \pm |--\rangle\right) \tag{5.88}$$

The coupling with the dot R serves to disentangle the photons from the electron states. Furthermore, the antisymmetric state $|\psi_-\rangle$ is suppressed due to destructive interference. Then, the state of the

photons is found by finding the projection of the state $|\Psi\rangle$ with $|\psi_+\rangle$. That is, the outgoing photons are described by:

$$\langle\psi_+|\Psi\rangle \propto |\Phi_+\rangle = \frac{1}{\sqrt{2}}\left(|++\rangle + |--\rangle\right) \tag{5.89}$$

which is a state with maximal entanglement.

5.5.2 RECEIVER

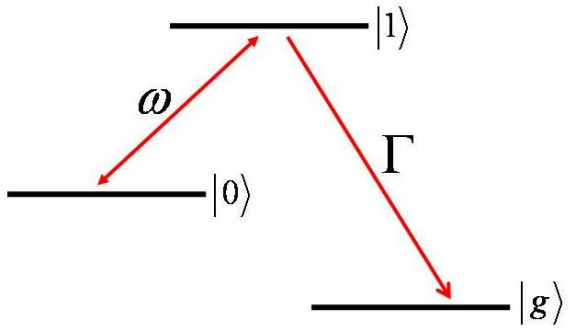

Figure 5.14: Energy levels and decay paths of proposed microwave sensing metamaterial [88, 89]. The device absorbs a photon of frequency ω and has a decay rate Γ to the long-lived stable ground state $|g\rangle$.

Photon detection is a well known technology widely used in the visible and near-visible regimes [19, 25, 83, 87]. However, the design and development of single photon detectors in the microwave regime present a large number of theoretical and experimental challenges [88, 89]. Some of these difficulties include the unavailability of cryogenic linear amplifiers capable of working with low photon number counts, as well as the problem of synchronizing the detection process with the arrival of the measured field.

However, a novel sensing technique has recently been proposed that circumvents most of the problems associated to the task of detecting single photons in the microwave regime [88, 89]. The idea rests in the design of a novel metamaterial[4]. The proposed metamaterial is designed to absorb microwave photons and can be used to perform single-shot photodetection.

The proposed design of the system consists of a linear waveguide coupled to a set of three-level photo-absorbing particles in arbitrary positions. The three energy levels of the absorber are depicted in Figure 5.14. It can be shown that these absorbers are able to capture a microwave photon from the initial state $|0\rangle$ and transition to the excited state $|1\rangle$. Subsequently, the state decays into a long-lived stable ground state $|g\rangle$ with a decay rate Γ. The photon counting then boils down to a counting of

[4]Metamaterials are artificially engineered materials designed to have specific physical properties. Furthermore, the mechanical and electromagnetic properties of a metamaterial are a consequence of its molecular structure rather than its composition.

those absorbers found in the ground state $|g\rangle$. Therefore, this detector resembles photographic film in the sense that once a photon has been absorbed by the metamaterial, the device is changed into a stable and mesoscopically distinguishable state.

One potential problem with the proposed design is its small operational bandwidth, which has to be small in comparison to the time it takes to absorb a photon. That is:

$$\Delta\omega < \frac{1}{\Gamma} \tag{5.90}$$

However, this may not be an important issue in its application towards a quantum radar receiver.

Another potential problem is that if the decay process $1 \rightarrow 0$ takes place, then there will be incoming photons that will not be counted. However, recent experiments appear to suggest that this process happens with a rate of a few MHz, and therefore it will affect long wavepackets [45]. It remains to be seen if this issue could present a serious limitation to the use of these devices for quantum radar applications in the X-band.

5.6 SUMMARY

Quantum radar is a standoff sensor that could be used to beat the standard quantum limit of current sensing devices. Two major designs have been proposed: interferometric quantum radar and quantum illumination. The hardware to enable quantum radar is still in the design process, but some work has been done towards the development of entanglement generators and photodetectors able to operate in the radar region.

Unfortunately, to date it is very difficult to predict the performance of a quantum radar in an operational environment. First, most quantum radars proposals presume a perfectly reflecting target oriented in the specular direction. Second, we cannot use the standard definition of the radar cross section.

Indeed, regardless of the underlying system or states used, the important point of quantum radars is that, as their name suggests, they operate on the quantum regime. That is, they use a relatively small number of photons. As a consequence, theoretical consistency requires that the electromagnetic fields have to be described as quantum fields. Thus, the radar pulse is not described by classical electrodynamics, but by quantum electrodynamics. Therefore, just as the radar cross section was defined through Maxwell equations for classical fields, it is necessary to define a quantum radar cross section σ_Q based on quantum electrodynamics.

CHAPTER 6

Quantum Radar Cross Section

So far our discussion on quantum radar has ignored the geometry and composition of the target. In practice, of course, targets will present intricate geometries that will reflect the incoming photons on a complex pattern. Within the realm of classical radar theory, the radar cross section σ_C is used to determine the "radar visibility" of a specific target.

We recall from Chapter 4 that σ_C is defined as the ratio between the power reflected back to the receiver per unit solid angle and the incident power density. As we discussed, σ_C emerges as a critical concept in classical radar theory, as it offers an objective measure of performance for the radar system and the stealth capabilities of modern weapon platforms.

As quantum radars emit a handful of photons at the time, the radar-target interaction in this regime is described through photon-atom scattering processes governed by the laws of quantum electrodynamics. As such, it is theoretically inconsistent to use the same σ_C to characterize the visibility of a target illuminated with a quantum radar. As a consequence, there is a need to develop the concept of a *quantum radar cross section* σ_Q to objectively measure the "quantum radar visibility" of a specified target. That is, we need to define σ_Q to analyze the performance of quantum radars in the scenario where the targets are not perfectly reflective objects and the radar signal is made of a handful of photons [61].

6.1 DESIRED FEATURES OF σ_Q

There are several conceptual challenges that make it difficult to define σ_Q. For instance, energy in the classical regime is proportional to the amplitude. But in the quantum realm the energy of a single photon is proportional to its frequency. Furthermore, as we discussed in Chapter 2, photons are nonlocalizable.

However, we can attempt to establish the basic properties that are desired in a conceptually robust definition of σ_Q. In simple analogy to the classical radar cross section, the quantum radar cross section should have these properties:

Operational Meaning: The reason to define σ_Q in the first place is to have an objective measure of the quantum radar visibility of a target.

Energy Conservation: As with σ_C, σ_Q should entail energy conservation in the optical regime when absorption effects are ignored.

Strong Dependencies: Similarly, to σ_C, it is desirable that σ_Q strongly depends on properties of the target: geometry (absolute and relative size, shape and orientation), as well as its composition (material properties).

Weak Dependencies: In the same manner, it is desired that σ_Q is approximately independent on the properties of the radar system. That is, σ_Q should depend very weakly on the strength, architecture, physical implementation, and range of the radar system.

Multiplatform Comparison: To better understand the advantages and disadvantages of quantum radars, it would be desirable to be able to directly compare σ_C and σ_Q.

Asymptotic Behavior: In the large photon limit, the quantum realm gives way to classical physics and σ_Q should be proportional to σ_C:

$$\lim_{n_\gamma \to \infty} \sigma_Q \propto \sigma_C \tag{6.1}$$

6.2 INCIDENT AND SCATTERED QUANTUM FIELDS

As we discussed in Chapter 3, it is possible to describe all the physical properties of specular reflections exclusively using QED processes of absorption and emission of photons by the atoms in a mirror [62]. Following an interferometric analysis, we found that the intensity measured by a detector after a photon is reflected by N atoms is given by:

$$\langle \hat{I}_s(\mathbf{r}_s, \mathbf{r}_d, t) \rangle = \frac{1}{N} \left| \sum_{i=1}^{N} \Psi_\gamma^{(i)}(\Delta R_i, t) \right|^2 \tag{6.2}$$

where the photon wave functions are:

$$\Psi_\gamma^{(i)}(\Delta R_i, t) = \frac{\mathcal{E}_0}{\Delta r_{id}} \Theta(t - \Delta R_i/c)\, e^{-(i\omega + \Gamma/2)(t - \Delta R_i/c)} \tag{6.3}$$

with:

$$\mathcal{E}_0 = -\frac{\omega^2\, |\hat{\vec{\mu}}|_{ab}\, \sin\eta}{4\pi\epsilon_0\, c^2\, \Delta r_{id}} \tag{6.4}$$

and Γ represents the inverse of the lifetime of the excited state of the atom:

$$\Gamma \equiv \frac{1}{\tau} = \frac{1}{4\pi\epsilon_0} \frac{4\omega^3 |\hat{\vec{\mu}}|_{ab}^2}{3\hbar c^3} \tag{6.5}$$

In the above expressions ω is the frequency of the incoming photon, and η is the angle between the electric dipole moment of the atom $\vec{\mu}$ and $\Delta\mathbf{r}_{id} = \mathbf{r}_i - \mathbf{r}_d$ is the distance between the i^{th} atom and the detector. In the context of quantum radar, ΔR_i is the total interferometric distance from the radar transmitter to the target, and from the target to the radar receiver.

For monostatic radars the source and the detector are at the same spatial location:

$$\mathbf{r}_s = \mathbf{r}_d \tag{6.6}$$

and therefore

$$\begin{aligned} \Delta R_i &= \Delta r_{si} + \Delta r_{id} \\ &= |\mathbf{r}_s - \mathbf{r}_i| + |\mathbf{r}_i - \mathbf{r}_d| \\ &= 2|\mathbf{r}_i - \mathbf{r}_d| \end{aligned} \tag{6.7}$$

where $\mathbf{r}_s$, $\mathbf{r}_d$, and $\mathbf{r}_i$ are the positions of the source, the detector, and the i^{th} atom, respectively.

From an operational point of view, the definition of σ_Q has to be able to provide an objective measure of the quantum radar visibility of the target. Therefore, σ_Q has to depend explicitly on $\langle \hat{I}_s(r, \theta, \phi, t) \rangle$, the scattered intensity at the receiver:

$$\sigma_Q \propto \langle \hat{I}_s(r, \theta, \phi, t) \rangle \tag{6.8}$$

because in the large photon limit:

$$\lim_{n_\gamma \to \infty} \langle \hat{I}_s(r, \theta, \phi, t) \rangle \propto |\mathbf{E}_{s@r}|^2 \tag{6.9}$$

On the other hand, the resulting average intensity incident over all the N atoms that make the target is (assuming the target behaves as a photodetector):

$$\begin{aligned} \langle \hat{I}_i(\mathbf{r}_s, t) \rangle &= \frac{1}{N} \sum_{i=1}^{N} \left| \Psi_\gamma^t(\Delta r_{si}, t) \right|^2 \\ &= \frac{1}{N} \sum_{i=1}^{N} \left(\frac{\mathcal{E}_0}{\Delta r_{si}} \right)^2 \left| \Theta(t - \Delta r_{si}/c)\, e^{-(i\omega + \Gamma/2)(t - \Delta r_{si}/c)} \right|^2 \\ &\approx \frac{1}{N} \left(\frac{\mathcal{E}_0}{R} \right)^2 \sum_{i=1}^{N} \left| \Theta(t - R/c)\, e^{-(i\omega + \Gamma/2)(t - R/c)} \right|^2 \end{aligned} \tag{6.10}$$

where we have presumed that in the region of interest:

$$\Delta r_{si} = |\mathbf{r}_s - \mathbf{r}_i| \approx R \quad \forall i \tag{6.11}$$

It is important to note that we can make this approximation because the exponential terms in the equation of $\langle \hat{I}_i(\mathbf{r}_s, t) \rangle$ do not form an interference pattern. Indeed, the absolute value is inside the summation symbol. In other words, there is only one possible path from the emitter to the target.

The Θ step function merely indicates that the signals will not propagate faster than the speed of light. With this understanding, we can remove it from the equation to simplify the notation. Therefore:

$$\langle \hat{I}_i(\mathbf{r}_s, t) \rangle \approx \left(\frac{\mathcal{E}_0}{R} \right)^2 e^{-\Gamma(t - R/c)} \tag{6.12}$$

and as a consequence, the integration over the orthogonal projected area of the target gives:

$$\int_{T_\perp(\theta,\phi)} \langle \hat{I}_i(\mathbf{r}_s, t)\rangle \, dS \approx A_\perp(\theta,\phi)\, \langle \hat{I}_i(\mathbf{r}_s, t)\rangle \tag{6.13}$$

If we ignore absorption effects, energy conservation in the optical regime requires that all the incident energy has to be reflected in some direction. Thus, we can derive expressions similar to those obtained in Section 4.9. That is, integrating the position of the detector over a spherical surface S_{R_d} of radius R_d:

$$\int_{T_\perp(\theta,\phi)} \langle \hat{I}_i(\mathbf{r}_s, t)\rangle \, dS \approx \lim_{R_d\to\infty} \int_{S_{R_d}\supset T} \langle\, \hat{I}_s(\mathbf{r}_s, \mathbf{r}_d, t)\rangle \, R_d^2 \, d\Omega_d \tag{6.14}$$

which can be approximated by:

$$A_\perp(\theta,\phi)\, \langle \hat{I}_i(\bar{\mathbf{r}}_t, t)\rangle \approx \lim_{R_d\to\infty} \int_0^{2\pi}\int_0^{\pi} \langle\, \hat{I}_s(\mathbf{r}_s, \mathbf{r}_d, t)\rangle \, R_d^2 \, \sin\theta \, d\theta \, d\phi \tag{6.15}$$

6.3 OPERATIONAL DEFINITION OF σ_Q

In analogy to σ_C, it is reasonable to define σ_Q as:

$$\sigma_Q \equiv \lim_{R\to\infty} 4\pi R^2 \, \frac{\langle \hat{I}_s(\mathbf{r}_s, \mathbf{r}_d, t)\rangle}{\langle \hat{I}_i(\mathbf{r}_s, t)\rangle} \tag{6.16}$$

and if we assume energy conservation in the optical regime, then σ_Q for a monostatic quantum radar can be approximated by:

$$\sigma_Q \approx 4\pi A_\perp(\theta,\phi) \lim_{R\to\infty} \frac{\langle \hat{I}_s(\mathbf{r}_s = \mathbf{r}_d)\rangle}{\int_0^{2\pi}\int_0^{\pi} \langle\, \hat{I}_s(\mathbf{r}_s, \mathbf{r}_d)\rangle \, \sin\theta_d \, d\theta_d \, d\phi_d} \tag{6.17}$$

where the expectation value of the scattered intensity is taken at the receiver [61].

Unfortunately, this "simplified" expression for σ_Q remains problematic for the analytic study of quantum radar. In general, numerical methods have to be employed to elucidate the behavior of the quantum radar cross section.

It is possible, however, to get an analytical expression for the quantum radar cross section of a spherical target. Indeed, for this target is safe to assume that $\sigma_Q^{(sphere)}$ will showcase spherical symmetry and it will be independent of the angular variables θ and ϕ. Then:

$$\int_0^{2\pi}\int_0^{\pi} \sigma_Q^{(sphere)} \, \sin\theta \, d\theta \, d\phi = 4\pi\sigma_Q^{(sphere)} \tag{6.18}$$

In addition, the expression for $\sigma_Q^{(sphere)}$ in the optical regime leads to:

$$\int_0^{2\pi}\int_0^{\pi} \sigma_Q^{(sphere)} \, \sin\theta \, d\theta \, d\phi \approx 4\pi A_\perp \tag{6.19}$$

and as a consequence:

$$\sigma_Q^{(sphere)} \approx A_\perp \tag{6.20}$$

which means that, in the case of a spherical target, the classical radar cross section and the quantum radar cross section are the same:

$$\sigma_Q^{(sphere)} = \sigma_C^{(sphere)} \tag{6.21}$$

In general, for non-spheric targets, the quantum and the classical radar cross sections may be different.

6.4 THE QUANTUM RADAR EQUATION

We are now in position to derive a quantum radar cross section based on the definition of quantum radar cross section. From the previous definition for the quantum cross section we have that:

$$\sigma_Q = \lim_{R\to\infty} 4\pi R^2 \frac{\langle I_s\rangle}{\langle I_i\rangle} \tag{6.22}$$

and using the previously obtained expressions for the intensities we get in the large R limit:

$$\begin{aligned} \langle I_s\rangle &\approx \frac{\langle I_i\rangle \sigma_Q}{4\pi R^2} \\ &\approx \frac{\Psi_\gamma \Psi_\gamma^* \ \sigma_Q}{4\pi \ R^2} \\ &\approx \frac{\mathcal{E}_0^2 \ \sigma_Q}{4\pi \ R^4} \\ &\approx \frac{4\pi \ \mathcal{E}_0^2 \ \sigma_Q}{(4\pi)^2 \ R^4} \end{aligned} \tag{6.23}$$

This last expression resembles the classical radar equation. Indeed, if we make the replacements:

$$\begin{aligned} P_t^Q &= 4\pi \ \mathcal{E}_0^2 \\ P_r^Q &= \langle I_s\rangle A_r \end{aligned} \tag{6.24}$$

where P_t^Q is the transmitted power of the quantum radar and P_r^Q is the received power at the quantum radar. Then:

$$P_r^Q = \frac{P_t^Q \ A_r \ \sigma_Q}{(4\pi)^2 \ R^4} \tag{6.25}$$

which for all means and purposes can be considered as the *quantum radar equation*.

6.5 SIMULATION OF σ_Q FOR RECTANGULAR TARGETS

We have developed computer programs to simulate σ_C and σ_Q for a finite, flat rectangular plate. The geometry of the sensor-target system is the same as the one shown in Chapter 4 and shown again in Figure 6.1. As before, we will ignore diffraction and absorption effects.

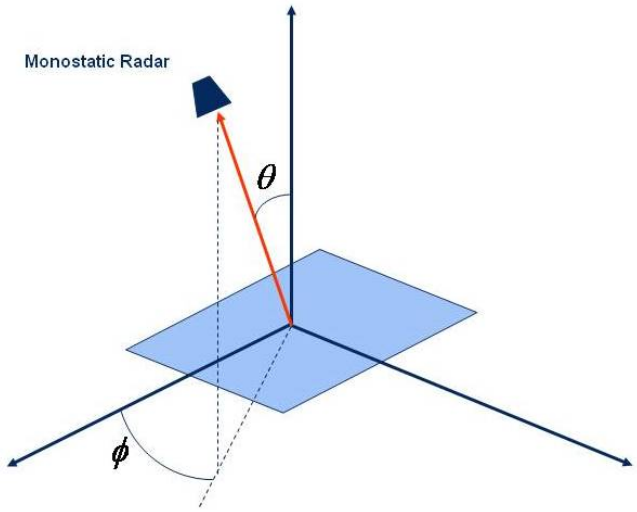

Figure 6.1: Sensor-target geometry.

Even though it is not computationally efficient, we decided to perform the coding using *Mathematica*^{TM} because it allows the rapid prototyping of simulation programs [75]. As a consequence, the target size and atomic composition had to be severely limited by the available computational resources.

For instance, a σ_Q simulation of a target made of 10,000 atoms and a single quantum radar signal photon took over 4 hours on a 1.6 GHz Intel desktop. Furthermore, multiple incoming radar photons contribute an exponentially large number of terms in the simulation. Thus, our computer simulations were limited by 5 radar photons and 100,000 atoms. By any means this is a very simple radar-target system. Nevertheless, this model offers a useful way to obtain valuable insight on the physical properties of σ_Q.

Finally, it is interesting to mention that the simulation of σ_Q appears to be an ideal task to be solved by quantum computers [63].

6.5.1 ANALYTICAL EXPRESSION

Using the equations for the expectation value of the intensity we obtain:

$$\begin{aligned}
\sigma_Q &\approx 2\pi A_\perp(\theta,\phi) \lim_{R\to\infty} \frac{\left|\sum_{i=1}^{N} \Psi_\gamma^{(i)}(\Delta R_i, t)\right|^2}{\int_0^{2\pi}\int_0^{\pi}\left|\sum_{i=1}^{N} \Psi_\gamma^{(i)}(\Delta R_i{}', t)\right|^2 \sin\theta'\, d\theta'\, d\phi'} \qquad (6.26)\\
&\approx 2\pi A_\perp(\theta,\phi) \lim_{R\to\infty} \frac{\left|\sum_{i=1}^{N} \frac{\mathcal{E}_0}{\Delta r_{id}}\, e^{-(i\omega+\Gamma/2)(t-\Delta R_i/c)}\right|^2}{\int_0^{2\pi}\int_0^{\pi}\left|\sum_{i=1}^{N} \frac{\mathcal{E}_0}{\Delta r_{id}}\, e^{-(i\omega+\Gamma/2)(t-\Delta R_i'/c)}\right|^2 \sin\theta'\, d\theta'\, d\phi'}\\
&\approx 2\pi A_\perp(\theta,\phi) \lim_{R\to\infty} \frac{\left(\frac{\mathcal{E}_0}{R}\right)^2\left|\sum_{i=1}^{N} e^{-(i\omega+\Gamma/2)(t-\Delta R_i/c)}\right|^2}{\int_0^{2\pi}\int_0^{\pi}\left(\frac{\mathcal{E}_0}{R}\right)^2\left|\sum_{i=1}^{N} e^{-(i\omega+\Gamma/2)(t-\Delta R_i'/c)}\right|^2 \sin\theta'\, d\theta'\, d\phi'}\\
&\approx 2\pi A_\perp(\theta,\phi) \lim_{R\to\infty} \frac{\left|\sum_{i=1}^{N} e^{-(i\omega+\Gamma/2)(t-\Delta R_i/c)}\right|^2}{\int_0^{2\pi}\int_0^{\pi}\left|\sum_{i=1}^{N} e^{-(i\omega+\Gamma/2)(t-\Delta R_i'/c)}\right|^2 \sin\theta'\, d\theta'\, d\phi'}\\
&\approx 2\pi A_\perp(\theta,\phi) \lim_{R\to\infty} \frac{\left|\sum_{i=1}^{N} e^{-(i\omega+\Gamma/2)t}\, e^{(i\omega+\Gamma/2)\Delta R_i/c}\right|^2}{\int_0^{2\pi}\int_0^{\pi}\left|\sum_{i=1}^{N} e^{-(i\omega+\Gamma/2)t}\, e^{(i\omega+\Gamma/2)\Delta R_i'/c}\right|^2 \sin\theta'\, d\theta'\, d\phi'}\\
&\approx 2\pi A_\perp(\theta,\phi) \lim_{R\to\infty} \frac{\left|\sum_{i=1}^{N} e^{(i\omega+\Gamma/2)\Delta R_i/c}\right|^2}{\int_0^{2\pi}\int_0^{\pi}\left|\sum_{i=1}^{N} e^{(i\omega+\Gamma/2)\Delta R_i'/c}\right|^2 \sin\theta'\, d\theta'\, d\phi'}
\end{aligned}$$

where we have assumed that outside the interference terms, we can approximate:

$$\Delta r_{id} = |\mathbf{r}_d - \mathbf{r}_i| \approx R \quad \forall i \qquad (6.27)$$

in the amplitudes.

We can further assume that $\Gamma \approx 0$, which leads to:

$$\sigma_Q \approx 2\pi A_\perp(\theta,\phi) \lim_{R\to\infty} \frac{\left|\sum_{i=1}^{N} e^{i\omega\Delta R_i/c}\right|^2}{\int_0^{2\pi}\int_0^{\pi}\left|\sum_{i=1}^{N} e^{i\omega\Delta R_i'/c}\right|^2 \sin\theta'\, d\theta'\, d\phi'} \qquad (6.28)$$

6.5.2 SIDELOBE STRUCTURE

Figure 6.2 shows the plot of σ_Q vs. θ for $\phi = 0$. Similarly, to σ_C, the highest value of σ_Q is reached when the target is oriented in the specular direction at $\theta = 0$. In addition, a sidelobe structure is observed. However, while the sidelobe structure for σ_C was due to end-region returns, the sidelobe structure for σ_Q is a purely quantum mechanical effect due to quantum interference.

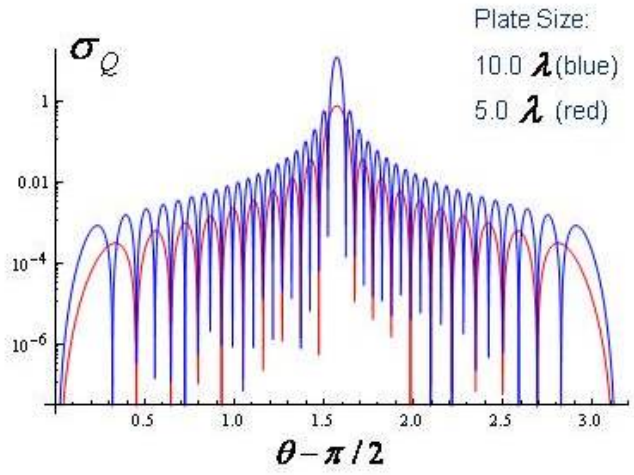

Figure 6.2: Simulation of σ_Q vs. θ ($\phi = 0$) for a 2D flat plate. As with σ_C, the highest value of σ_Q is reached when the target is oriented in the specular direction. The sidelobe structure, however, is a purely quantum mechanical effect. Diffraction and absorption effects have been ignored.

6.5.3 σ_Q VS. σ_C

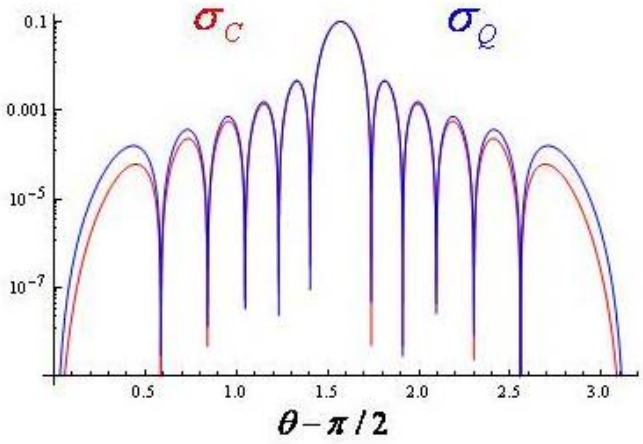

Figure 6.3: Comparison of σ_Q vs. σ_C for a rectangular target.

It is possible to compare σ_C and σ_Q because both have the same units of area and they have the same operational definition of ratio of intensities. The result is shown in Figure 6.3. It can be observed that σ_Q is approximately equal to σ_C for most values of the angular variable θ.

We need to remark that this result is valid only for the rectangular target. In addition, let us recall that for a spherical target, $\sigma_Q = \sigma_C$. However, it remains to be shown what is the behavior of σ_Q in relation to σ_C for singly curved surfaces. This is something we will explore in the future.

We also observe that the values of σ_Q and σ_C are different towards the region of large scattering angles. This, however, may be due to the error in the approximation used in the equation for σ_Q. Indeed, let us recall that the physical optics approximation tends to fail at large scattering angles. For example, a similar behavior is observed in the classical approximation with respect to the exact solution.

However, it is important to remark that, even though σ_Q and σ_C are equal, the sidelobe structure has a completely different physical origin. In the classical case, the sidelobes are a consequence of discontinuities in the surface currents, while in the quantum case the sidelobes are a result of quantum interference. Of course, the mathematical description of both is the same, which results in their similar cross sections.

Nevertheless, these results appear to offer the prospect of exploiting the quantum sidelobe structure of σ_Q to detect targets oriented off the specular direction. While current tapering will tend to suppress the classical sidelobes, most probably it will not have an effect on the quantum sidelobes. Furthermore, it is worth exploring any possible sensing mechanism that could enhance the quantum sidelobe structure of a target. These are subjects that we will consider in more detail in the future.

6.5.4 TARGET'S GEOMETRY

Let us assume now three rectangular targets of the same area, but different proportions:

$$\begin{aligned} A_1 &= 2.5 \times 4.0\ \lambda^2 \\ A_2 &= 5.0 \times 2.0\ \lambda^2 \\ A_3 &= 10.0 \times 1.0\ \lambda^2 \end{aligned} \tag{6.29}$$

The plot of σ_Q vs. θ at $\phi = 0$ for these targets is shown in Figure 6.4. It can be seen that, even though they have the exact same area, the difference in their proportions alters their σ_Q. It can be observed that the maximal value of σ_Q is the same in all cases, but the sidelobe structure is different. This result is equivalent to the one seen for σ_C in Chapter 4.

6.5.5 RANGE INDEPENDENCE

Figure 6.5 shows that σ_Q is indeed independent of the range to the target R, one of the most important features of a well-defined σ_Q. The plot shows σ_Q vs. θ ($\phi = 0$) for $R/a = 1, 5, 10, 10^2, 10^3, 10^4$ and 10^6.

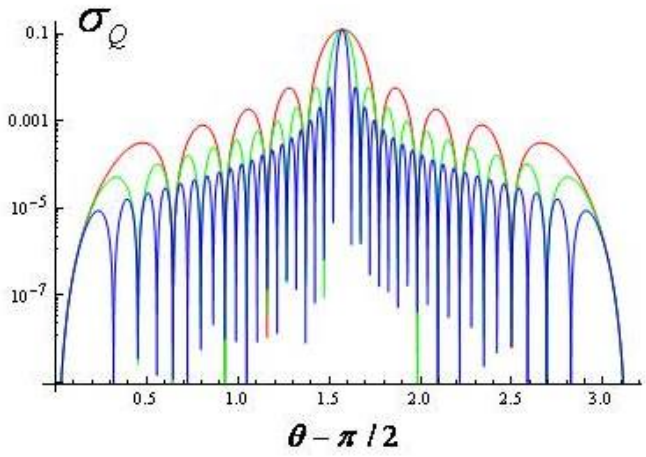

Figure 6.4: Simulation of σ_Q vs. θ ($\phi = 0$) for a 2D rectangular plate of the same area but different proportions (2.5×4.0 [red], 5.0×2.0 [green], and 10.0×1.0 [blue]).

6.5.6 SMALL SIZE TARGETS

Figure 6.6 shows σ_Q in the case of small targets (in comparison to the radar wavelength). For $a = 5\,\lambda$ we have the usual sidelobe structure. For $a = \lambda$ there are only two sidelobes. And for $a = 0.1\,\lambda$ the quantum radar cross section is approximately constant. This behavior is also seen for the classical radar cross section. For small targets, the radar system cannot elucidate any details, as the target appears to have spherical symmetry. This final observation is not surprising, an optical-based sensor is only good to resolve objects larger than its wavelength.

6.5.7 HIGH FREQUENCY PHOTONS

The case of very high radar frequencies is shown in Figure 6.7. In the figure we show σ_Q for a wavelength of the same size as the interatomic distance δ. The result is a plot similar to a crystallographic spectrum. Indeed, the quantum radar is probing the atomic structure of the target.

Of course, this is not a desired feature of a quantum radar. This simply means that the quantum radar model has an upper and lower limit of valid frequencies. But then again, this is the exact same situation as with a classical radar.

6.5.8 ATOMIC STRUCTURE

Figure 6.8 explores how σ_Q depends on the atomic structure of the target. We consider a target of the same dimensions, but with different number of atoms and interatomic distances. The plots depict σ_Q vs. θ ($\phi = 0$). The cases considered are arrays of 100×2, 1000×2, and 2500×2 atoms with interatomic distances $\delta = 10^{-3}$, 10^{-4}, and $4 \times 10^{-5}\,\lambda$, respectively. We observe a slight variation

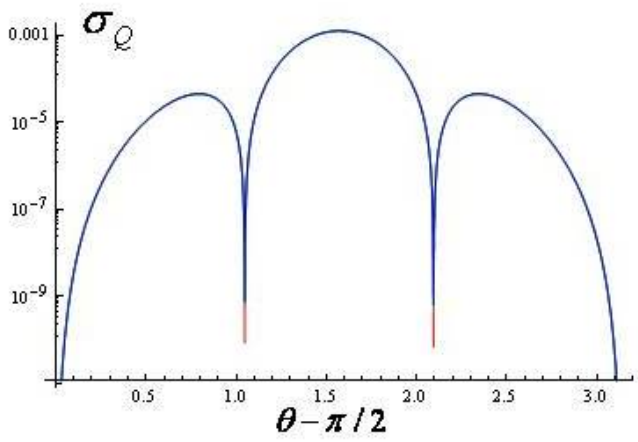

Figure 6.5: σ_Q vs. θ ($\phi = 0$) for $R/a = 1, 5, 10, 10^2, 10^3, 10^4$ and 10^6. The plots make evident that σ_Q is independent of the range to the target R.

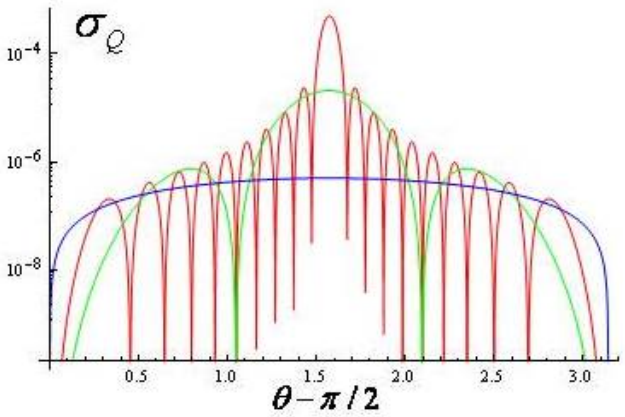

Figure 6.6: Behavior of σ_Q for small targets.

in the amplitude values of σ_Q for high incidence angles, but all the cases retain the same periodic structure.

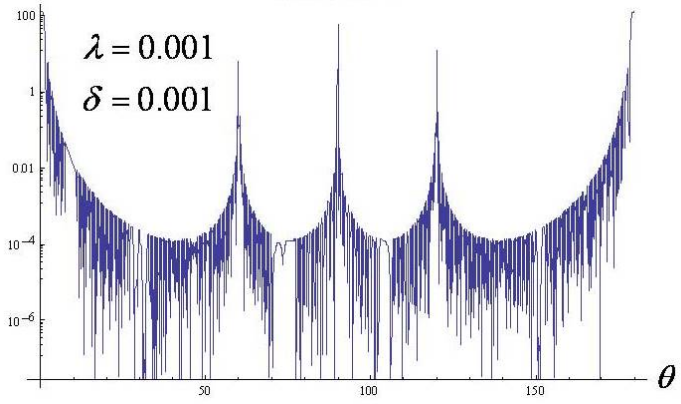

Figure 6.7: Quantum radar cross section for high frequency photons ($\lambda = 0.001$ and $\delta = 0.001$).

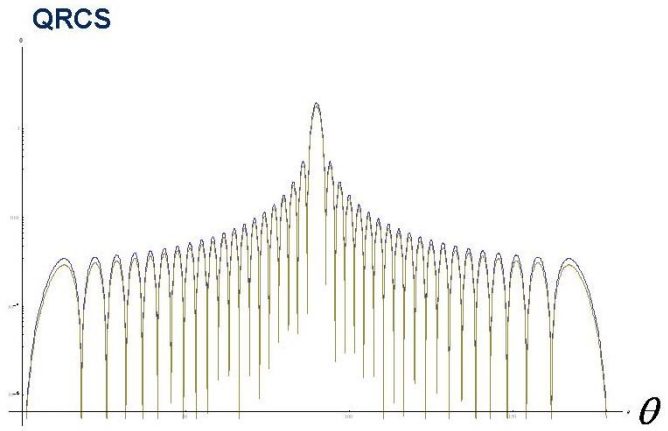

Figure 6.8: Plots of σ_Q vs. θ ($\phi = 0$) for arrays of 100×2, 1000×2, and 2500×2 atoms with interatomic distances $\delta = 10^{-3}$, 10^{-4}, and 4×10^{-5}, respectively.

6.5.9 MULTIPLE PHOTONS

So far we have considered the structure of σ_Q for the case of single photon signals in the quantum radar pulse. It is very easy to generalize the equations to describe quantum radar pulses with n_γ photons. The definition of σ_Q is the same, but we need to obtain a new expression for $\langle \hat{I}_s(\mathbf{r}_d, t) \rangle$.

Let us consider as an example the case of two photons, $n_\gamma = 2$, one with momentum $\mathbf{p}$ and the other with momentum $\mathbf{q}$ (and for simplicity we ignore the polarization states). We can follow the same steps used in Chapter 2 to obtain expressions for the probability of photodetection. In this case, the photodetector needs to detect two photons, one at $(\mathbf{r}, t)$ and another at $(\mathbf{r}', t')$. Then, the

transition amplitude of the detector signaling the detection of the two photons is given by:

$$a_f(\mathbf{r}, t, \mathbf{r}', t') = \langle 0|\hat{E}^{(+)}(\mathbf{r}, t)\ \hat{E}^{(+)}(\mathbf{r}', t')|1_{\mathbf{p}}1_{\mathbf{q}}\rangle \tag{6.30}$$

and the measured intensity is:

$$\begin{aligned}\langle \hat{I}_{\mathbf{pq}}(\mathbf{r}, t, \mathbf{r}', t')\rangle &= |a_f(\mathbf{r}, t, \mathbf{r}', t')|^2 \\ &= \left|\langle 0|\hat{E}^{(+)}(\mathbf{r}, t)\ \hat{E}^{(+)}(\mathbf{r}', t')|1_{\mathbf{p}}1_{\mathbf{q}}\rangle\right|^2 \\ &= \left|\Psi_{\mathbf{pq}}(\mathbf{r}, t, \mathbf{r}', t')\right|^2\end{aligned} \tag{6.31}$$

Now, using the expressions for the quantum fields and the Fock states we get:

$$\begin{aligned}\Psi_{\mathbf{pq}}(\mathbf{r}, t, \mathbf{r}', t') &= \langle 0|\hat{E}^{(+)}(\mathbf{r}, t)\ \hat{E}^{(+)}(\mathbf{r}', t')|1_{\mathbf{p}}1_{\mathbf{q}}\rangle \\ &\propto \langle 0|(\hat{a}_{\mathbf{p}}e^{-i(\omega_p t-\mathbf{p}\cdot\mathbf{r})} + \hat{a}_{\mathbf{q}}e^{-i(\omega_q t-\mathbf{q}\cdot\mathbf{r})}) \\ &\quad \times(\hat{a}_{\mathbf{p}}e^{-i(\omega_p t'-\mathbf{p}\cdot\mathbf{r}')} + \hat{a}_{\mathbf{q}}e^{-i(\omega_q t'-\mathbf{q}\cdot\mathbf{r}')})|1_{\mathbf{p}}1_{\mathbf{q}}\rangle \\ &\propto\ e^{-i(\omega_p t-\mathbf{p}\cdot\mathbf{r})}e^{-i(\omega_p t'-\mathbf{p}\cdot\mathbf{r}')}\langle 0|\hat{a}_{\mathbf{p}}\hat{a}_{\mathbf{p}}|1_{\mathbf{p}}1_{\mathbf{q}}\rangle \\ &\quad + e^{-i(\omega_p t-\mathbf{p}\cdot\mathbf{r})}e^{-i(\omega_q t'-\mathbf{q}\cdot\mathbf{r}')}\langle 0|\hat{a}_{\mathbf{p}}\hat{a}_{\mathbf{q}}|1_{\mathbf{p}}1_{\mathbf{q}}\rangle \\ &\quad + e^{-i(\omega_q t-\mathbf{q}\cdot\mathbf{r})}e^{-i(\omega_p t'-\mathbf{p}\cdot\mathbf{r}')}\langle 0|\hat{a}_{\mathbf{q}}\hat{a}_{\mathbf{p}}|1_{\mathbf{p}}1_{\mathbf{q}}\rangle \\ &\quad + e^{-i(\omega_q t-\mathbf{q}\cdot\mathbf{r})}e^{-i(\omega_q t'-\mathbf{q}\cdot\mathbf{r}')}\langle 0|\hat{a}_{\mathbf{q}}\hat{a}_{\mathbf{q}}|1_{\mathbf{p}}1_{\mathbf{q}}\rangle \\ &\propto\ e^{-i(\omega_p t-\mathbf{p}\cdot\mathbf{r})}e^{-i(\omega_q t'-\mathbf{q}\cdot\mathbf{r}')} + e^{-i(\omega_q t-\mathbf{q}\cdot\mathbf{r})}e^{-i(\omega_p t'-\mathbf{p}\cdot\mathbf{r}')} \\ &\propto\ \Psi_{\gamma_{\mathbf{p}}}(\mathbf{r}, t)\ \Psi_{\gamma_{\mathbf{q}}}(\mathbf{r}', t') + \Psi_{\gamma_{\mathbf{q}}}(\mathbf{r}, t)\ \Psi_{\gamma_{\mathbf{p}}}(\mathbf{r}', t')\end{aligned} \tag{6.32}$$

where we have used the fact that:

$$\begin{aligned}\langle 0|\hat{a}_{\mathbf{p}}\hat{a}_{\mathbf{q}}|1_{\mathbf{p}}1_{\mathbf{q}}\rangle = \langle 0|\hat{a}_{\mathbf{q}}\hat{a}_{\mathbf{p}}|1_{\mathbf{p}}1_{\mathbf{q}}\rangle &\propto 1 \\ \langle 0|\hat{a}_{\mathbf{p}}\hat{a}_{\mathbf{p}}|1_{\mathbf{p}}1_{\mathbf{q}}\rangle = \langle 0|\hat{a}_{\mathbf{q}}\hat{a}_{\mathbf{q}}|1_{\mathbf{p}}1_{\mathbf{q}}\rangle &\propto 0\end{aligned} \tag{6.33}$$

which is a consequence that $\hat{a}_{\mathbf{p}}$ ($\hat{a}_{\mathbf{q}}$) destroys a photon of momentum $\mathbf{p}$ ($\mathbf{q}$).

Therefore, the intensity is given by:

$$\langle I_{\mathbf{pq}}(\mathbf{r}, t, \mathbf{r}', t')\rangle \propto |\Psi_{\gamma_{\mathbf{p}}}(\mathbf{r}, t)\ \Psi_{\gamma_{\mathbf{q}}}(\mathbf{r}', t') + \Psi_{\gamma_{\mathbf{q}}}(\mathbf{r}, t)\ \Psi_{\gamma_{\mathbf{p}}}(\mathbf{r}', t')|^2 \tag{6.34}$$

which is a symmetric bipartite wave function as required by Bose-Einstein statistics. Furthermore, notice that in general:

$$\langle I_{\mathbf{pq}}(\mathbf{r}, t, \mathbf{r}', t')\rangle \neq |\Psi_{\gamma_{\mathbf{p}}}(\mathbf{r}, t)|^2\ |\Psi_{\gamma_{\mathbf{q}}}(\mathbf{r}', t')|^2 \tag{6.35}$$

or equivalently:

$$\langle I_{\mathbf{pq}}\rangle \neq \langle I_{\mathbf{p}}\rangle\langle I_{\mathbf{q}}\rangle \tag{6.36}$$

which means that the two photodetections at $(\mathbf{r}, t)$ and $(\mathbf{r}', t')$ are not independent but are correlated [73]. The reason for this behavior is that each of the detection events gives some information about the state of the quantum field, and this information has an influence on the estimates of subsequent detections. As a consequence, this is a quantum mechanical effect due to the interference

between the photon states in the symmetric bipartite state shown in Equation (6.34). Indeed, it is only possible to factorize the contributing intensities for states that represent classical light.

Let us now consider the case of three atoms ($N = 3$) scattering two photons ($n_\gamma = 2$). In this case:

$$\langle \hat{I}(\mathbf{r}_d, t)\rangle \propto \frac{1}{3}\left|\Psi_{\gamma_1}^{(1)}\Psi_{\gamma_2}^{(2)} + \Psi_{\gamma_1}^{(2)}\Psi_{\gamma_2}^{(3)} + \Psi_{\gamma_1}^{(3)}\Psi_{\gamma_2}^{(1)}\right|^2 \tag{6.37}$$

where the wave function subindex marks the photon and the upper index identifies the scattering atom. That is, the two photons can interact with any of the three atoms, and all possible combinations contribute to the interference pattern. Notice that there is no permutation over the photon indices because the photons are bosons, and therefore indistinguishable from each other.

Then, for N atoms and n_γ photons:

$$\langle \hat{I}(\mathbf{r}_d, t)\rangle = \frac{1}{\binom{N}{n_\gamma}}\left|\Gamma_{a_1 a_2 \ldots a_{n_\gamma}} \prod_{j=1}^{n_\gamma} \Psi_{\gamma_j}^{(a_j)}\right|^2 \tag{6.38}$$

where $a_i = 1, 2, \ldots N$, and sum over equal "a_i" indices is implied.

The simulation of multiple incoming photons has exponential complexity because of the binomial combinatorial summation in the equation. Indeed, the simulation of $(n_\gamma + 1)$ photons requires this number of operations:

$$\begin{aligned}\binom{N}{n_\gamma + 1} &= \frac{N!}{(n_\gamma + 1)!\,(N - n_\gamma - 1)!} \\ &= \frac{N!}{(n_\gamma)!\,(N - n_\gamma)!}\,\frac{N - n_\gamma}{n_\gamma + 1} \\ &= \binom{N}{n_\gamma}\,\frac{N - n_\gamma}{n_\gamma + 1}\end{aligned} \tag{6.39}$$

And, if $N \gg n_\gamma$:

$$\frac{N - n_\gamma}{n_\gamma + 1} \approx \mathcal{O}(N/n_\gamma) \tag{6.40}$$

That is, the simulation of a single extra photon requires a factor of N extra operations. Then, the simulation of n_γ photons requires:

$$\mathcal{O}\left((N/n_\gamma)^{n_\gamma}\right) \tag{6.41}$$

operations.

Figure 6.9 shows the plots of σ_Q vs. θ ($\phi = 0$) for $n_\gamma = 1, 2$, and 5 photons (for a rectangular target made of 10×5 atoms). It can be observed that as the number of photons increases, so does the peak of the maximum value of σ_Q at the specular orientation. That is, a target near the specular direction appears to look bigger when illuminated with a quantum radar. For example, we will observe the magnification of the quantum cross section at the specular direction when we use an interferometric quantum radar using NOON states. This appears to be a pure quantum-mechanical

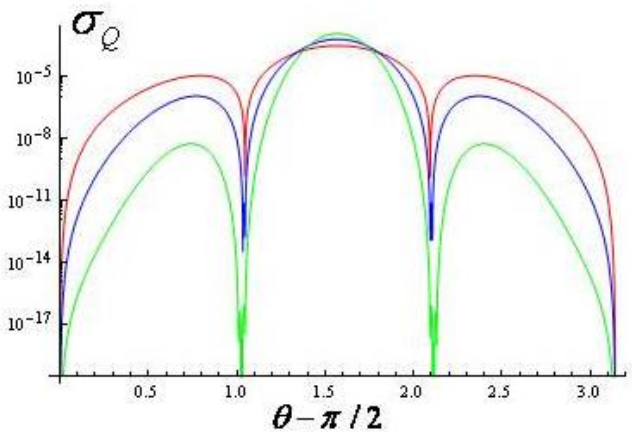

Figure 6.9: Plots of σ_Q vs. θ ($\phi = 0$) for $n_\gamma = 1$ (red), 2 (blue), and 5 (green) photons.

effect due to the interference terms that lead to Equation (6.36). Thus, only in the case of beams of classical light will we expect to see the same cross sections without regard to the number of photons per beam.

However, as the number of photons increases, the sidelobe structure decreases dramatically and the width of the specular orientation peak becomes more narrow. Such behavior is to be expected. Indeed, the interferometric analysis only takes into consideration specular returns and the associated sidelobe structure due to quantum interference. As the number of photons increases, the dynamics of the scattering transition to the classical domain. In such a case, we would expect that σ_Q will be extremely narrow at the specular direction and without sidelobes. That is, this behavior makes evident the large photon number limit for σ_Q:

$$\lim_{n_\gamma \to \infty} \sigma_Q \propto \sigma_C \propto \delta(\theta) \tag{6.42}$$

which corresponds to specular returns without end-region contributions. This further shows that the quantum side lobe structure is not related to the side lobe structure observed in the context of classical radar cross sections. That is, the quantum side lobe structure is a purely quantum mechanical feature.

Numerical values for the peak value of the quantum radar cross section on the main ($\theta = 0$) and secondary ($\theta = \pi/4$) lobes are given in Table 6.1. It almost appears that the main lobe peak value increases by a constant factor as a result of adding an extra photon. However, this is not the case. Indeed, let us define the growth ratio $G_r(n_\gamma)$ as:

$$G_r(n_\gamma) = \frac{\sigma_Q^{Max}(n_\gamma)}{\sigma_Q^{Max}(n_\gamma - 1)} \tag{6.43}$$

where $\sigma_Q^{Max}(n_\gamma)$ is the maximal value of σ_Q for n_γ photons. Thus, we can observe a steady decrease in its value as we increase the number of photons. Furthermore, we can expect that the growth ratio will steadily decrease to zero for a large number of photons.

On the other hand, the peak of the lateral lobes appears to decrease exponentially faster with the number of photons. It is also worth mentioning that the "damping" of the quantum side lobes due to the addition of extra photons to the radar pulse depends on the ratio N/n_γ. In more realistic examples, where $N \gg n_\gamma$, the damping will not be as severe as the one shown in the figure.

Table 6.1: Peak values of the quantum radar cross section on the main ($\theta = 0$) and lateral ($\theta = \pi/4$) lobes.

No. of Photons	Main Lobe Peak	Growth Ratio	Lateral Lobe Peak
1	0.0003152		1.12×10^{-5}
2	0.0006474	2.054	1.14×10^{-6}
3	0.0009444	1.459	8.06×10^{-8}
4	0.0012262	1.298	4.84×10^{-9}

At this point is worth discussing the two main quantum mechanical effects that contribute to the behavior of the quantum radar cross section:

- First, the sidelobe structure is a pure quantum mechanical effect due to the interference of the photon wave functions and it has no classical counterpart. Indeed, classically there would be no sidelobes without discontinuous surface currents due to edge effects.
- And second, the maximal value of the quantum radar cross section increases with the number of photons in the quantum radar beam. This effect is also due to the interference between the photons as expressed by Equation (6.36).

Because of the correspondence principle, we expect that the quantum radar cross section will become the classical radar cross section for a large number of photons. The first effect appears to obey this principle, as the sidelobe structure disappears as the number of photons increases. However, the second effect appears to persist in the large photon number, as the maximal value of the quantum radar section continues to increase with the number of photons.

At this point it is important to recall the second footnote of Section 2.5, where we mentioned that a large number of photons is not enough to guarantee the correspondence principle. Indeed, the Fock states used for the computation of the quantum radar cross section are non-classical even with a large number of photons. To obtain the principle of correspondence for the second effect one needs to explicitly use coherent states with large average photon numbers. It is only in such a case that the expression for the contributions to the intensity becomes an equality:

$$\langle I_{12} \rangle = \langle I_1 \rangle \langle I_2 \rangle \tag{6.44}$$

which means that there are no interference effects and as a consequence there will be no change to the value of the radar cross section.

Therefore, in the small photon number regime, it appears that specular returns and quantum interference are the principal contributors to the value of σ_Q. Therefore, it may be worth considering if it is possible to detect targets using the sidelobe structure of quantum radars operating in the small photon number regime. In such a case, not only an optimal value for n_γ will need to be found, but also explore strategies and protocols that amplify the quantum sidelobe structure of a target.

6.6 SUMMARY

In this chapter we have discussed the need to define a quantum radar cross section σ_Q. The definition taken follows the same structure as the one for classical radar σ_C. We used interferometric arguments based on quantum electrodynamics to determine the intensity measured by the radar receiver. It was found that for single photon quantum radars, σ_Q has a sidelobe structure which is a purely quantum mechanical effect (in contrast, the sidelobe structure of σ_C is a consequence of end-region returns). We also observed that $\sigma_Q \geq \sigma_C$ for rectangular targets near the specular direction if the quantum radar pulse has more than one photon. In addition, just as multiple photon pulses tend to increase the specular return of σ_Q, they also narrow the peak and reduce the sidelobe structure.

These results suggest that it may be possible to detect targets using the sidelobe structure of quantum radars. This is an idea that deserves to be explored in more detail.

CHAPTER 7

Conclusions

Preliminary results show that interferometric quantum radar using entangled photons can provide a quadratic increase of resolution over non-entangled photons even in an attenuating environment [97]. Quantum illumination offers higher signal-to-noise ratio which increases the detectability and identification of stealth targets even in the presence of noise or a jamming signal [67]. In addition, defining the quantum radar cross section using quantum electrodynamics leads to the result that the "effective visibility" of a target near the specular direction is increased if observed with a quantum radar instead of a classical radar [61, 62]. Furthermore, a quantum sidelobe structure offers the possibility of detecting RF stealth targets [61].

As a consequence, quantum radars may be able to detect, identify, and resolve RF stealth platforms and weapons systems. In the electronic battlefield, quantum radar may become a revolutionary technology just as RF stealth technology was in the last three decades of the 20th century.

7.1 OPEN QUESTIONS

Quantum radar is a novel technological concept and its development presents a variety of multidisciplinary, experimental, and theoretical research challenges. Some of these include:

1. What is the most optimal way to entangle photons in the X-band frequency regime?
2. What is the most optimal frequency to be used by quantum radars?
3. What is the best physical design of a quantum radar?
4. What is the best way to measure the operational performance of a quantum radar?
5. How to deal with the effects of noise in the atmosphere?
6. How to describe the capacity of a quantum radar channel?
7. How to simulate quantum radar cross sections?
8. What is the optimal number of coherent photons per radar pulse?
9. How to design low observable quantum stealth platforms?
10. How to use weak measurements to enhance detection?
11. How to exploit other quantum resources to enhance target detection?

12. How to perform signal detection from quantum radar measurements?
13. How to ruggedize a quantum radar for its deployment in an operational environment?
14. What are the effects of geometry on the quantum radar cross section?
15. How do these results change when using realistic targets in arbitrary motion?
16. What type of signal analysis is needed to detect and track targets using a quantum radar?
17. Is there a quantum sensing strategy that amplifies the quantum sidelobe structure?

7.2 THE BOTTOM LINE

Quantum radar is a promising technology that could have a strong impact on the civilian and military realms. It is important to note that, even though quantum sensing technology is not as mature as quantum computation, the engineering of a full-blown multi-qubit quantum computer is a much harder challenge than the design of deployable quantum sensors. As a consequence, quantum radar is a high risk, high payoff proposal. By any means, the concept of a quantum radar is worth investigating in further detail.

Bibliography

[1] D. Alexander, *Stealth Warfare*, Alpha, 2004. Cited on page(s) 1, 58

[2] E.H. Allen and M. Karageorgis, "Radar Systems and Methods Using Entangled Quantum Particles", US Patent 7375802, 2008. Cited on page(s) 3

[3] N.W. Ashcroft and N.D. Mermin, *Solid State Physics*, Brooks/Cole, 1976. Cited on page(s) 40

[4] K.M.R. Audenaert, et.al. "The Quantum Chernoff Bound", *Phys. Rev. Lett.* 98, 160501, 2007. DOI: 10.1103/PhysRevLett.98.160501 Cited on page(s) 86

[5] O. Benson, et.al., "Regulated and Entangled Photons from a Single Quantum Dot", *Phys. Rev. Lett.* 84, 2513, 2000. DOI: 10.1103/PhysRevLett.84.2513 Cited on page(s) 88

[6] V.B. Bereststetskii, E.M. Lifshitz, and L.P. Pitaesvskii, *Quantum Electrodynamics*, Volume 4 of the Landau and Lifshitz Course of Theoretical Physics, Second Edition, Pergamon Press, 1982. Cited on page(s) 5, 11, 12, 13, 24, 25, 26, 27, 28, 29, 30

[7] R.S. Bondurant and J.H. Shapiro, "Squeezed states in phase-sensing interferometers", *Phys. Rev. D* 30, 2548–2556, 1984. DOI: 10.1103/PhysRevD.30.2548 Cited on page(s) 65

[8] M. Born and E. Wolf, *Principles of Optics*, Seventh Edition, Cambridge University Press, 1999. Cited on page(s) 5, 18, 21, 22, 31, 40, 41, 53, 60

[9] A.N. Boto, et.al. "Quantum Interferometric Optical Lithography: Exploiting Entanglement to Beat The Diffraction Limit", *Phys. Rev. Lett.* 85, 2733, 2000. DOI: 10.1103/PhysRevLett.85.2733 Cited on page(s) 69

[10] V.B. Braginsky and F.YA. Khalili, *Quantum Measurement*, Cambridge University Press, 1992. Cited on page(s) 64

[11] L. Brown, *A Radar History of World War II: Technical and Military Imperatives*, Taylor and Francis, 1999. Cited on page(s) 1

[12] J. Calsamiglia, et.al., "The quantum Chenoff bound as a measure of distinguishability between density matrices: application to qubit and Gaussian states", *Phys. Rev. A* 77, 032311, 2008. DOI: 10.1103/PhysRevA.77.032311 Cited on page(s) 86

[13] J.C. Carrison and R.Y. Chiao, *Quantum Optics*, Oxford University Press, 2008. Cited on page(s) 5, 15, 25

[14] C.M. Caves, "Quantum-Mechanical Noise in an Interferometer", *Phys. Rev. D*, V.23, No. 8, 1981. DOI: 10.1103/PhysRevD.23.1693 Cited on page(s) 64

[15] C.M. Caves, "Quantum-Mechanical Radiation-Pressure Fluctuations in an Interferometer", *Phys. Rev. Lett.*, Vol.45, No. 2, 1980. DOI: 10.1103/PhysRevLett.45.75 Cited on page(s) 64

[16] C. Cohen-Tannoudji, J. Dupont-Roc, and G. Grynberg, *Atom-Photon Interactions*, Wiley-VCH, 2004. Cited on page(s) 10, 23

[17] Darpa Quantum Sensor Program. http://www.darpa.mil/sto/space/qsp.html Cited on page(s) 3

[18] B. Dayan, et.al., "Two Photon Absorption and Coherent Control with Broadband Down-Converted Light", *Phys. Rev. Lett.* 93, 023005, 2004. DOI: 10.1103/PhysRevLett.93.023005 Cited on page(s) 87

[19] E.L. Dereniak and D.G. Crowe, *Optical Radiation Detectors*, Wiley, 1984. Cited on page(s) 90

[20] L.D. Didomenico, H. Lee, P. Kok, and J.P. Dowling,"Quantum Interferometric Sensors", *Proceedings of SPIE Quantum Sensing and Nanophotonic Devices*, 2004. Cited on page(s) 68, 69, 70

[21] S.M. Dutra, *Cavity Quantum Electrodynamics*, Wiley-Interscience, 2005. Cited on page(s) 19

[22] Z. Dutton, J. H. Shapiro, and S. Guha, "LADAR Resolution Improvement using Receivers Enhanced with Squeezed-Vacuum Injection and Phase-Sensitive Amplification," *J. Opt. Soc. Am. B* 27, A63, 2010. DOI: 10.1364/JOSAB.27.002007 Cited on page(s) 67

[23] Z. Dutton, J. H. Shapiro, and S. Guha, "LADAR Resolution Improvement using Receivers Enhanced with Squeezed-Vacuum Injection and Phase-Sensitive Amplification: Erratum," *J. Opt. Soc. Am. B* 27, 2007. Cited on page(s) 67

[24] M. Derrick, et.al., "Precision test of QED by direct comparison of $e^+e^- \rightarrow \gamma\gamma$ and $e^+e^- \rightarrow e^+e^-$ at 29 GeV", *Phys. Lett. B*, Vol. 166, 4, 1986. DOI: 10.1016/0370-2693(86)91600-X Cited on page(s) 5

[25] S. Donati, *Photodetectors: Devices, Circuits, and Applications*, Prentice Hall, 2000. Cited on page(s) 90

[26] J.P. Dowling, "Quantum optical metrology - the lowdown on high-NOON states", *Contemporary Physics*, Vol. 49, No. 2, 2008. DOI: 10.1080/00107510802091298 Cited on page(s) 3

[27] C. Emary, B. Trauzettel, and C.W.J. Beenakker, "Entangled Microwave Photons From Quantum Dots", *Phys. Rev. Lett.* 95, 127401, 2005. DOI: 10.1103/PhysRevLett.95.127401 Cited on page(s) 3, 88, 89

[28] H.B. Fei, et.al. "Entanglement-Induced Two-Photon Transparency", *Phys. Revl Lett.*, V. 78, 1679, 1997. DOI: 10.1103/PhysRevLett.78.1679 Cited on page(s) 87

[29] R.P. Feynman and A.R. Hibbs, *Quantum Mechanics and Integrals*, McGraw-Hill, 1965. Cited on page(s) 33, 39

[30] R.P. Feynman, *QED: The strange theory of light and matter*, Princeton University Press, 1985. Cited on page(s) 21, 39

[31] D.R. Frieden (ed.), *Principles of Naval Weapons Systems*, Naval Institute Press, 1988. Cited on page(s) 3, 43

[32] G. Gilbert, M. Hamrick, and Y. S. Weinstein, "Practical Quantum Interferometry Using Photonic N00N States", *Proceedings of SPIE*, E. J. Donkor, A. R. Pirich, H. E. Brandt, Vol. 6573, SPIE, Orlando, 2007. DOI: 10.1080/09500340802428314 Cited on page(s) 3, 70, 71

[33] G. Gilbert, and Y.S. Weinstein, "Aspects of Practical Remote Quantum Sensing", *Journal of Modern Optics*, Vol. 55, Nos. 19-20, 10-20 November 2008. Cited on page(s) 3, 70, 71

[34] V. Giovannetti, S. Lloyd, and L. Maccone, "Quantum Enhanced Positioning and Clock Synchronization", *Nature* 412, 417, 2001. DOI: 10.1038/35086525 Cited on page(s) 3

[35] V. Giovannetti, S. Lloyd, and L. Maccone, "Quantum-Enhanced Measurements: Beating the Standard Quantum Limit", *Science*, 306, 2004. DOI: 10.1126/science.1104149 Cited on page(s) 64, 65, 68

[36] V. Giovannetti, S. Lloyd, and L. Maccone, "Quantum Metrology", *Phys. Rev. Lett.* **96**, 010401, 2006. DOI: 10.1103/PhysRevLett.96.010401 Cited on page(s) 65

[37] S. Guha and J.H. Shapiro, "Enhanced standoff sensing resolution using quantum illumination", arXiv:1012.2548v1 [quant-ph], 2010. DOI: 10.1063/1.3630159 Cited on page(s) 86

[38] S. Guha, "Receiver design to harness quantum illumination advantage", arXiv:0902.2932v3 [quant-ph], 2009. DOI: 10.1109/ISIT.2009.5205594 Cited on page(s) 87

[39] S. Guha and B.I. Erkmen, "Gaussian-state quantum illumination receivers for target detection", *Phys. Rev. A* 80, 052310, 2009. DOI: 10.1103/PhysRevA.80.052310 Cited on page(s) 87

[40] F. Halzen and A.D. Martin, *Quarks & Leptons: An Introductory Course in Modern Particle Physics*, Wiley, 1984. Cited on page(s) 5, 10, 13, 23, 25

[41] N.D. Hardy and J.H. Shapiro, "Reflective Ghost Imaging Through Turbulence", arXiv:1110.0845v1 [quant-ph], 2011. Cited on page(s) 67

[42] Harris, *Quantum Sensors Program*, Final Technical Report, AFRL-RI-RS-TR-2009-208, 2009. Cited on page(s) 65

[43] E. Hecht, *Optics*, Fourth Edition, Addison Wesley, 2002. Cited on page(s) 17, 21, 22, 31, 41, 60

[44] C.W. Hellstrom, *Quantum Detection and Estimation Theory*, Academic Press, 1976. Cited on page(s) 63, 86

[45] M. Hofheinz, et.al, "Synthesizing arbitrary quantum states in a superconducting resonator", *Nature*, **459**, 546-549, 2009. DOI: 10.1038/nature08005 Cited on page(s) 91

[46] M.J. Holland and K. Burnett, "Interferometric detection of optical phase shifts at the Heisenberg limit", *Phys. Rev. Lett.* 71, 1355–1358, 1993. DOI: 10.1103/PhysRevLett.71.1355 Cited on page(s) 65

[47] R. Horodecki, P. Horodecki, M. Horodecki, and K. Horodecki, "Quantum Entanglement", *Rev Mod Phys* Vol. 81, No. 2, 2009. DOI: 10.1103/RevModPhys.81.865 Cited on page(s) 3

[48] S. Hui-Tan, B.I. Erkmen, V. Giovannetti, S. Guha, S. Lloyd, L. Maccone, S. Pirandola, and J.H. Shapiro, "Quantum Illumination with Gaussian States", *Phys. Rev. Lett.* 101, 253601, 2008. DOI: 10.1103/PhysRevLett.101.253601 Cited on page(s) 3, 86

[49] B. Huttner and S.M. Barnett, Quantization of the Electromagnetic Field in Dielectrics, *Phys. Rev. A*: 46, 7, 1992. Cited on page(s) 19

[50] S.D. Huver, C.F. Wildfeuer, and J. P. Dowling, "Entangled Fock states for robust quantum optical metrology, imaging, and sensing", *Phys Rev A* 78, 063828, 2008. DOI: 10.1103/PhysRevA.78.063828 Cited on page(s) 3

[51] J.D. Jackson, *Classical Electrodynamics*, Second Edition, Wiley, 1975. Cited on page(s) 5, 6, 18, 21, 25, 27

[52] J.R. Jeffers, N. Imoto, and R. Loudon, Quantum optics of traveling-wave attenuators and amplifiers, *Phys. Rev. A*, 47: 4, 3346,1993. Cited on page(s) 3, 19, 20

[53] D.C. Jenn, *Radar and Laser Cross Section Engineering*, Second Edition, AIAA Press, 2005. Cited on page(s) 44, 45, 47, 48, 49, 50, 51, 52, 53, 55, 56, 61

[54] H. Klinkrad, *Space Debris: Models and Risk Analysis*, Springer-Praxis, 2006. Cited on page(s) 1

[55] L. Knoll, et.al., "QED in Dispersing and Absorbing Dielectric Media", in *Coherence and Statistics of Photons and Atoms*, J. Perina (ed.), Wiley-Interscience, 2001 Cited on page(s) 19

[56] E.F. Knott, J.F. Shaeffer, and M.T. Tuley, *Radar Cross Section*, Second Edition, SciTech Publishing, 2004. Cited on page(s) 47, 48, 49, 50, 55, 56, 57, 58, 61

[57] P. Kok and B.W. Lovett, *Optical Quantum Information Processing*, Cambridge University Press, 2010. Cited on page(s) 64, 65

[58] P. Kumar, V. Grigoryan, and M. Vasilyev, "Noise-Free Amplification: Towards Quantum Laser Radar," *Proceedings of the 14th Coherent Laser Radar Conference*, Snowmass CO, July 9-13, 2007. Cited on page(s) 67

[59] P. Lacomme, J.P. Hardange, J.C. Marchais, and E. Normant, *Air and Spaceborne Radar Systems*, SciTech Publishing, 2001. Cited on page(s) 3, 43

[60] L.D. Landau and L.M. Lifshitz, *Quantum Mechanics*, Volume 3 of the Landau and Lifshitz Course of Theoretical Physics, Third Edition, Pergamon Press, 1981. Cited on page(s) 11, 13, 24, 26, 63

[61] M. Lanzagorta, "Quantum Radar Cross Sections", *Proceedigns of the Quantum Optics Conference*, SPIE Photonics Europe, 2010. DOI: 10.1117/12.854935 Cited on page(s) 3, 21, 41, 42, 93, 96, 111

[62] M. Lanzagorta, "A Quantum Description of Specular Reflections", submitted to the *American Journal of Physics*, 2011. Cited on page(s) 3, 21, 94, 111

[63] M. Lanzagorta, "A Quantum Algorithm for the Simulation of Quantum Radar Cross Sections", in preparation, 2011. Cited on page(s) 98

[64] D. Lear, et.al., "STS-118 Radiator Impact Damage", NASA Technical Report, 2008. Cited on page(s) 1

[65] T.W. Lee et.al., "Optimization of quantum interferometric metrological sensors in the presence of photon loss", *Phys Rev A* 80, 063803, 2009. Cited on page(s) 3

[66] H. Lee, P. Kok, and J.P. Dowling, "A Quantum Rosetta Stone for Interferometry", *J. Mod. Opts.*, **49**, 2325, 2002. DOI: 10.1080/0950034021000011536 Cited on page(s) 68, 69, 70

[67] S. Lloyd, "Enhanced Sensitivity of Photodetection via Quantum Illumination", *Science*, Vol. 321, Issue 5895, 2008. DOI: 10.1126/science.1160627 Cited on page(s) 3, 79, 86, 87, 111

[68] R. Loudon, *The Quantum Theory of Light*, Third Edition, Oxford University Press, 2000. Cited on page(s) 3, 5, 6, 7, 19, 20, 64

[69] A. Luks and V. Perinova, *Quantum Aspects of Light Propagation*, Springer, 2009. Cited on page(s) 19

[70] D. Lynch Jr., *Introduction to RF Stealth*, SciTech Publishing, 2004. Cited on page(s) 48, 53, 56

[71] F.H. Madjid, J.M. Myers, "Lessons for pulsed-array radar from quantum light detection", *Proceedings of SPIE*, 1629, 368, 1992. DOI: 10.1117/12.137136 Cited on page(s) 3

[72] M. Malik, H. Shin, P. Zerom, and R.W. Boyd, "Quantum Ghost Image Discrimination With Single Photon Pair", *Proceedings of the Conference on Lasers and Electro-Optics / International Quantum Electronics Conference*, Optical Society of America, 2009. Cited on page(s) 3

[73] L. Mandel and E. Wolf, *Optical Coherence and Quantum Optics*, Cambridge University Press, 1995. Cited on page(s) 5, 6, 9, 16, 25, 26, 64, 86, 105

[74] R. Matloob, "Canonical theory of electromagnetic field quantization in dielectrics", *Optics Communications*, 192, 287-297, 2001. DOI: 10.1016/S0030-4018(01)01094-X Cited on page(s) 20

[75] Mathematica.
http://www.wolfram.com/ Cited on page(s) 98

[76] A.D. McAulay, *Military Laser Technology for Defense*, Wiley, 2011. Cited on page(s) 67

[77] R. Meyers, K.S. Deacon, and Y. Shih, "Ghost-Imaging Experiment by Measuring Reflected Photons", *Phys Rev A* 77, 041801, 2008. DOI: 10.1103/PhysRevA.77.041801 Cited on page(s) 3

[78] D. Morrison, et.al., "Dealing with the Impact Hazard", in Asteroids III, W. Bottke, et.al. (eds), University of Arizona Press, 2003. Cited on page(s) 1

[79] J.M. Myers, "Speaking of sensing in the language of quantum mechanics", *Proceedings of SPIE* 6573, 657302, 2007. DOI: 10.1117/12.723412 Cited on page(s) 3, 67

[80] F. Neri, *Introduction to Electronic Defense Systems*, Second Edition, Artech House Publishers, 2001. Cited on page(s) 45

[81] M.A. Nielsen and I.L. Chuang, *Quantum Computation and Quantum Information*, Cambridge University Press, 2000. Cited on page(s) 2

[82] Office of Naval Research Reunion on Quantum Topics.
https://secure.onr.navy.mil/events/docs/587_Agenda_020310.pdf Cited on page(s) 4

[83] G.R. Osche, *Optical Detection Theory*, Wiley-Interscience, 2002. Cited on page(s) 90

[84] Z.Y. Ou, *Multi-Photon Quantum Interference*, Springer, 2007. Cited on page(s) 88

[85] A. Price, *Instruments of Darkness: The history of Electronic Warfare, 1939-1945*, Greenhill Books, 2006. Cited on page(s) 1, 48

[86] D. Richardson, *Stealth Warplanes*, MBI, 2001. Cited on page(s) 1, 53, 58

[87] G. Rieke, *Detection of Light: From the Ultraviolet to the Submillimeter*, Second Edition, Cambridge University Press, 2003. Cited on page(s) 90

[88] G. Romero, JJ Garcia-Ripoll, and E. Solano, "Photodetection of propagating microwaves in circuit QED", *Phys. Scr.* **T137** 014004, 2009. DOI: 10.1088/0031-8949/2009/T137/014004 Cited on page(s) 3, 90

[89] G. Romero, JJ Garcia-Ripoll, and E. Solano, "Microwave Photon Detector in Circuit QED", *Phys. Rev. Lett.*, **102** 173602, 2009. DOI: 10.1103/PhysRevLett.102.173602 Cited on page(s) 3, 90

[90] L.H. Ryder, *Quantum Field Theory*, Cambridge University Press, 1996. Cited on page(s) 5, 6, 9, 11, 21, 25

[91] K.S. Schifrin, *Physical Optics of Ocean Water*, American Institute of Physics, 1983. Cited on page(s) 17, 18, 72

[92] M.O. Scully and M.S. Zubairy, *Quantum Optics*, Cambridge University Press, 1997. Cited on page(s) 5, 6, 7, 8, 15, 16, 25, 32, 33, 64, 86

[93] J.H. Shapiro, "Quantum Pulse Compression Laser Radar", *Proceedings of SPIE*, Vol. 6603, 660306, 2007. DOI: 10.1117/12.725025 Cited on page(s) 3, 67

[94] J.F. Shapiro and S. Lloyd, "Quantum illumination versus coherent-state target detection", *New J. Phys.* **11** 063045, 2009. DOI: 10.1088/1367-2630/11/6/063045 Cited on page(s) 3, 86

[95] M.L. Skolnik, *Introduction to Radar Systems*, Third Edition, McGraw Hill, 2001. Cited on page(s) 3, 43, 44, 48, 61, 71, 72

[96] M.L. Skolnik, *Radar Handbook*, Third Edition, McGraw Hill, 2008. Cited on page(s) 3, 43, 44, 48, 61, 71, 72

[97] J.F. Smith, "Quantum entangled radar theory and a correction method for the effects of the atmosphere on entanglement", *Proceedings of the SPIE Quantum Information and Computation VII conference*, 2009. DOI: 10.1117/12.819918 Cited on page(s) 3, 77, 79, 111

[98] J.F. Smith, personal communication with the author, 05/20/2010. Cited on page(s)

[99] T.M. Stace, G.J. Milburn, and C.H.W. Barnes, "Entangled two-photon source using biexciton emission of an asymmetric quantum dot in a cavity", *Phys. Rev. B* 67, 085317, 2003. DOI: 10.1103/PhysRevB.67.085317 Cited on page(s) 88

[100] B. Sweetman, "Chinese J-20 Stealth Fighter in Taxi Tests", *Aviaion Week*, Jan. 3, 2011. Cited on page(s) 1

[101] R. Tyson, *Principles in Adpative Optics*, Third Edition, CRC Press, 2010. Cited on page(s) 78

[102] A.R. Usha Devi and A.K. Rajagopal, "Quantum Target Detection Using Entangled Photons", *Phys Rev A* 79, 062320, 2009. DOI: 10.1103/PhysRevA.79.062320 Cited on page(s) 3

[103] S.A. Vakin, L.N. Shustov, and R.H. Dunwell, *Fundamentals of Electronic Warfare*, Artech House Publishers, 2001. Cited on page(s) 45

[104] M. Xiao, L.A. Wu, and H.J. Kimble, "Precision measurement beyond the shot-noise limit", *Phys. Rev. Lett.* 59, 278–281, 1987. DOI: 10.1103/PhysRevLett.59.278 Cited on page(s) 65

[105] R.C. Watson, *Radar Origins Worldwide: History of its Evolution in 13 Nations Through World War II*, Trafford Publishing, 2009. Cited on page(s) 1

[106] S. Weinberg, *The Quantum Theory of Fields I*, Cambridge University Press, 1995. Cited on page(s) 5, 9, 11, 21, 25

[107] P.R. Weissman, et.al., "Galileo NIMS Direct Observation of the Shoemaker-Levy 9 Fireballs and Fall Back", in *Abstracts of the Lunar and Planetary Science Conference*, volume 26, page 1483, 1995. Cited on page(s) 1

[108] W.G. van der Wiel, et.al., "Electron Transport Through Double Quantum Dots", *Rev. Mod. Phys.* 75, 1-22, 2002. DOI: 10.1103/RevModPhys.75.1 Cited on page(s) 88

[109] J.G. Williams and J.O. Dickey, "Lunar Geophysics, Geodesy, and Dynamics, *Proceedings of the 13th International Workshop on Laser Ranging*, 2002. Cited on page(s) 77

[110] N.E. Zirkind and J.H. Shapiro, "Adaptive Optics for Large Aperture Coherent Laser Radars', *Proceedings of the Laser Radar III Conference*, 1989. Cited on page(s) 78

[111] N.E. Zirkind, *Adaptive Optics for Large Aperture Coherent Laser Radars*, MIT PhD Thesis, 1989. Cited on page(s) 78

Author's Biography

MARCO LANZAGORTA

Dr. Marco Lanzagorta is Technical Fellow and Director of the Quantum Technologies Group of ITT Exelis. In addition, Dr. Lanzagorta is Affiliate Associate Professor and Member of the Graduate Faculty at George Mason University, and co-editor of the Quantum Computing series of graduate lectures published by Morgan and Claypool. Dr. Lanzagorta is a recognized authority on the research and development of advanced information technologies and their application to combat and scientific systems. Dr. Lanzagorta has over 100 publications in the areas of physics and computer science, and he is coauthor of the books *Quantum Computer Science* (2008), and *Introduction to Reconfigurable Supercomputing* (2010). Dr. Lanzagorta received a doctorate degree in theoretical physics from Oxford University in the United Kingdom. In the past, Dr. Lanzagorta worked as a scientific consultant at the US Naval Research Laboratory in Washington DC, at the European Organization for Nuclear Research (CERN) in Switzerland, and at the International Centre for Theoretical Physics (ICTP) in Italy.